Radiometric Instrumentation and Measurements Guide for Photovoltaic Performance Testing

D. Myers

NREL

NOTICE

This report was prepared as an account of work sponsored by an agency of the United States government. Neither the United States government nor any agency thereof, nor any of their employees, makes any warranty, express or implied, or assumes any legal liability or responsibility for the accuracy, completeness, or usefulness of any information, apparatus, product, or process disclosed, or represents that its use would not infringe privately owned rights. Reference herein to any specific commercial product, process, or service by trade name, trademark, manufacturer, or otherwise does not necessarily constitute or imply its endorsement, recommendation, or favoring by the United States government or any agency thereof. The views and opinions of authors expressed herein do not necessarily state or reflect those of the United States government or any agency thereof.

Available to DOE and DOE contractors from:
Office of Scientific and Technical Information (OSTI)
P.O. Box 62
Oak Ridge, TN 37831
Prices available by calling (423) 576-8401

Available to the public from:
National Technical Information Service (NTIS)
U.S. Department of Commerce
5285 Port Royal Road
Springfield, VA 22161
(703) 487-4650

Printed on paper containing at least 50% wastepaper, including 20% postconsumer waste

CONTENTS

CONTENTS (Concluded)

List of Figures

List of Figures (Continued)

List of Tables

1. INTRODUCTION

The Photovoltaic Module and Systems Performance and Engineering Project at the National Renewable Energy Laboratory performs indoor and outdoor standardization, testing, and monitoring of the performance of a wide range of photovoltaic (PV) energy conversion devices and systems. The PV Radiometric Measurements and Evaluation Team (PVSRME) within that project is responsible for measurement and characterization of natural and artificial optical radiation which stimulates the PV effect.

The PV manufacturing and research and development community often approaches project members for technical information and guidance. A great area of interest is radiometric instrumentation, measurement techniques, and data analysis applied to understanding and improving PV cell, module, and system performance. At the Photovoltaic Radiometric Measurements Workshop conducted by the PVSRME team in July 1995, the need to communicate knowledge of solar and optical radiometric measurements and instrumentation, gained as a result of NREL's long-term experiences, was identified as an activity that would promote improved measurement processes and measurement quality in the PV research and manufacturing community (Myers, 1995b).

The purpose of this document is to address the practical and engineering need to understand optical and solar radiometric instrument performance, selection, calibration, installation, and maintenance applicable to indoor and outdoor radiometric measurements for PV calibration, performance, and testing applications. An introductory section addresses radiometric concepts and definitions. Next, concepts essential to spectral radiometric measurements are discussed. Broadband radiometric instrumentation and measurement concepts are then discussed. Each type of measurement serves as an important component of the PV cell, module, and system performance measurement and characterization process.

Specific applications and examples of spectroradiometry and broadband radiometry applied to photovoltaic performance evaluation are described. In each case, the measurements, calibrations and reference standards, instrument performance, and instrument applications (installation, maintenance, quality assurance) are addressed.

2. PV AND OPTICAL RADIOMETRIC CONCEPTS

This section defines the concepts and terms used in the context of this document. NBS Technical Notes 910-1 through 910-5, "Self Study Manual on Optical Radiation Measurements" published by the National Bureau of Standards (NBS), now the National Institute of Standards and Technology (NIST) (Nicodemus, 1976,1977,1978,1979,1982) is an excellent source of very detailed information on the radiometric topics discussed here. NBS Special Publication SP-300, Volume 7, *Precision Measurement and Calibration Radiometry and Photometry* (Hammond and Mason, 1971) published by NBS, and McCluney (1994), *An Introduction to Radiometry and Photometry*, along with references in the bibliography, are highly recommended.

2.1 Spectral Concepts

Electromagnetic radiation is present everywhere around us in the form of waves or photons ("particles" or packets of light) with a wide distribution, or spectrum, of energies. These waves originate from and are radiated by every object in the universe, the most important of which are stars, and especially by the star most important to us, our sun. Common broad energy groupings have evolved in the scientific community for regions of the spectrum, usually referred to with names such as gamma rays, X-rays, cosmic rays, ultraviolet (UV), visible, infrared (IR), microwaves, and radio waves.

We refer to "optical" or "solar" radiation in the UV-visible-IR region of the electromagnetic spectrum, where photons and waves can be manipulated with lens, mirrors, filters, etc. This spectral region corresponds roughly with the peak intensity of the sun's spectral distribution, which is utilized by the human eye, photosynthesis in plants, and the photovoltaic conversion systems of interest here. The technical term "light" is reserved for the radiation that can be sensed by the human eye (McCluney,1994). The bibliography lists reference books and specific publications discussing optical radiation and applications to photovoltaic performance testing.

The photovoltaic energy conversion devices being developed and marketed to replace fossil fuel energy sources generate energy by dislodging electrons bound to the atoms of certain materials, leaving "holes" and "free" electrons to generate electric current, and the transport of electrical energy. This process uses only waves or photons in the "middle part" of this broad spectral range (UV, visible, and IR radiation), and the effectiveness (efficiency) of the conversion process varies depending on the distribution of energy within the spectrum.

PV cells are single, "integrated" devices made up of one or more layers of various semiconductor materials. A cell is the smallest PV device that generates electrical power. PV modules consist of a number of interconnected cells packaged to protect the cells from the environment, and produce larger amounts of electrical power. PV arrays consist of a number of interconnected modules. Finally, a PV system is comprised of interconnected PV arrays and the associated balance of systems, or elements required to interconnect the arrays, condition the power (convert direct current to alternating, etc.), and connect the PV system to the load or the power grid.

Properties of radiation related to location within the overall spectrum are described as spectral properties. The term broadband optical radiation refers to radiation within a broad wavelength range within the total spectrum, such as ultraviolet radiation, and sometimes total radiation, referring to the entire (optical) spectrum. PV device performance is spectrally dependent.

Common terms encountered in optical radiometric physics are:

- *irradiance*: the power (or energy) density per unit area of the radiation. Symbol: E. Units are usually watts per square meter (W/m^2) or Joules per square meter (J/m^2).

- *wavelength*: the distance between wave crests in the electromagnetic wave. Symbol: λ.

2

-   *spectral irradiance*: irradiance as a function of wavelength. Symbol: E(λ). Units are usually watts per square meter per nanometer (W/m²/nm).

The units of wavelength are usually nanometers (nm), or $1 * 10^{-9}$ meter (m). Other units often seen are micrometers or microns ($1 * 10^{-6}$ m), Angstroms ($1 * 10^{-10}$ m) or millimicrons ($1 * 10^{-9}$ m, equal to nanometers). Figure 2.1 is graph of a typical irradiance versus wavelength for natural sunlight, showing the wavelength regions of interest to the PV community, and the wavelength regions where certain PV materials respond.

Table 2.1 shows descriptive names associated with the wavelength regions labeled UV, visible, and infrared (IR).

Figure 2.2 shows relative spectral response, or current generation efficiency versus wavelength, for materials from which PV modules and systems are manufactured. Figure 2.2 illustrates that different spectral regions are important to different PV materials.

This variation in material response makes it difficult to compare performance from one material to another, or understand the variations in performance of a given material under different conditions. Further, laboratory light sources have different spectral distributions than natural sunlight, and of course the spectral distribution of natural sunlight varies both in amplitude and in the relative distribution of energy with respect to wavelength under various conditions.
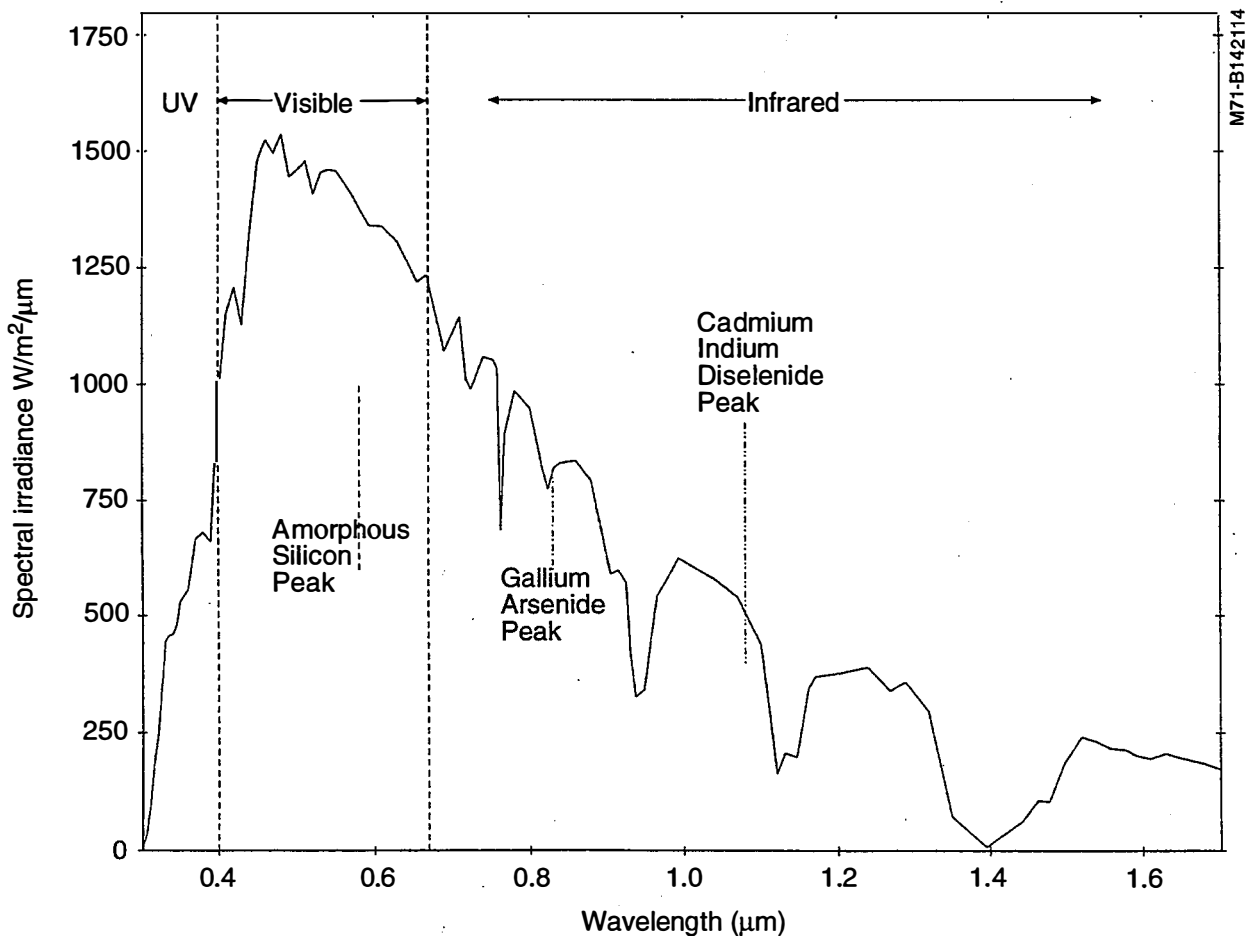
Figure 2.1. Typical solar spectral distribution showing regions of interest to PV

3

Table 2.1. Descriptive Names for Optical Spectral Regions

Spectral Region	Wavelength Boundary (nm)
Ultraviolet (UV)	150 nm-400 nm
Vacuum UV	150 nm- 250 nm
UV-C	250 nm-280 nm
UV-B	280 nm-320 nm
UV-A	320 nm-400 nm
Visible	380 nm-750 nm
Near Infrared	750 nm-1000 nm
Infrared	1000 nm-4000 nm
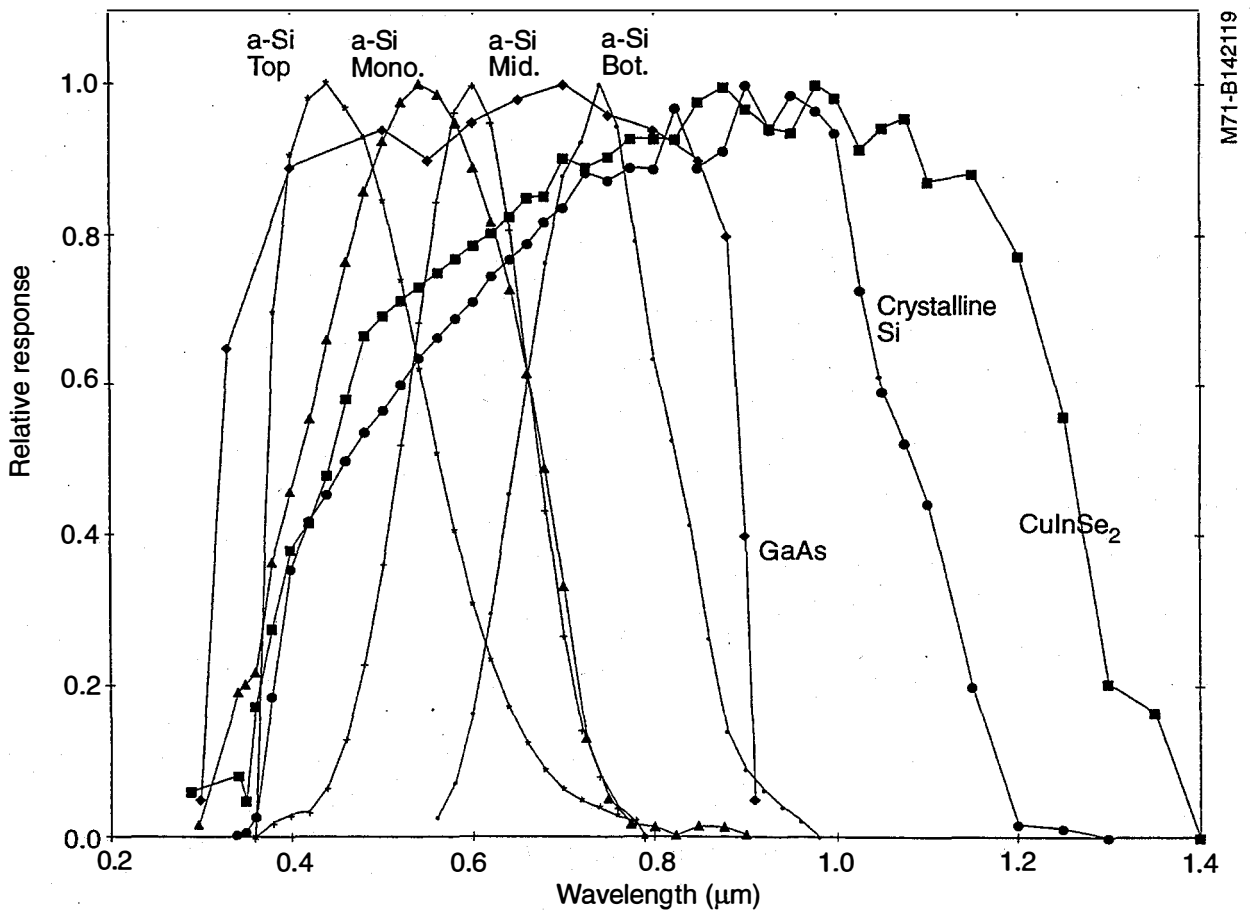
Figure 2.2. Relative spectral response functions for a variety of PV materials

The PV community has established reference spectral distributions which represent specific atmospheric conditions, and means of computing spectral mismatch corrections to correct test results made under different sources and different atmospheric conditions to those that would be obtained under the reference spectrum. Figure 2.3 displays spectral distributions of laboratory sources often used in PV performance testing and evaluation.

Spectral variations in natural sunlight are due to the changes in atmospheric properties, such as the amount of water, ozone, aerosols, particles, and clouds in the atmosphere. One other major contributor to natural sunlight spectral variation is the length of the path the sunlight must traverse from the top of the atmosphere to the ground, known as the air mass, which we denote by M. Air mass 1 is the shortest path length possible, when the sun is directly overhead (elevation of $90°$). As the sun moves toward the horizon, the elevation angle decreases from $90°$ to $0°$ at the horizon, and the path length increases.

Geometrical air mass is often described with respect to the complement of the elevation angle, known as the zenith angle, Z. Thus $Z = 90°$-e, where e is the elevation of the sun (i.e., the center of the solar disk) above the horizon. The relationship between elevation and zenith angles, and the air mass M is that M = secant of Z, or $1/\cos(Z)=M$. At a solar elevation of $30°$, $Z = 90°-30°= 60°$, $\cos(Z) = 0.5$, and $1/\cos(Z) = M = 2.0$. The effects of the curvature of the earth and atmospheric refraction were investigated by Kasten (1964,1966) and Kasten and Young (1989), who developed the equation
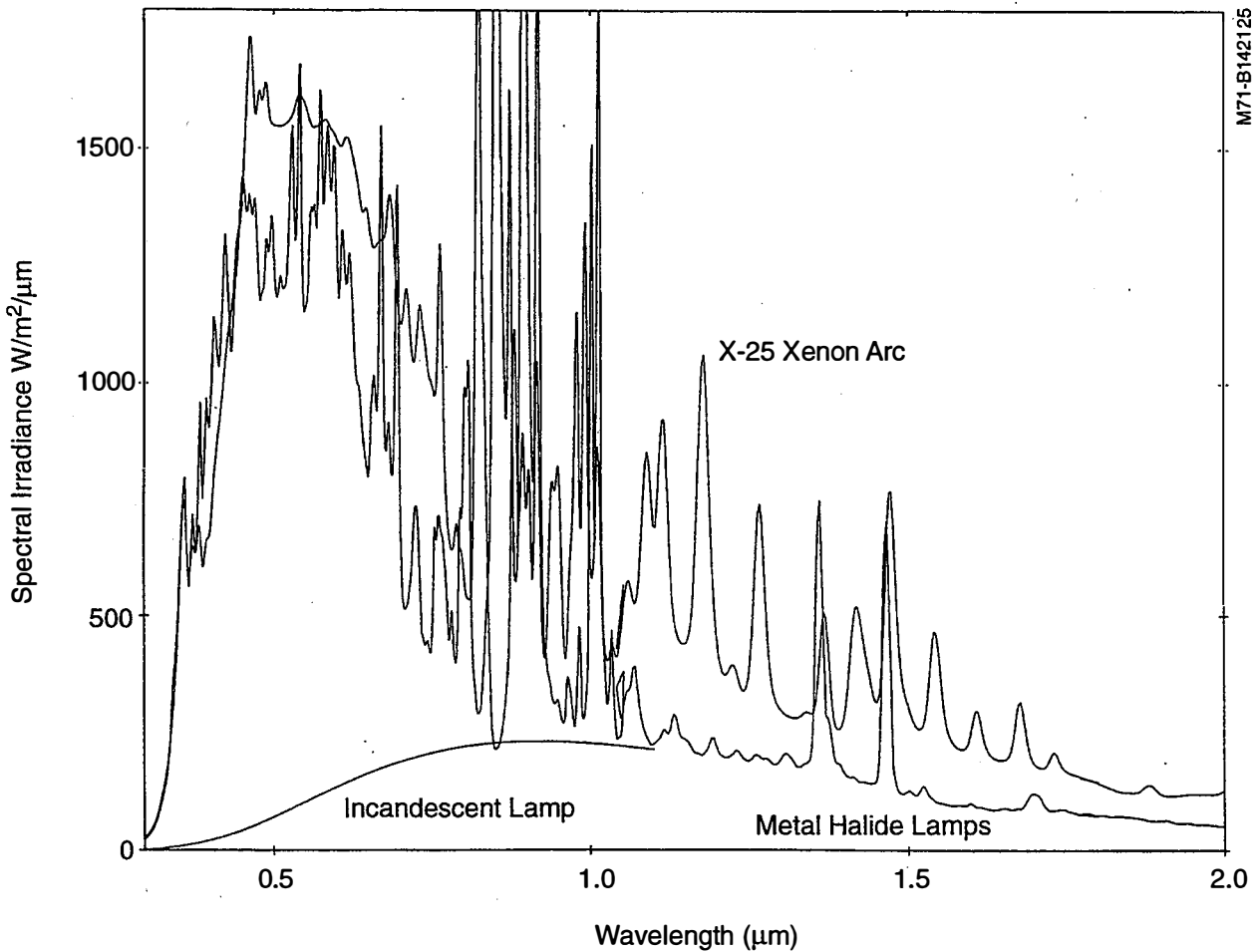
Figure 2.3. Spectral distributions of different laboratory lamps for PV materials evaluation

$$M = [\cos (Z) + 0.50572 / (96.07995 - Z)^{1.6364}]^{-1}$$

for the effective air mass, where the observed zenith angle is **Z**. Finally, the absolute air mass scales M for air pressure, by multiplying M by the ratio **P/P₀** of station barometric pressure, **P**, to standard barometric pressure at sea level, **P₀** (760 mm of mercury or 1013.25 millibars). Figure 2.4 illustrates how the solar spectrum varies for different values of air mass. Figure 2.5 shows definitions of angles involved in solar geometry considerations.

The large air mass when the sun is near the horizon in the morning and evening is responsible for red skies at sunrise and sunset. Preferential (Rayleigh) scattering of the short wavelength (UV and blue wavelengths) by the larger number of molecules encountered by the sunlight as it passes through the longer path in the atmosphere, redistributes the "blue" photons, leaving the longer wavelength ("red") photons to reach the eye. The wide variation in possible combinations of spectral response and source spectral distributions means it is important to be able to measure spectral response and spectral distribution information, as described in the next section.

Since the changing position of the sun throughout the day has such an impact on the character of the radiation, we need to compute the position of the sun at any time of day at any location on earth. Appendix I contains the computer code used by NREL to perform calculations of the sun's position, and parameters such as air mass.
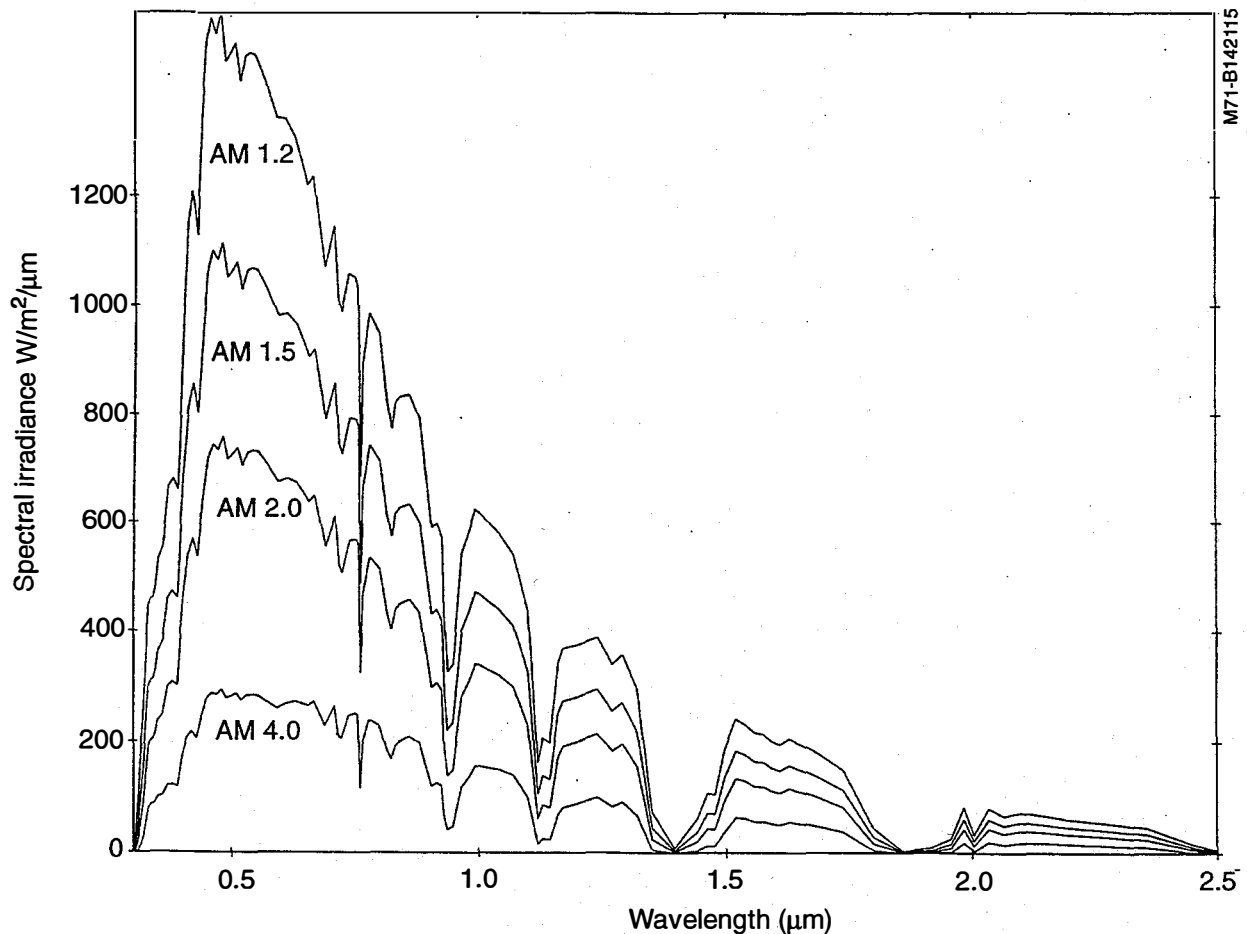
Figure 2.4. Changes in solar spectral distribution with increasing air mass M
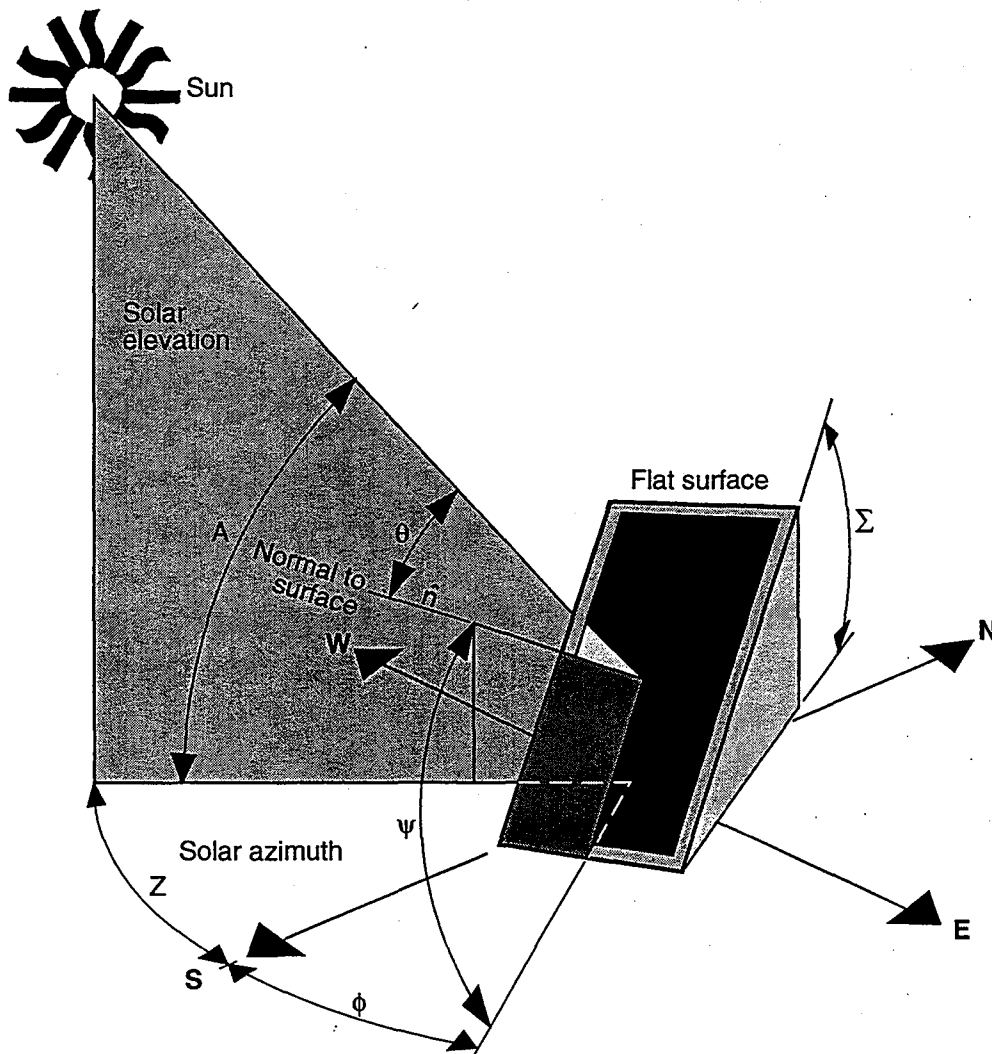
Figure 2.5. Solar geometry definitions for normal, zenith, incidence, and azimuth angles

2.2 Broadband Concepts

We conclude this section with a few concepts and definitions related to both spectral and broadband optical radiation. The optical radiation reaching the earth's surface arrives at the top of the atmosphere as a beam of (nearly) parallel, or collimated, rays called the direct beam radiation, **B**. The disk of the sun subtends a plane angle of about 0.5° on the sky dome, and the rays fill a cone (the base being the solar disk) with half angle of 0.25°, as seen from a point on the surface of a radiometer detector, or PV device. This cone defines a solid angle, prescribed by a point on the receiver and a closed curve in space (circumference of the solar disk). The solid angle is the area on the surface of a unit sphere within the closed curve projected onto the unit sphere with center at the point of observation. A pyrheliometer is designed to capture radiation within a solid angle of usually 5° to 6°, centered on the solar disk. A pyrheliometer accepts the direct beam and a small amount of circumsolar, or aureole, radiation from the sky near the sun.

As the direct beam encounters the atmosphere, short wavelength (UV and blue) photons are preferentially scattered out of the direct beam, contributing to the sky brightness and blue color. The radiation reaching a surface from all of the sky dome except the solar disk is called diffuse radiation, **D**.

Some of the radiation reaching the surface may be reflected by the ground (or buildings, plants, etc.) back to the sky, contributing to the diffuse sky radiation. Total or global radiation, **G**, is the combination of direct, reflected,

and diffuse radiation at a surface. A pyranometer measures total, or global, radiation at a surface. Ideally, it has a field of view, or solid angle of acceptance of 180°, or 2-pi steradians.

On an arbitrarily oriented surface, the collimated (essentially parallel) rays of the solar direct beam are spread over a given area in proportion to the cosine of the angle at which the beam strikes the surface. The normal to a surface is the direction of a line perpendicular to the surface, and the angle of incidence, i, of the direct beam is the angle between the normal to the surface and the beam radiation. Reflected and diffuse radiation consist of rays from random directions and are not collimated.

A horizontal surface is a plane parallel to the local plane tangent to the earth's surface. Global radiation on a horizontal surface can be computed from the following equation:

$$G = B \bullet \cos(i) + D \qquad (1)$$

where D, the diffuse radiation, includes both sky and reflected radiation seen by the surface.

The normal to a horizontal surface points to the zenith, the direction defined by the line connecting the center of the earth with the location on the earth's surface, continuing directly overhead. For a horizontal surface, the direct beam incidence angle, i, and the zenith angle, Z, defined above, are equal.

The field of view of a radiometer (or PV device) is the solid angle (angular extent of the scene in azimuth and elevation) from which the detector accepts radiation. Because radiometric sensors and radiometers usually consist of collecting and absorption surfaces that are plane, or defined by planes, knowledge of the geometrical relationship between the sensor planes, the direct beam, and the amount of diffuse radiation in the field of view of the sensor is useful, as we can apply Equation 1 when i or Z, and two of the three radiation components, B,D, or G are known.

As the incidence angle, i varies from normal (0°) to tangent (90°) on a perfect radiometer that generates a signal s_0 from a beam of radiation at normal incidence, the radiometer produces a signal s proportional to the cosine of the incident angle. This is known as Lambert's law, or the cosine law:

$$s = s_0 \bullet \cos(i) \qquad (2)$$

Such a radiometer has a "Lambertian" response. Imperfections in the manufacture of sensors or detectors, and variations in the absorption and reflectance of sensor materials result in detectors which do not agree exactly with the desired theoretical response as the direction of the beam radiation changes. The change in a radiometer signal as a function of incidence angle of collimated radiation is referred to as the cosine response of the radiometer. This term may describe deviations from agreement with Lambert's law, as well as the absolute variation in response versus incidence angle.

Similarly, the signal from a perfect radiometer would be constant for a constant collimated beam of radiation, independent of the azimuth angle (angle in the plane of the surface between two planes perpendicular to the receiving surface: a reference direction and the plane containing the beam). The variation in signal as a function of the azimuth angle is referred to as the azimuthal response of the radiometer. Both azimuthal and cosine response are sometimes referred to in combination as the geometrical response of the radiometer. Figure 2.5 depicts these angles.

Environmental factors other than the geometry of the radiation and the sensor geometrical response, can affect radiometer detectors and readout instrumentation in both short and long time scales. These factors include (but are not limited to) temperature fluctuations, vibration, and electromagnetic interference (EMI), the relative

strength of the UV portion of the spectrum, and humidity. Each of these factors can cause changes or variations in radiometer performance, stability, and the long-term accuracy of radiometric instruments.

2.3 Measurement Processes, Uncertainty, and the True Value

An important principle of uncertainty analysis is that the quantity we want to measure may not be exactly the quantity we actually do measure as the indication on our instrumentation. Due to lack of knowledge of the details of the "measurement process," the desired (true) value may be quite different than what we measure or record.

For example, we may be trying to read the temperature of a material using a thermocouple attached to the material. In effect, we do not measure the temperature of the material the thermocouple is in contact with, but the temperature of the thermocouple junctions. There may be a significant difference between these two quantities, depending on the quality of thermal conduction path between the material and the thermocouple, gradients, how close or far away the system is from equilibrium, and many other factors.

For optical radiation measurements, the response of a sensor might be the result of the geometry, temperature, and electromagnetic environment of the detector. The data recorded by a data logger will include errors inherent in the data logger electronics as well. Therefore an understanding of what is measured versus what is desired, the sources and magnitudes of various components of uncertainty, and the desired accuracy (level of uncertainty) that is needed and that can be obtained is important. An excellent discussion of uncertainty analysis applied to the radiometric disciplines can be found in Wells (1995). An application to radiometers is found in Myers, 1989a.

3. SPECTRAL RADIOMETRIC INSTRUMENTATION AND MEASUREMENTS

Systems used to separate broadband optical radiation into spectral components are called spectroradiometers. These systems consist of an optical receiver or "front end" which defines the field of view and captures the radiation, a dispersion element (monochromator) for separating the light by wavelength, scanning control to "tune" the radiometer to different wavelengths, a detector for collecting and determining the amplitude of the signal proportional to the photons (sorted by wavelength), and a signal-processing unit (computer) to control the system, record, process, and store the data. This section describes the calibration, operation, and applications of such instrumentation for PV performance measurements and characterization.

3.1 Optical Receiver

The input optics of the spectroradiometric system are used to collect the radiation for sorting by wavelength. Whether measuring a lamp in the laboratory, or natural sunlight, several points need to be kept in mind regarding input optics and their relationship with PV devices under test.

The input optic field of view should match that of the PV device. If testing a large, flat PV module, a diffuser plate, integrating sphere, or other diffusing element with a limiting aperture field of view of 180° is required. If testing or calibrating a solar cell outdoors against a pyrheliometer with a given field of view (usually 5° or so), a view-limiting device must be designed to closely match the field of view of the spectroradiometer input optics, the broadband reference instrument, and the PV device. This includes getting the orientation (slope and azimuth) of the receiving surfaces as close to identical as possible. If the test device or the spectroradiometer "see" different amounts of radiation it is more difficult to make accurate statements about the correct amount of the radiation used by the PV device, and consequently the device performance.

Whether the input optic is an integrating sphere or another diffusion element (plates or domes of ground quartz, Teflon, etc.) there will be deviations from perfect Lambertian response (cosine response). We recommend both laboratory (Nann and Riordan, 1992; Michalsky et al., 1990) and outdoor tests (Myers, 1990) to determine the magnitude of these deviations. Either the source (lamp or sun), the input optic/radiometer, or a combination of the two can be arranged to move in order to acquire data for different geometries (Springsteen, 1989).

3.2 Dispersive Element

The heart of any spectroradiometric instrument is the dispersive element, which separates the broadband light into its various wavelength components. The simplest dispersive element to use (though not to make) is the optical filter. This consists of various combinations of solid, liquid, or gaseous materials, glass, metal, or perhaps chemical elements (dyes) which allow only certain wavelengths to be reflected or transmitted, absorbing or blocking others. See Driscoll and Vaughn's *Handbook of Optics*, Section 8, 1978, for descriptions of absorption, interference, reflection, scattering, and polarization properties of materials.

Filters can be made to transmit (reflect) only radiation above (cut-on filters) or below (cut-off filters) or within (passband) given wavelength limits. Basic concepts associated with optical passband filters are shown in Figure 3.1, a generic passband filter transmission curve.

The figure shows the central wavelength as the point where the maximum transmission occurs.

The passband is the difference between wavelength limits in which optical radiation is made available to the detector. The term passband most often refers to the half-power band width (HPBW) or full-height half power (FHHP), which is the difference between the longer and shorter wavelengths at which 50% of the peak
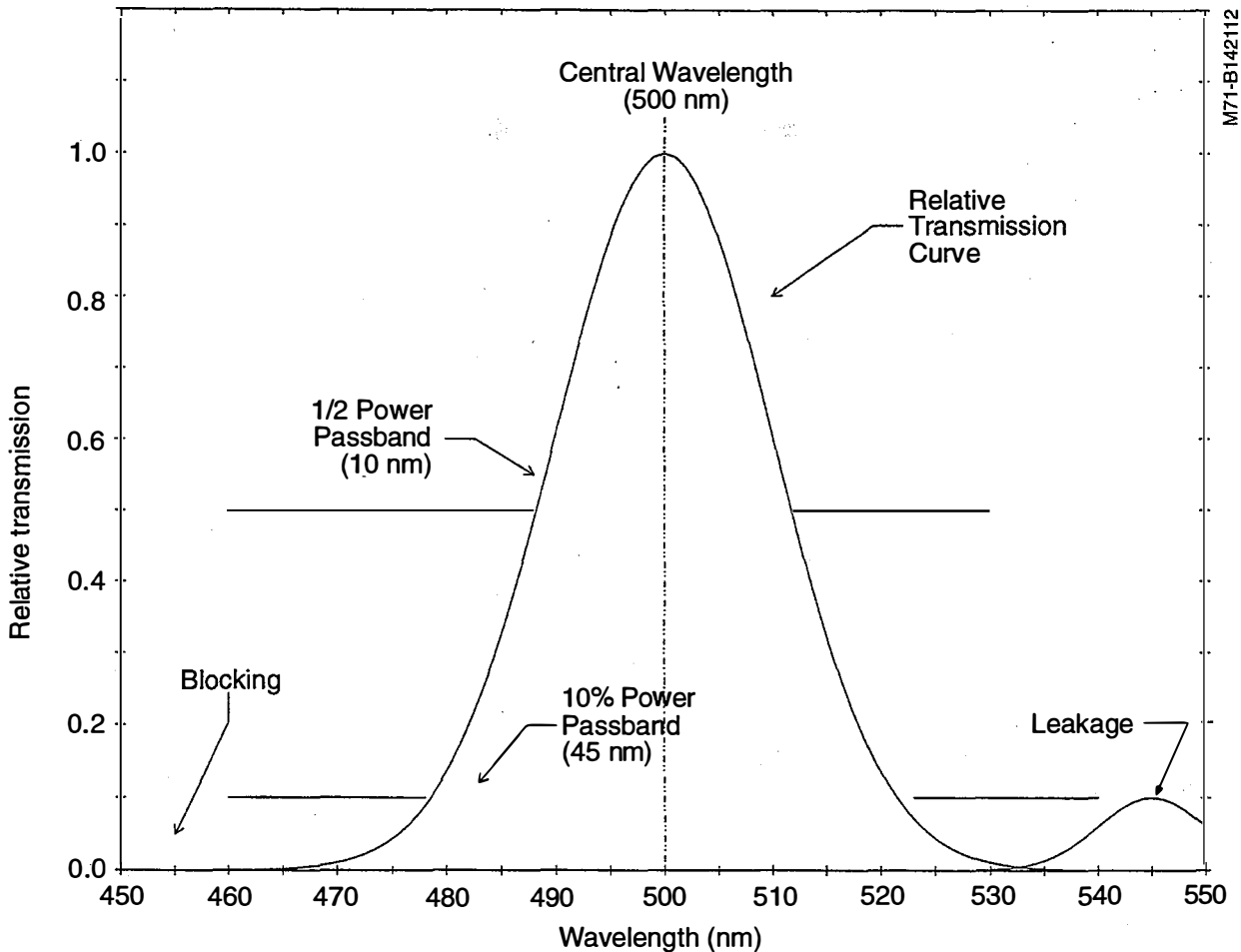
Figure 3.1. Optical filter parameters

transmission occurs. Sometimes the bandwidth at the 10% transmission points is specified. Another important parameter is the degree of blocking outside the passband, expressed usually as a fraction of the peak transmittance, i.e., 1 x 10^{-4}, since "leakage" outside the passband can contribute to the detector signal, resulting in errors in the measurement at the desired central wavelength.

An issue for filter radiometry is the stability of their materials and optical properties, which usually change with time. Very minute changes in materials and physical dimensions, and alignment (i.e., transmission is a function of angle of incidence of the radiation) can cause changes in the throughput of the filters over time, when used in the outdoor environment.

Filter spectroradiometers interpose a series of filters with different central wavelengths and possibly different passbands, between the input optic and the detector, which provides a signal proportional to the spectral irradiance at the input optic. Typical examples are described in Schneider, et al., 1967, and Correll et al., 1992.

Narrow slits, in combinations with prisms (Schneider, et al., 1967; Stair, 1966; Zerlaut, 1986) and diffraction gratings (Chap. 7, Sec. 7.7 of Lipson and Lipson, 1969; Hutley, 1982; Sommerfield, no date, Chap. V & VI) are the classical means of spectral dispersion. The Fabry-Pero interferometer (Sommerfield, no date, Chap. I, Sec. 7-G) used in instruments such as Fourier Transform Infrared Radiometers (FTIR) have also been used as the basis for spectroradiometers.

The primary specifications of concern with respect to the dispersion component of the spectral measurement system are the wavelength accuracy and stability (repeatability), spectral resolution, passband, and throughput or efficiency of the element. Each is discussed in general below.

The accuracy of wavelength-related parameters depends on the quality of filters or wavelength drive mechanisms and grating quality. Filter passband and central wavelength have been discussed above. For the classical monochromator based on slits, diffraction gratings, and drive mechanisms, there are more complications. These include mechanical mounting and drives for moving gratings and other optical components, the quality of gratings (mechanically ruled, or holographically produced) and grating properties such as efficiency with respect to wavelength, which is related to the grating groove spacing and shape. Gratings re-distribute the broadband energy into spectral orders, denoted zeroth, first, second, etc., and to eliminate spectral "crosstalk" between the various orders, cut-on filters known as order-sorting filters may be required to ensure that only the wavelengths of interest are allowed to reach the detector. Gratings with optimized throughput for specific spectral regions have special groove shapes and spacing, and are said to be blazed to the spectral region or wavelength.

Spectral resolution is the ability to separate spectral features that may be in close proximity in wavelength. It is usually quoted in terms of wavelength units, as in 0.1 nm or 0.5 nm. Usually, the smallest usable slit width, rather than the grating, will determine the spectral resolution. For larger slits, resolution is the product of the slit width (usually in millimeters, mm) and the grating reciprocal linear dispersion (i.e., nm/mm for the combination of grating angular dispersion related to the number of grooves per mm, and focal length of the monochromator).

For scanning grating dispersion instruments (monochromators), spectral resolution is a combination of slit widths through which the radiation enters the monochromator and the grating properties. For fixed grating, multi-channel detector radiometers, grating properties, width of the detector elements and geometry determine the spectral resolution.

For classical monochromators, the responsivity function, which is the product of the slit scattering function and detector responsivity, is the rough analog of the filter passband discussed above. In NBS technical note 910-4, Chapter 7, these functions and their determination are described in great detail. This topic will be outlined here to give the reader an idea of the concepts and techniques involved, and their importance.

The slit-scattering function is the mirror image of the irradiance "profile" of a very narrow spectral line (such as a narrow emission line or laser line) incident on the slits as the line is scanned in wavelength. The detector responsivity is the relative output of the detector as a function of wavelength, assuming input radiation that is constant in amplitude with respect to wavelength, and is similar to the spectral response or quantum efficiency of PV devices shown in Figure 2.2.

The combination of slits (input and output), gratings, filters, and detector responsivity as a function of wavelength is needed to fully characterize the performance of a given monochromator system with the utmost accuracy. The signal recorded by the spectroradiometric system at a specific wavelength is the mathematical convolution (integral of the products of functions) of the system responsivity function at that wavelength setting with the true spectral distribution of the source. It is possible, and common, for the responsivity function to vary at different wavelength settings.

If the system responsivity function at wavelength λ_o is denoted by $r(x,y,\lambda_o,\lambda)$ where x,y are spatial coordinates over the detector area, A, λ_o is the wavelength setting, λ is wavelength, and the source spectral distribution amplitude is $E(x,y,\lambda)$, the output signal, $S(A, \Delta\lambda,\lambda_o)$ of the monochromator/detector system will be

$$S(A,\Delta\lambda,\lambda_o) = \int_{\Delta\lambda}\int_A E(x,y,\lambda) \cdot r(x,y,\lambda_o,\lambda) \cdot dA \cdot d\lambda \qquad (3)$$

where $\Delta\lambda$ is the region where the responsivity function is non-zero. For a filter radiometer, $r(x,y,\lambda_o,\lambda)$ includes the filter passband function, as shown in Figure 3.1. Thus, it is apparent, and important to note, that for any type of spectroradiometer, the signal will change if the relative spectral shape over the range $\Delta\lambda$ is changed.

This is particularly important because the calibration sources used (discussed below) often have smooth, relatively slowly changing spectral distributions (lowest curve in Figure 2.3) as opposed to the sometimes rapidly changing distributions of the sun or solar simulator lamps (top curves of Figure 2.3, solar curves in Figure 2.4). Applying Equation 3 when calibrating with a lamp having spectral distribution $E^s(\lambda)$, say we obtain the signal $S^s(A, \Delta\lambda,\lambda_o)$, and when measuring an unknown source, we obtain $S(A, \Delta\lambda,\lambda_o)$. If we assume the calibration source irradiance, $E^s(\lambda)$, is constant over $\Delta\lambda$, bring the $E^s(\lambda_o)$ term (for the calibration lamp) outside the integral, and multiply the ratio of the two equations, S/S^s, times the calibration lamp irradiance, $E^s(\lambda_o)$, we have:

$$E^o(\lambda_o) = \frac{S}{S^s} \cdot E^s(\lambda_o) = \frac{\int_{\Delta\lambda} E(\lambda) \cdot r(\lambda_o,\lambda)\, d\lambda}{\int_{\Delta\lambda} r(\lambda_o,\lambda)\, d\lambda} \qquad (4)$$

where we have designated $E^o(\lambda_o)$ as the observed irradiance, derived from the ratio of signals times the calibration irradiance. This is commonly done, and omits taking into account the convolutions with the detector responsivity function.

Figure 3.2 illustrates schematically how using Equation 4 will distort the actual spectral distribution for a sample spectral distribution for the responsivity function shown in the figure. Note the underestimates and overestimates of spectral irradiance as a result of the responsivity function shape.

Unless the spectral responsivity functions of a system are known and a deconvolution process is followed (see NBS Technical Note 910-4, Chapter 8), there are inherent errors in the spectral measurements made with radiometers calibrated against NIST standard lamps, and used to measure other spectral distributions. The errors vary depending on the slope of the spectral distribution at each λ_o. They are largest when there is a great disparity in the slopes of the calibration and unknown spectral distributions at a given λ_o. For example, in Figure 2.4 above, in the wavelengths short of 350 nm in the solar spectra, comparison with the lowest curve (1000-watt tungsten halogen lamp) in Figure 2.3 shows dramatic differences in slope between the two curves. Thus, the absolute accuracy of solar UV measurements is much less, and varies greatly between radiometers with different responsivity functions. See the discussions in Stair (1967) and Koskela (1994).

Within the present uncertainty limits of spectral irradiance calibration sources, and over the spectral region of greatest interest for PV applications, these sorts of corrections are not large enough to contribute greatly to the overall uncertainty, so they are not accounted for. However, for short-wavelength solar ultraviolet measurements, or highly accurate determination of spectral emission peaks and bandwidths, the knowledge of the responsivity function can be crucial.

Diode array spectroradiometers have become relatively inexpensive and readily available from many optical instrumentation manufacturers. These spectrographs or spectroradiometers acquire spectral information in milliseconds that would take minutes to acquire with traditional scanning grating spectroradiometers such as those used at NREL, and which have been described previously. In the course of experimenting with such an instrument, we have become aware of many of the difficulties associated with using such a device to take spectra of pulse solar simulators.
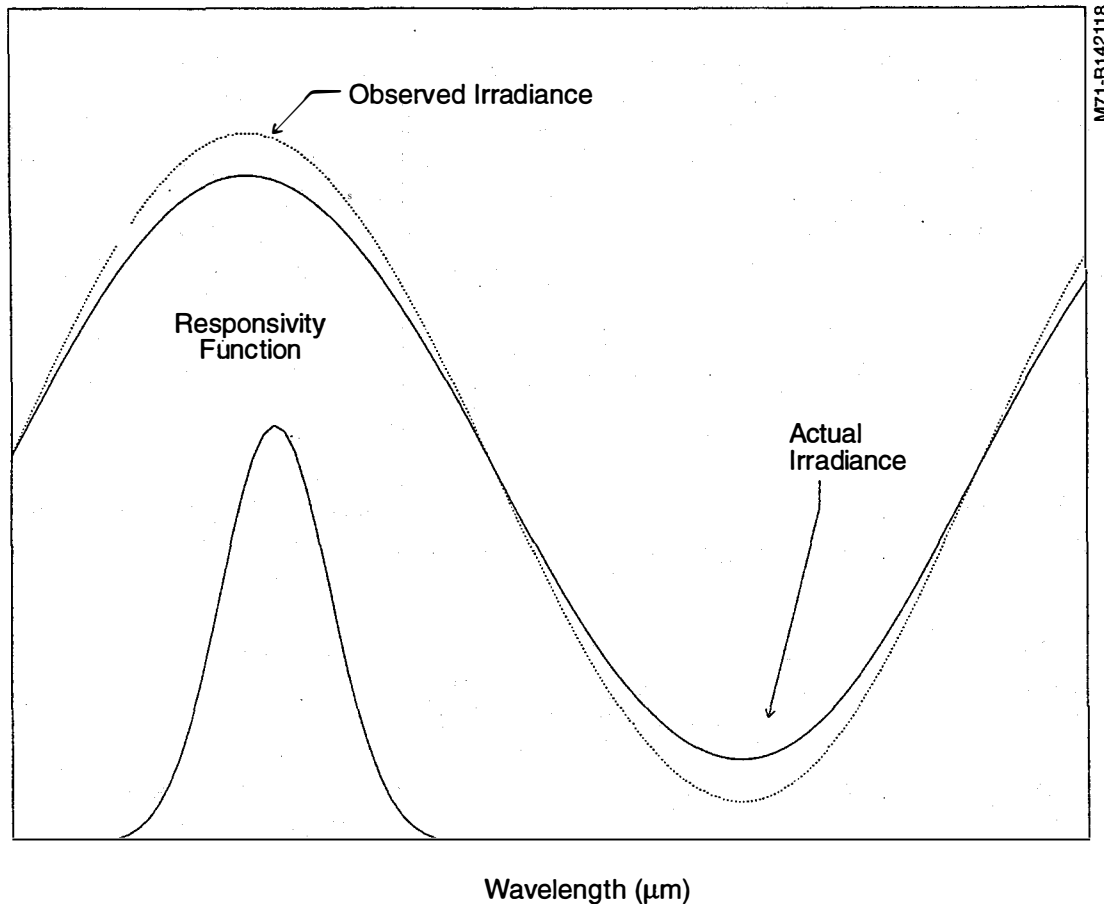
Figure 3.2. Schematic of variation in indicated versus true irradiance when using Equation (4)

The device covered the wavelength region from 300 nm to 1100 nm with an array of 1024 diode elements, or an equivalent spectral resolution of about 1 nm. The spectrograph grating was blazed (had optimum throughput) at 1000 nm. The unit was calibrated for absolute spectral measurements by determining the responsivity (watts per square meter per nanometer)/(digital count) when measuring a 200-watt tungsten halogen lamp with a known spectral distribution.

Spectral data were then collected under the NREL Spire 204A pulsed solar simulator, which generates a 3-millisecond (ms) light pulse at 15 hertz, or a period of 66.67 ms. Figure 3.3 compares the array radiometer and NREL scanning grating radiometer (Pulse Analysis Spectro-radiometer System, PASS, see Myers, Cannon, and Trudell, 1993) data, and shows the relative spectral distribution of the calibration lamp in the lower part of the figure.

Figure 3.3 shows the array radiometer data exceed the PASS radiometer data greatly in the above 800 nanometers, and is lower than the PASS data in the region from 400 nm to 700 nm. The reasons for these discrepancies are: (1) lack of spectral order sorting filters in the diode array instrument, (2) great disparity in the spectral distributions of the calibration and simulator sources, (3) increased stray light due to the lack of an exit slit in front of the detector(s), and (4) time synchronization between the pulse source and the array data collection.

14
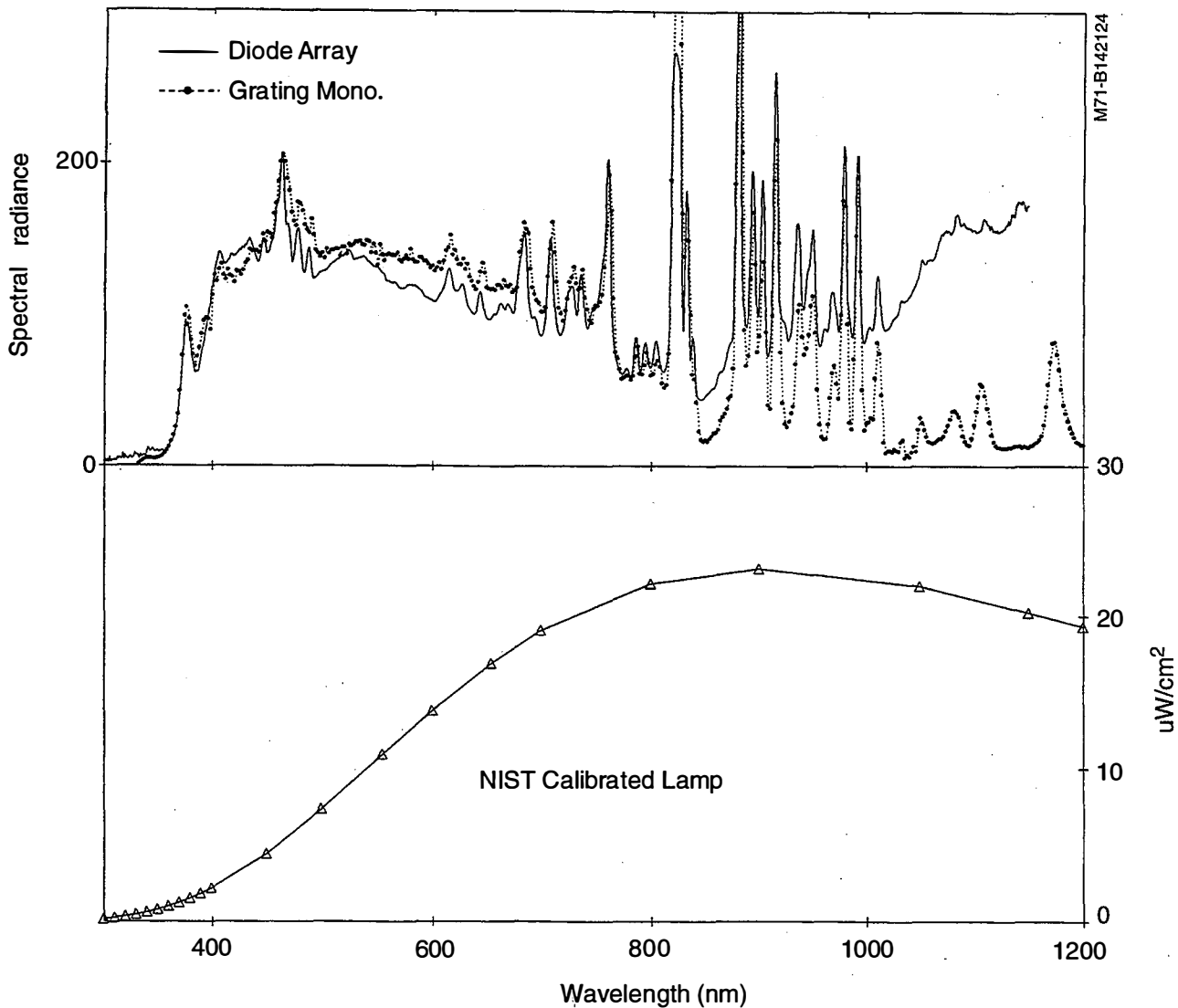
Figure 3.3. Relative spectral distribution of Spire 240A measured with diode array and scaning grating spectroradiometers compared with calibration lamp spectrum

Gratings used in modern monochromators obey the grating equation, relating the grating spacing (d), the wavelength of impinging radiation (λ), the angle the radiation is incident at (ϕ), and the angle the radiation is diffracted with respect to the normal (θ), and the order number (m) via: d (sin ϕ + sin θ) = m λ. The equation indicates that monochromatic light will be diffracted in a number of different directions (θ_m for each order multiple m of the wavelength). When broadband light is diffracted from the grating, higher orders of shorter wavelength light can overlap the first order of longer wavelength light, and contribute to the signal in the longer wavelength radiation. For example, second-order 400 nm radiation will add to the first-order 800 nm radiation seen by a detector selecting the 800 nm wavelength radiation. This is the primary cause of the excess radiation beyond 800 nm in the array data of Figure 3.3. The second-order radiation from the high irradiance levels at 400 nm to 800 nm overlaps the first-order radiation in the 800 to 1000 nm region and contributes a significant error to the signal beyond 800 nm.

Selection of an order-sorting (cut-on) filter to pass radiation of wavelength greater than about 600 nm, and rejection of radiation below that wavelength, would allow only first-order 600 nm to 1100 nm light to reach the detector, and produce a more accurate spectrum. This complicates the calibration and use of the array radiometer. Several (at least two) array spectral measurements are required, since the low wavelength data would have to be acquired without the filter in place, and the longer wavelength data with the filter in place. This requires a calibration (see Section 3.4 below) for the array radiometer with and without the filter in place, and a combination

15

of the two measured spectra to produce the final composite spectrum. Some array detectors are available with integral order-sorting filters deposited on the elements for detecting longer wavelengths.

The significantly different shapes of the calibration and measurement spectra, together with the problem of order sorting, further complicates the interpretation of the measured data. There is relatively low energy in the 300 to 600 nm region of the standard lamp spectrum. The contribution of the higher orders of shortwave radiation to the first-order longer wave radiation is completely different than in the case of the pulse simulator xenon source. Thus, the "calibration," without the use of order sorting, carries appropriate information only for sources with similar relative spectral distributions and not for any other unknown spectral distribution to be measured.

In addition to the above concerns, an understanding of the operation of this particular array radiometer is essential to obtaining meaningful data. A very simplified outline of the operation of the radiometer follows to illustrate the point.

The array used in the spectrograph is continually accumulating charge ("counts") as long as the instrument is running. An operational cycle is carried out continuously by the instrument. The cycle consists of accumulating charge for a "blanking time" of at least 6.84 ms, then "reading" the array by reading out (discharging) the array (so it does not eventually saturate) during the next 13.16 ms. The "blanking" time, or time of data acquisition, can be extended by the user. When light reaches the detector array, charge builds up in each array element over the 6.84 blank time, and is read out and processed during the 13.16 ms read time. Figure 3.4 is a diagram of this process compared to the duty cycle of a typical pulse simulator.
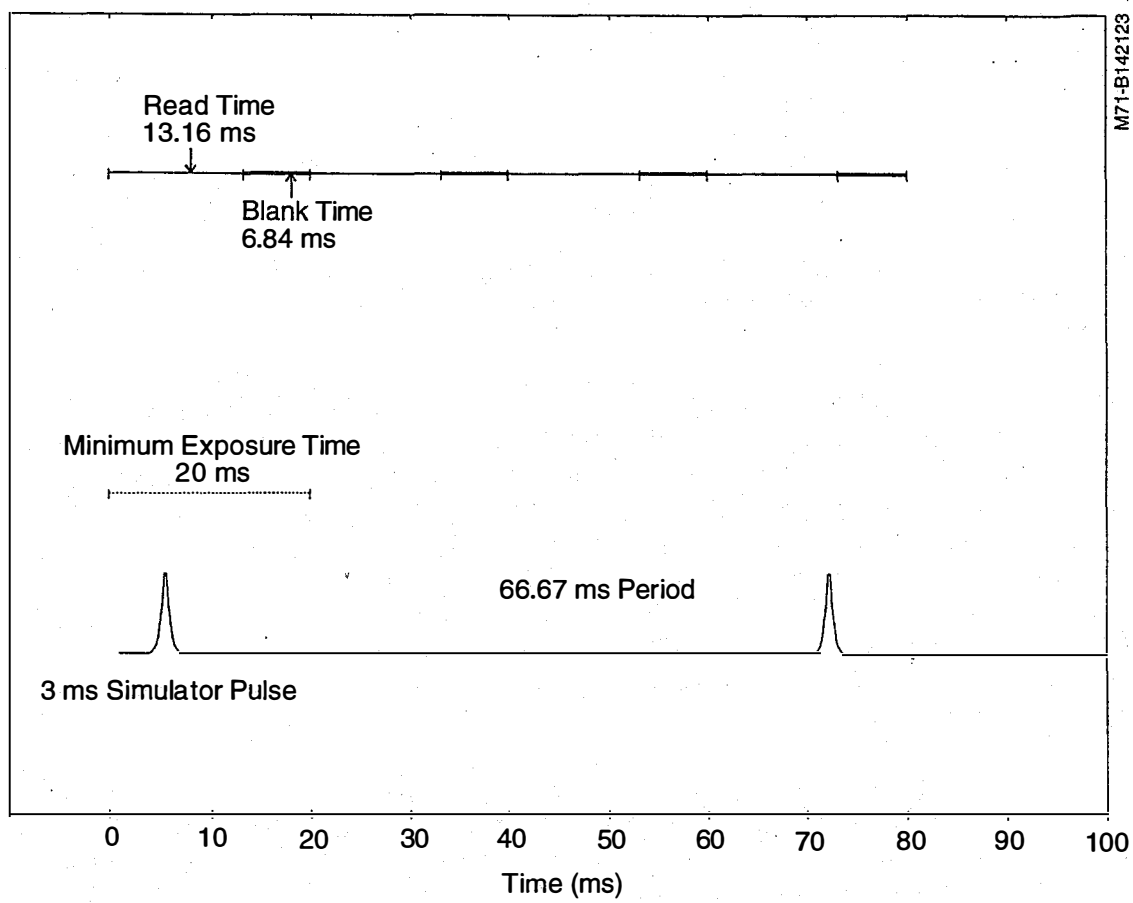
Figure 3.4. Timing diagram for array spectroradiometer data collection

16

During calibration, the standard source is on continuously, so charge accumulates during each (minimum) 8.64-ms blanking interval. During the measurement of a 3-ms pulse from the Spire 240A, charge only builds up over the short 3-ms period, which may or may not occur totally within the blanking interval. The temporal duration of the charge buildup must be accounted for in the two different situations in order to get easily interpreted measured spectra.

The array essentially produced a signal proportional to the *energy* seen during the blanking period. Without knowledge of the pulse shape and appropriate time synchronization between the pulse and the operational cycle of the array radiometer, only a portion, or none, of a pulse may be captured. Thus, the amplitude of the spectra could vary wildly as well.

These issues point out that though these instruments may be relatively inexpensive and easy to set up and use, compared with classical scanning grating instruments, attention to the details of their operation and knowledge of the principles behind the measurements are required to obtain meaningful data.

3.3 Spectroradiometric Detectors

The radiation that is collected by the input optics and sorted by the dispersion element of the spectroradiometric system finally is measured with the detector at the output side of the monochromator or disperser. Detector types range from photomultiplier tubes for photon counting and other low-level applications (such as in the ultraviolet region) to silicon and more complex sensitive materials, such as Mercury Cadmium Zinc Telluride (HgCdZnTe), Indium Gallium Arsenide (InGaAs), or Lead Sulfide (PbS), avalanche photodiodes (APD), photodiode arrays (PDA), charge-coupled devices (CCD), and Multi-Anode Microchannel Array (MAMA) detectors (Cole and Smeins, 1989). Each material or detector technology has its own spectral responsivity curve, and optimum region of usefulness.

The variation in spectral responsivity of a measurement system is a combination of the slit-scattering function, grating properties, and detector responsivity. In addition, the signal collection, processing techniques (chopped, or AC techniques, versus DC signal processing), and electronics may vary depending on detector signal-to-noise ratio, etc., and contribute to variations in the total system responsivity. Several detectors and/or grating combinations may be required to obtain spectral data over the entire spectral range of interest.

3.4 Spectroradiometric Standards and Calibrations

Calibration of spectroradiometric instrumentation is based on sources with known spectral distributions, and Equation 4, as described above. A known spectral distribution is measured with a system, and the response as a function of wavelength is compared with the response or signal when an unknown spectral distribution is scanned, using the ratio method of Equation 4.

Sources (lamps) of known spectral distribution are the calibration standards of spectral irradiance issued by various national standardizing laboratories, such as NIST in the United States, Physicalishes Technische Bureau (PTB) in Germany, the National Physical Laboratory (NPL) of Great Britain, etc. A long chain of intercomparisons, and conversions are performed by the standardizing laboratories to generate the lamps. The process is described in detail in NBS Special Publication 250-20, *Spectral Irradiance Calibrations*, by Walker et al.

Briefly, the spectral irradiance scale is derived from the spectral radiance scale (Walker, Saunders, and Hattenburg, 1987), which is based on the realization of the International Temperature Scale (ITS) (Waters, Walker, and Hattenburg, 1987), starting with a black body radiator at the freezing temperature of gold. The resulting scale is realized in a set of lamps maintained at NIST, and is transferred from those primary standard lamps to the 1000-watt lamps that are provided to the user, using a well-characterized, high-accuracy

spectroradiometric transfer system called FASCAL (Facility for Automated Spectroradiometric Calibrations), described in NBS 250-20. The resulting absolute uncertainty with respect to System Internationale (SI) units, as reported by NIST, is shown in Table 3.1. This process is also costly, resulting in lamps that cost approximately $8,500.00 (in 1996) and have a lifetime of 50 hours. Instructions for the use of spectral irradiance standard lamps are given in Appendix C.

Table 3.1. 1986 Spectral Irradiance Scale Transfer Uncertainty (3 σ)
(from Table V, NBS 250-20)

Wavelength (nm)	250	350	656.4	900	1300	1600	2000	2400
Uncertainty (percent)	2.23	1.35	1.01	1.34	1.42	1.89	3.29	6.51

In 1991 an international intercomparison of 12 national spectral irradiance scales, sponsored by the *Comite Consultatif de Photometrie et Radiometrie of the Comite International des Poids et Mesures* (Walker, et al., 1991) indicated the uncertainties in Table 3.1 may be somewhat optimistic, as the range of mean deviations from the NIST-derived values of several lamps at various wavelengths ranged from + 5% to -4% at 300 nm, from +2% to -1% at 600 nm, and +5% to -5% at 2000 nm. Twenty-one percent of the UV measurements (250 to 350 nm), 19% of the visible (400 nm to 800 nm), and 47% of the infrared (900 nm to 2400 nm) exceeded 1.1 times the NIST-quoted uncertainty.

NREL depends on both NIST-supplied lamps, and working standards derived by transfer from NIST lamps to secondary standard lamps for research and routine calibration work, plus the additional precision equipment (power supplies, shunts, meters) needed to operate the lamps as prescribed by NIST. Instructions for using the lamps are provided by NIST as described in Appendix C.

Figure 3.5 displays typical spectral irradiance standard lamp data as a curve with the error bars at each wavelength quoted above superimposed.

The uncertainty in a spectral calibration is a combination of the uncertainties due to the source (NIST uncertainty, current regulation, and distance measurements) and uncertainties in the instrumentation (such as wavelength accuracy, wavelength repeatability, detector temperature coefficients, control electronics, and software performance). The uncertainty of subsequent spectral measurements will be a combination of all of the calibration and instrumentation uncertainties. Note that the instrumentation-related uncertainties may be different in the measurement environment than in the calibration environment (i.e., outdoor versus laboratory measurements). See Myers (1989a) for details of the propagation of errors in a spectroradiometric measurement.

As a result of the propagation of errors through the calibration and measurement process, it is generally very difficult to obtain spectral data with uncertainties less than about 5.0% over most of the spectral range of interest to PV. In the ultraviolet and infrared parts of the spectrum, the uncertainty will be larger still, usually due to higher detector noise, calibration uncertainty, and the increasing need for detailed knowledge of the spectral responsivity function mentioned above.

3.5 NREL Spectroradiometer Calibrations

NREL spectroradiometric instrumentation and some pertinent specifications for each are listed in Table 3.2. These radiometers are used to measure solar simulator spectral distributions to compare with the American Society for Testing and Materials (ASTM) standard spectra E891/892, and to classify simulators according to ASTM standard specification E-927 *Solar Simulation for Terrestrial Photovoltaic Testing*. They are also used
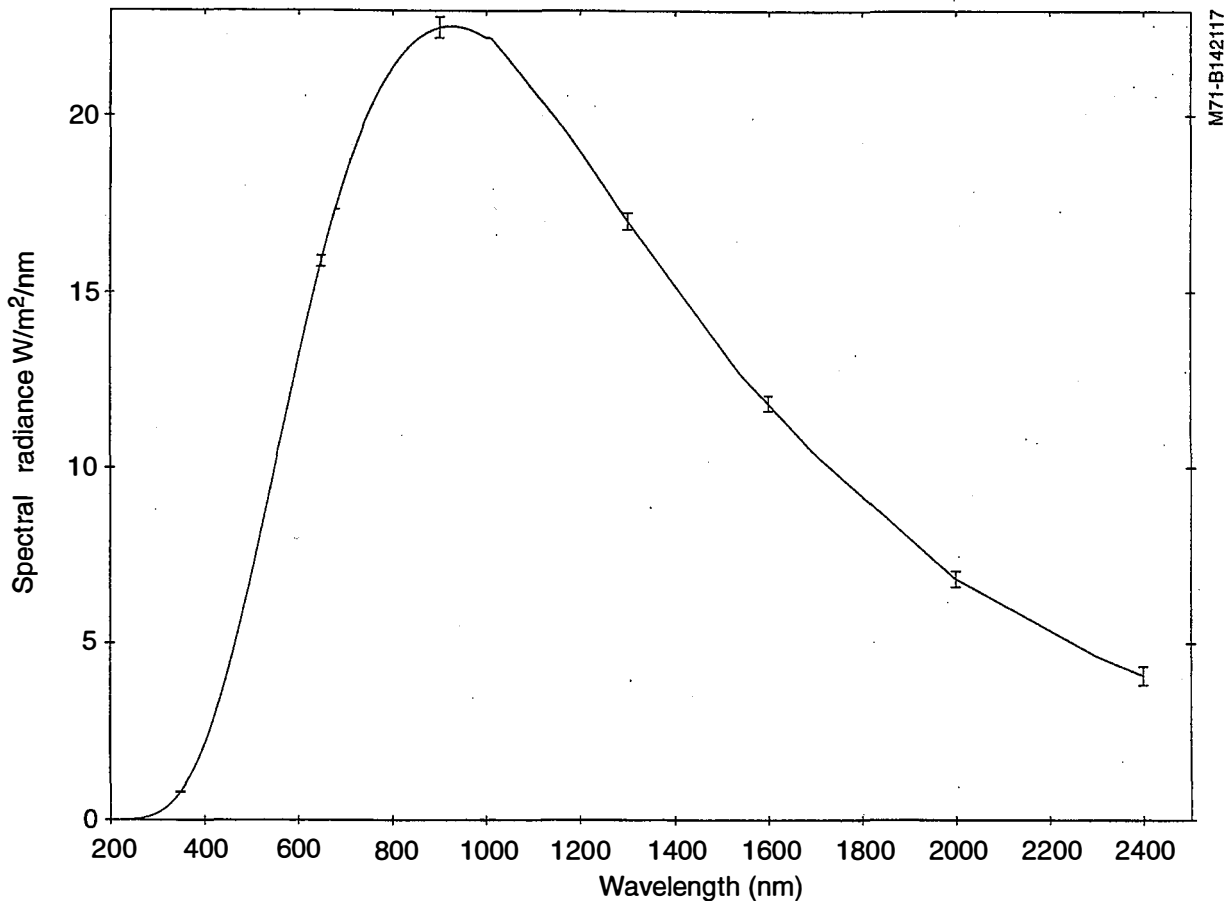
Figure 3.5. Standard of spectral irradiance lamp data with 3 σ error bars

to measure natural sunshine (outdoor spectra) during standardized outdoor module testing, and special experiments. See Appendix B for PV-related ASTM and some International Standards Organization (ISO) standards.

Table 3.2. NREL PV Spectroradiometric Systems

Instrument/System	Wavelength Region	Spectral Bandpass	Wavelength Accuracy
Licor LI-1800	300 nm-1100 nm	6 nm (1 mm slits) 3 nm (0.5 mm slits)	± 1.0 nm
Geophysical Environmental Research	300 nm-1800 nm	4 nm @ 500 nm to 8 nm @ 1800 nm	± 0.5 nm
Optronic Laboratories OL-750	180 nm-800 nm	2.5 nm (1.5 mm slits)	± 0.25 nm
Optronic Laboratories OL-746D	250 nm-2400 nm	2 nm (250 nm-000 nm) 5 nm (1000 nm-2400 nm)	± 0.25 nm
Optronic Laboratories OL-752	250 nm-2400 nm	2 nm (250 nm-1000 nm) 5 nm (1000 nm-2400 nm)	± 0.25 nm

To calibrate these radiometers, NREL uses 1000-watt standards of spectral irradiance purchased from the Radiometric Physics Division of the NIST.

NIST standard lamps are used only to provide primary calibrations to spectroradiometers which transfer calibration to working standard lamps. Working standard lamps are used for routine calibrations, unless the lower uncertainty of a calibration directly from the NIST standard lamp is necessary. Table 3.3 lists the equipment used to perform the calibration transfers. Included in the table are the uncertainties associated with each piece of equipment, which are needed to propagate uncertainty to the final statement of uncertainty during a rigorous uncertainty analysis.

In practice, a spectral calibration includes the following steps:

1. **Generate a calibration lamp data file.** Interpolate the NIST data sheet irradiance versus wavelength data to the appropriate wavelength interval (i.e., 1 nm steps if needed, or 10 nm steps if appropriate), converting, if need be, to the units desired (watt per square meter per nm, microwatt per square cm per micron, etc.).

   Note: Some spectroradiometer systems come with control software that allows the user to enter NIST data and generate the appropriate interpolated data files. For others, the interpolation must be done using custom software, and/or a text editor to generate the files. Either 3-point Lagrangian interpolation, cubic spline interpolation, or straightforward linear interpolation are acceptable, as any differences in the results are well within the uncertainty limits quoted for the raw data by NIST. There is also a NIST-recommended function fit described in the Instructions for use of spectral irradiance standards. NREL uses simple interpolation methods due to the uncertainty constraints mentioned earlier.

Table 3.3. NREL Spectroradiometer Calibration Equipment

Instrumentation	Application	Total Estimated Uncertainty	Estimated Radiometric Uncertainty
Standard lamp power supply	8.0 amps @ 110 V DC for lamp	± 0.01% current regulation	±0.1%
0.01 Ω shunt resistor	Monitor lamp current @ 8 amps, 110 V DC	± 1 part per million 0.000001Ω/0.01Ω or 0.01%	±0.1%
6-1/2 digit voltmeter	Readout lamp current (voltage drop across shunt)	±0.01% DC V @ 80 mV (0.08 V)	±0.1%
Optical bench and laboratory jack supports	Mount and align source and radiometer	±10° azimuth ±3 mm height	N/A
50-cm calibration distance spacer	Set distance from lamp current carrying pins to radiometer input optic (calibration plane)	±2 mm distance 0.4% of 500 mm	±0.8%
NIST 1000-watt calibration lamp	Radiometric source	±2.0% @250 nm ±1.0% @600 nm ±1.5% @900 nm ±3.0% @2000 nm	±2.0% @250 nm ±1.0% @600 nm ±1.5% @900 nm ±3.0% @2000 nm

2. **Store (enter, upload, or otherwise save) the calibration lamp data file** in the appropriate form for use by the radiometer system (i.e., it is uploaded to the Li-Cor on-board ROM memory, or stored as a *.STD file for use with the Optronics systems).

3. **Set up the radiometer** with the appropriate interconnections between input optics, dispersion unit, detector, and control unit or computer.

4. **Install the calibration lamp** to be used in the kinematic mount, with label/faceplate facing <u>opposite</u> the radiometer input optics. Observe the polarity markings on the lamp and the mounting.

5. **Set the 50-cm calibration distance** using a template bar with the cut-out end against the <u>lowest</u> part of the lamp envelope (to avoid scratching the central part of the envelope), use laboratory jacks to bring the input optic of the radiometer to the 50-cm calibration distance (flat end of the template) from the lamp. The template is designed to set the 50-cm calibration distance from the <u>plane tangent to the front surface of the pins</u> carrying the current to the lamp filament to the plane of the input optic.

6. **Adjust the height of center of the input optic** to as close as possible (within a few millimeters) to the height of the central part of the lamp filament.

7. **Insert the 3-panel radiation shield/baffle**, adjusted so the cut-out rectangle center is within 2-3 millimeters of the height of the central portion of the lamp filament and the central portion of the input optic, at about 25 cm from the lamp. The distance is not critical.

8. **Connect the lamp to the power source.** Attach the current-carrying leads to the power supply, in series with the four-terminal 0.01 ohm shunt resistor. Make sure the current flows through the "C," or current carrying, terminals, and <u>not</u> the "P" or potential terminals.

9. **Connect the potential terminals of the shunt resistor** to the DC voltage input terminals of the monitoring voltmeter.

10. **Power up the digital voltmeter**, after verifying all connections are correct and snug, power on the monitoring voltmeter and verify that the reading is within 5 nanovolts of zero.

11. **Power up the lamp power supply.** When ready to energize the lamp, program the appropriate current (usually 8.3 amperes), and toggle the lamp ON.

    NOTE: The lamps are run on DC power to eliminate "flicker" in the irradiance and to prevent crystallization of the filament. The current is ramped upwards slowly to avoid stressing the filament. (Ninety percent of the time when ordinary lamps burn out, it is at turn-on when the current rushes through the filament, shocking it thermally.)

Figure 3.6 is a photograph of a typical NREL spectroradiometric calibration in progress, showing the calibration lamp, baffles for allowing only the radiation from the lamp, and not extraneous reflected radiation to enter the input optic aperture.

12. **Prepare spectroradiometer to scan.** Using the software provided with the system, the preparations for performing the calibration scan are made. This includes selecting the calibration lamp data file, setting scan parameters, and issuing initialization commands to the hardware.
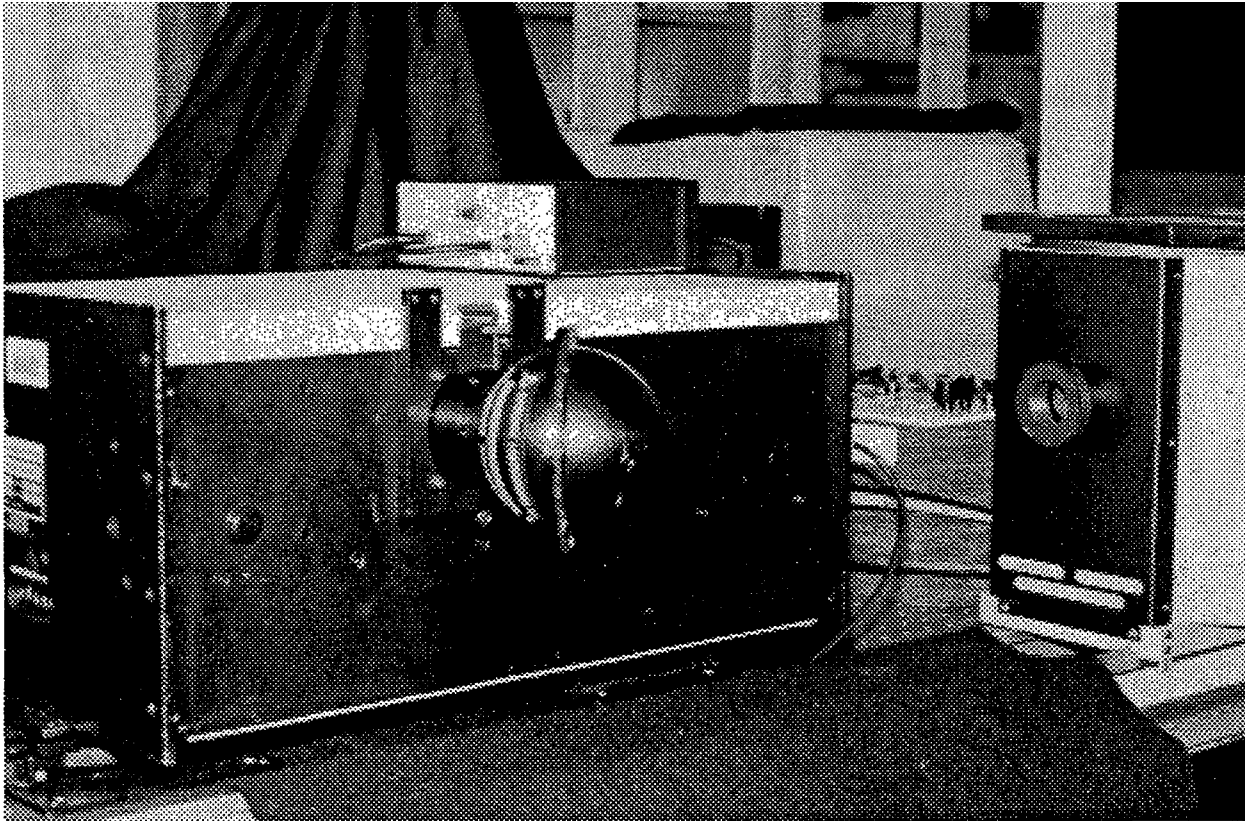
Figure 3.6. Photograph of NREL spectroradiometric calibration

13. **Issue the command(s) to perform the calibration scan.** Start the hardware scan and data acquisition process for the spectroradiometer.

14. ` **Save the calibration file and or data to disk.** Note, this may involve downloading data from on-board random access memory, or saving data stored in the computer controller memory.

At this point, the process of generating a calibration file for use with a specific system is complete. From this point on, quality assurance procedures are performed as follows:

(1)   The new calibration is compared with previous calibrations to establish whether major systematic changes are apparent, or have occurred, and to contribute information on the random and systematic uncertainties in the calibration and measurement system. Figure 3.7 illustrates relative changes between calibrations over a six month period for a Li-Cor Li-1800 spectroradiometer. The plot is the ratio of the newer calibration to the older.

(2)   Calibration information (source, date, and results) is archived as part of the instrument history, especially in case historical data needs "rehabilitation" in the future.
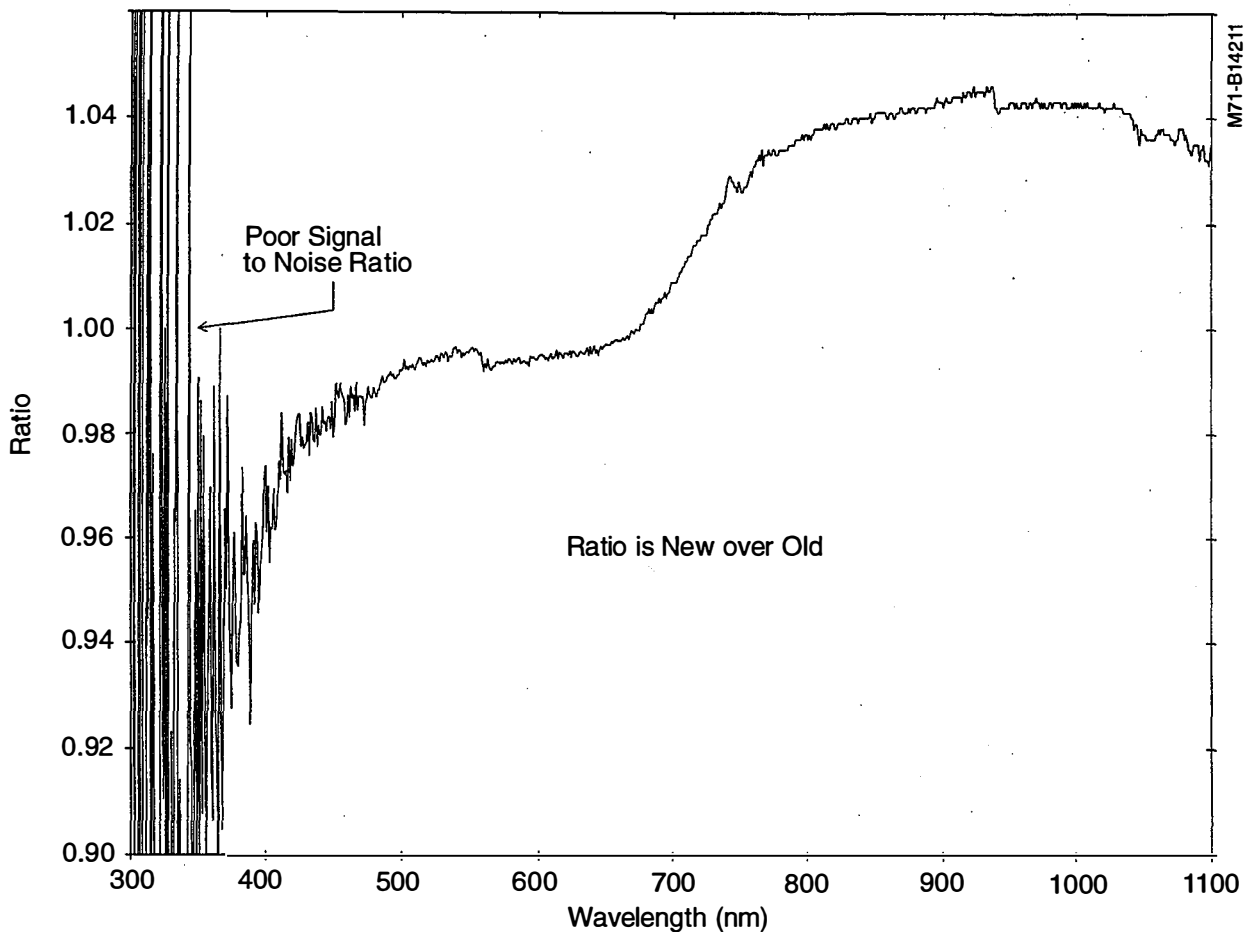
Figure 3.7 Ratio of calibration files taken six months apart for an NREL spectroradioemeter

(3) Calibration verification and "sanity" checks are made, such as test measurements of sources (solar simulators, other lamps) with previously determined and known spectral distributions, using the new (and possibly old) calibration files. These tests include scans of lamps containing material with emission at specific wavelengths, to check the wavelength calibration of the dispersive element. Figure 3.8 illustrates a wavelength calibration check scan. Distorted measurements of known sources can indicate problems with stray light in the calibration setup, light leaks or improper operation of instrumentation, detector instability, etc.

Figure 3.9 illustrates how the distorted shape in a scan of an incandescent lamp made stray light problems in a calibration setup apparent. The apparent shift in the distribution occurs because no baffle was in place between the lamp and the spectroradiometer input optic, so excess radiation (scattered and reflected from surrounding surfaces) reached the input optic during calibration. Only the optical radiation emitted by the lamp filament is considered to contribute to the flux density at the calibration plane.

(4) The calibration results, file names, and special considerations or observations noted are recorded in written documentation (memos to file, specifically for the NREL Metrology Center).
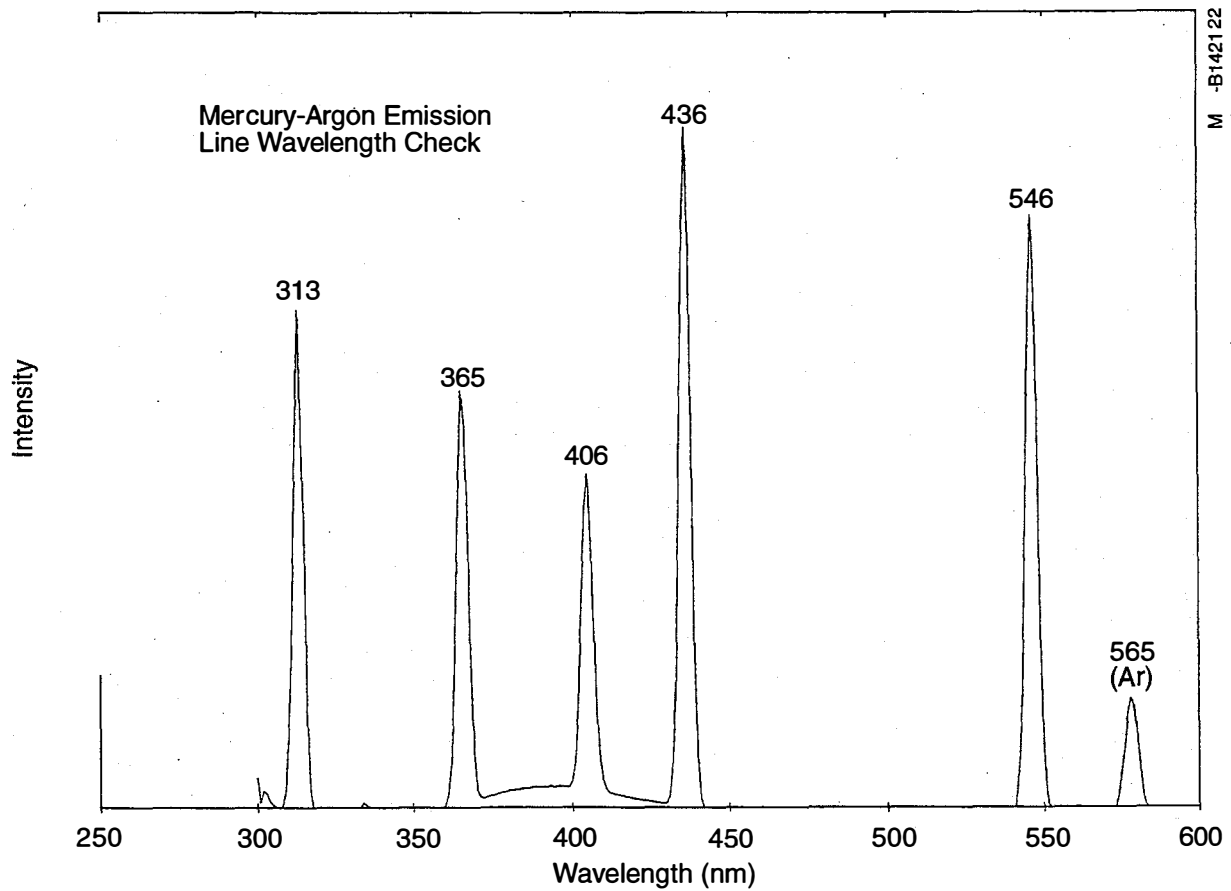
Figure 3.8. **Emission spectrum for Mercury-Argon lamp showing lines used for wavelength calibration**

With the completion of a calibration, the spectroradiometer systems are ready to measure and check unknown sources, perform outdoor measurements, continue monitoring of fixed indoor sources, or monitor the relative spectral effects of changes made to sources. In the process of performing the spectral measurements, one must think carefully about what is measured, as well as what is desired as the measurement, so that the needs of the research are met as closely as possible. The measurement performed must be evaluated with respect to the desired true value in the light of instrument and operator capability, and the possible sources of uncertainty that could contribute to errors in the measurements, and their interpretation.

The next section addresses the main application of spectroradiometric measurements within the PV community, namely the measurements of natural and simulated solar radiation for derivation of spectral mismatch correction factors.
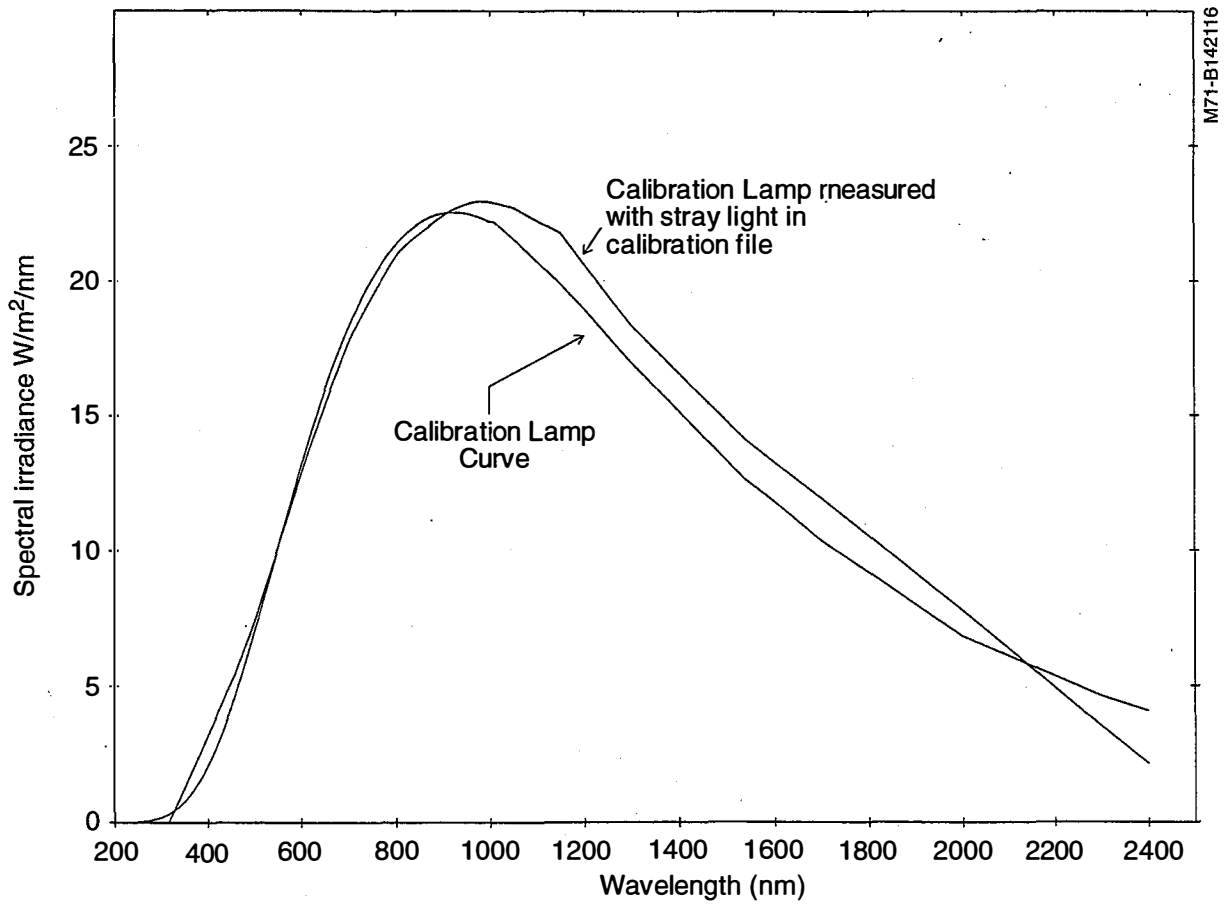
Figure 3.9. **Distorted spectral distribution for an incandescent lamp as the result of excess (reflected) radiation reaching an input optic during calibration**

4.0 SPECTRORADIOMETRIC APPLICATIONS TO PV

4.1 Solar Simulator Ratings and Spectral Mismatch

Because of the variability in spectral response of the various photovoltaic materials, as well as the wide variation in the spectral distributions resulting from a wide variety of laboratory light sources (lamps, solar simulators), and the range of variation in the spectral distribution of natural sunlight, it can be difficult to fairly compare or evaluate the performance of different (or even similar) photovoltaic devices. The photovoltaic community has worked to establish and use a consensus reference standard spectra and a solar simulator rating standard that can be used to provide a common basis for reporting performance.

Reference standard spectra were initially developed as separate standards for direct normal spectral irradiance, ASTM E-891, and global irradiance on a 37° south-facing tilted surface, ASTM E-892. These standards were developed and in use from 1987 until 1995. As of 1996, these standards were combined into a new, consolidated standard, *Standard Tables for Reference Solar Spectral Irradiance at Air Mass 1.5: Direct Normal and Hemispherical for a 37° Tilted Surface*. These fixed spectral distributions are the result of combining measured extraterrestrial spectra and modeled atmospheric effects to produce the spectra. These relatively arbitrary spectra are merely agreed upon distributions to which performance can be related, translated to, or corrected to. They have no other special meaning or significance.

The performance classification of solar simulators is described in terms of how closely the spectral distributions approach those of the standard spectra, and several other parameters, in *Standard Specification for Solar Simulators Used for Terrestrial Photovoltaic Testing* (ASTM E-927). Rather than a point-by-point comparison of the spectra, integrals over six specified bands of 100 nm to 200 nm width for the simulator are compared with those for the reference spectrum. In addition, the temporal stability, amount of the total radiation within a 30° field of view, and spatial uniformity are evaluated to classify the simulator as "Class A" (smallest departure from standard) to "Class C" (greatest departure from the standard), with "Class B" between the two. As mentioned in the standard, the "choice of the class of a solar simulator should be based on the needs of that particular measurement." For instance, the spectral agreement with the standard is not important if the simulator is used to sort production cells by voltage or current.

The means of translating and correcting to the standard spectral conditions mentioned above is prescribed in another standard, the *Standard Test Method for Determination of the Spectral Mismatch Parameter Between a Photovoltaic Device and a Photovoltaic Reference Cell* (ASTM E-971). To accurately determine a performance parameter for either a PV reference cell (or module) or a PV test cell (or module) measured under a test spectrum, knowledge of the reference spectrum, the spectral response of the reference and test devices, and spectrum of the test source, measured with a spectroradiometer, are used to compute the spectral mismatch correction factor, M. The performance parameter of the cell under test is divided by M. The equation for M, based on the reference spectral distribution, $E_o(\lambda)$; test spectral distribution, $E(\lambda)$; the reference device spectral response, $Rr(\lambda)$; and the test device spectral response, $R_t(\lambda)$ is:

$$M = \frac{\int_{\lambda_1}^{\lambda_2} E(\lambda)\, R_t(\lambda)\, d\lambda}{\int_{\lambda_3}^{\lambda_4} E(\lambda)\, R_r(\lambda)\, d\lambda} \cdot \frac{\int_{\lambda_3}^{\lambda_4} E_o(\lambda)\, R_r(\lambda)\, d\lambda}{\int_{\lambda_1}^{\lambda_2} E_o(\lambda)\, R_t(\lambda)\, d\lambda} \qquad (5)$$

where λ_1 and λ_2 correspond to the wavelength limits of the test device spectral response, and λ_3 and λ_4 to the wavelength limits of the reference device spectral response. Note that the $E_o(\lambda)$ is the reference spectrum tabulated in the standards.

26

Different digital integration algorithms will produce different integrals, and thus different M factors. The linear-trapezoid method is used at NREL. The response and test spectra data are computed using linear interpolation, if needed, at each wavelength of the reference spectrum, and trapezoid rule integration of the resulting curves is performed. See Myers, Cannon, and Trudell, (1995) pp. 182-183.

As an example of an application and use of the spectral mismatch correction factor, assume we wish to know the short-circuit current of a cadmium indium diselenide test cell under the global air mass 1.5 reference spectrum. We will use two sources to evaluate the CIS cell: a xenon arc simulator, and a 1000-watt incandescent tungsten-halogen lamp. As a reference, we will use an amorphous silicon reference cell.

The silicon reference cell will indicate the magnitude of the incident energy from each source through the reference cell's measured short-circuit current. We then measure the short-circuit current of the CIS device under each source. Figure 4.1 shows the spectral distribution of the global reference spectrum and the xenon arc source, with the spectral response curves of the CIS and silicon (Si) cells superimposed.
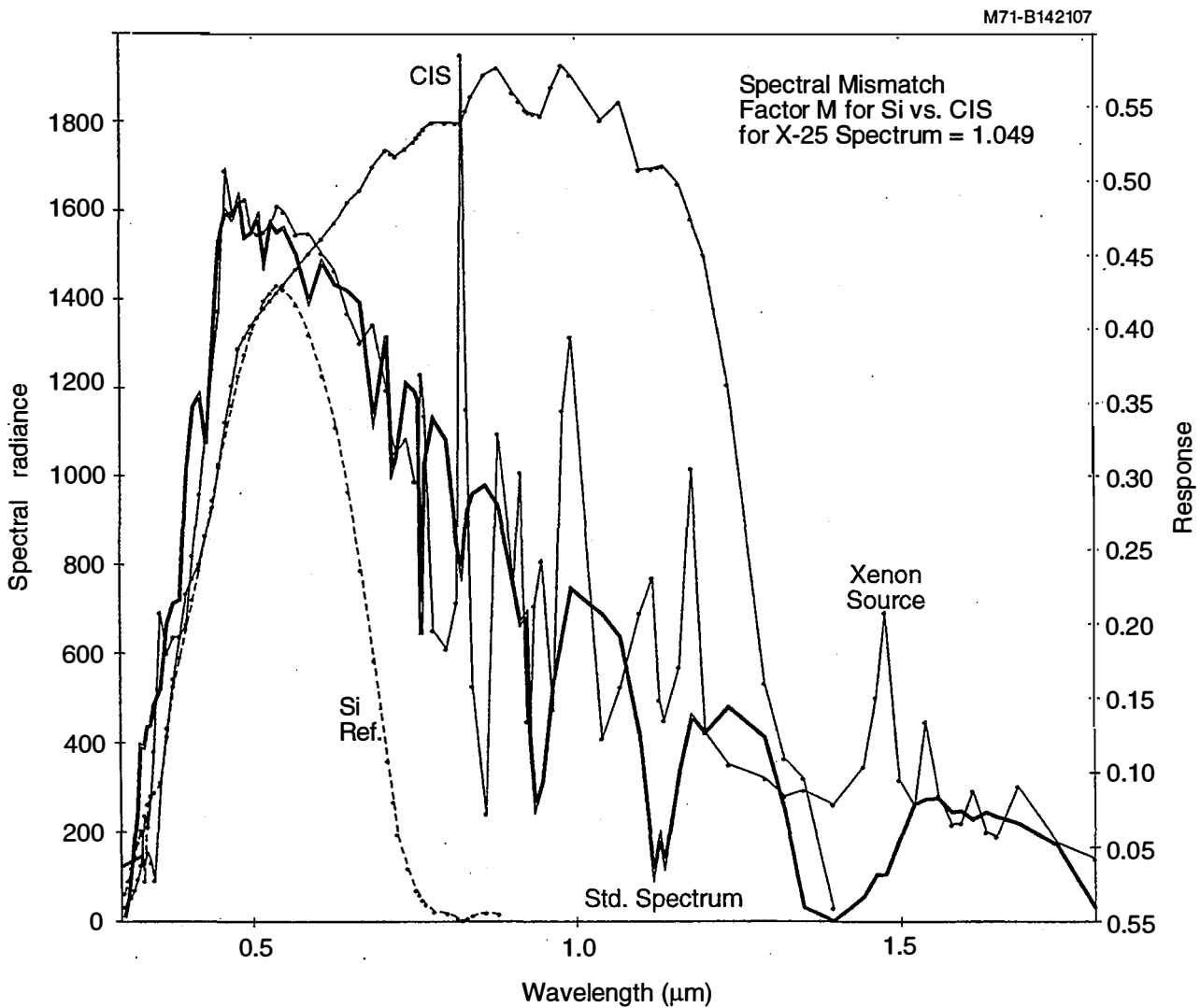
Figure 4.1. Spectral distribution of xenon source, ASTM E-892 global spectrum, and spectral responses of CIS and Si cells for spectral mismatch computation

It should be apparent that the CIS device will respond to much of the infrared part of the spectrum, where the Si device will not. From the absolute spectral responses (right-hand scale) it is apparent that more current would be generated by the CIS device if the spectra were uniform over the response regions. However, the falling intensity of the spectra over the region of the CIS peak response will reduce the "current excess" with respect to the Si device. The mismatch computation quantifies the relative contributions to each device's current, and allows them to be compared equitably.

Let $R_c(\lambda)$ and $R_s(\lambda)$ be the spectral response functions of the CIS and Si device as functions of the wavelength λ. Let $E_o(\lambda)$ and $E_x(\lambda)$ be the spectral distributions of the global reference spectrum and the xenon lamp, respectively. From the tabulated data that were used to generate the graph in Figure 1, we perform a linear interpolation of the spectral response data (measured) and the xenon spectrum (measured) at the wavelengths given in the global reference spectrum table. We then compute the trapezoid rule integrals on the tabular data to form the mismatch integrals in the equation

$$M = \frac{\int_{0.3}^{1.4} E_x(\lambda)\, R_c(\lambda)\, d\lambda}{\int_{0.3}^{0.85} E_x(\lambda)\, R_s(\lambda)\, d\lambda} \cdot \frac{\int_{0.3}^{0.85} E_o(\lambda)\, R_s(\lambda)\, d\lambda}{\int_{0.3}^{1.4} E_o(\lambda)\, R_c(\lambda)\, d\lambda} \tag{6}$$

and obtain the following numerical results:

$$M = \frac{\int_{0.3}^{1.4} E_x R_c\, d\lambda - 406.74}{\int_{0.3}^{0.85} E_x R_s\, d\lambda - 155.67} \cdot \frac{\int_{0.3}^{0.85} E_o R_s\, d\lambda - 155.9}{\int_{0.3}^{1.4} E_o R_c\, d\lambda - 388.03} = 1.049 \tag{7}$$

This means that if the silicon device is used to set the xenon source so that the Si device generates the short-circuit current it would under the reference spectrum, the CIS device will produce about 5% more current than it should under the reference spectrum. That is, setting the xenon source with the Si reference device, the CIS device current under that source must be divided by 1.049, to obtain the current which would be seen if the CIS device were under the reference spectrum.

Now let us do the same computation, using a 1000-watt incandescent tungsten-halogen lamp as the test source to compare the two devices. The spectral irradiances and spectral response data are shown in Figure 4.2.

Note that the left-hand integrals will remain the same as in Equation 2, since the spectral responses and the reference spectrum, E_o, remain the same. E_x now is the spectral distribution of the incandescent lamp. Computing the integrals as before, we obtain:

$$M = \frac{\int_{0.3}^{1.4} E_x R_c\, d\lambda - 82.55}{\int_{0.3}^{0.85} E_x R_s\, d\lambda - 11.55} \cdot \frac{\int_{0.3}^{0.85} E_o R_s\, d\lambda - 155.9}{\int_{0.3}^{1.4} E_o R_c\, d\lambda - 388.03} = 2.872 \tag{8}$$

As opposed to the 5% difference, or spectral error, computed for the xenon simulator, in this case the error is almost 300%. This much larger spectral error is due to the fact that the incandescent lamp spectrum peaks in the near infrared at 900 nm, near the peak of the CIS device response. In addition, the lamp spectrum is very weak where the Si device responds best, around 500 nm.
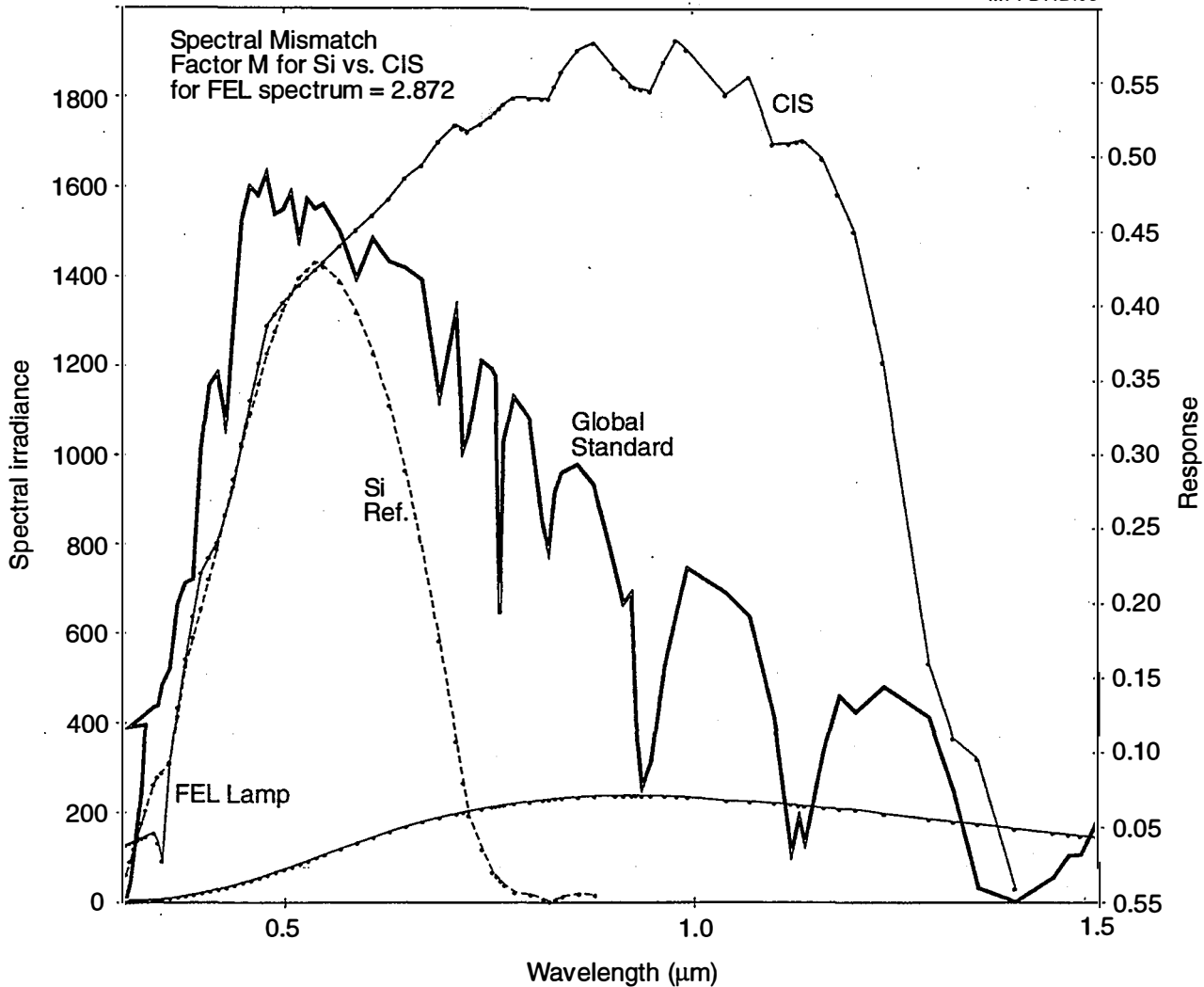
Figure 4.2. Spectral response and spectral irradiance curves for incandescent lamp source

The direct comparison of the currents from the two devices under the incandescent lamp (FEL) spectrum will be misleading, if we assume the same relationship will hold true under the reference spectrum. If the ratio of the CIS current, I_c, to the Si current, I_s, in the incandescent lamp case is I_c/I_s, the ratio under the reference spectrum would be { $I_c/(2.87)$ }/I_s.

Measurements of the spectral distribution of light sources used in testing (the **E** terms above) as well as for stimuli for the spectral response functions (the **R** terms above) require application of both spectral and broadband measurements and calibrations. As described by Field (1995), the measurement of spectral response can be accomplished using either bandpass filters or a monochromator to select the wavelengths of interest. In either case, the radiant power at the location of the test plane must be known (measured) for each wavelength interval of interest. This can be done using a broadband thermal or pyroelectric detector, a spectral measurement, or a calibrated semiconductor detector which responds well in the wavelength region of interest. Examples in the Field (1995) paper also illustrate how errors of gross magnitude (10% or more) can occur, and be corrected for by proper application of the spectral mismatch correction factor.

4.2 Primary Reference Cell Calibrations and Use

Primary PV reference cells are used to evaluate and verify (usually in side-by-side comparisons, or substitution) the performance of new cells, cell production lines, and PV modules and systems, in either the laboratory or outdoors. These highly characterized solar cells are usually defined as PV devices calibrated in natural sunlight, where the calibration is the determination of the ratio I_{sc}/I_{tot} of the short circuit-current (I_{sc}) of the device to the total irradiance (I_{tot}) when illuminated by a specified reference spectrum (terrestrial global, direct, or extraterrestrial) at a given temperature.

This ratio is known as the calibration number, CN. Computing CN requires accurate measurement of the cell temperature, electrical parameters, spectral response, the source (solar) spectral distribution(s), and the total irradiance on the cell. Since the natural solar source spectra are not likely to match the reference spectra, the spectral mismatch correction factor described in the previous section is used to modify the short-circuit current, and the CN. This methodology, its history, and uncertainty analysis on the techniques have been documented extensively by Emery et al. (1985,1988), Emery and Osterwald (1989), Emery et al. (1989), Osterwald et al. (1990), and Emery and Osterwald (1990). This method will be referred to as the "NREL" method.

The NREL method depends on natural solar direct beam irradiance measurements and testing, because of the improved accuracy (lower uncertainty) which can be attained. Test methods using the global irradiance have been tested, but found to be less accurate, as described in Emery et al. (1989). This method will be referred to as the "global" method.

Accurate knowledge of the test spectrum is needed to compute a calibration number. An alternative method of developing primary reference solar cells uses well-characterized laboratory lamps as the illuminating sources. This approach was used at Sandia National Laboratories by King, Hansen, and Jackson, (1993). Field and Emery (1993) compared this method, referred to as the "Sandia" method, with the NREL method. The next section describes the recent history of the calibration of terrestrial PV reference cells, introducing parameters affecting their characterization.

4.2.1 Early Terrestrial PV Cell Calibration Procedures

Procedures and measurement techniques to perform PV reference cell calibrations and outdoor module performance measurements evolved out of methodology developed by the National Aeronautics and Space Administration (NASA) in conjunction with the Energy Research and Development Administration (ERDA, now the U.S. Department of Energy).

The ERDA terrestrial PV program defined a set of reference atmospheric and spectral conditions after the 1976 Terrestrial PV Measurements Workshop at Baton Rouge, LA (NASA 1976), under which primary PV reference cells would be generated. NASA Lewis Research Center at Cleveland, OH, provided the reference cells required by the PV community.

NASA Lewis performed outdoor calibrations at a site with naturally occurring conditions close to agreed-upon specified reference conditions (see below). Calibrations occurred at sites on the west coast of Florida from 1976 until 1981, when primary reference cell calibrations were made the responsibility of the Solar Energy Research Institute (SERI), now NREL. The NASA Lewis procedures monitored direct solar irradiance with a pyrheliometer and atmospheric parameters that affect the terrestrial solar spectral distribution with a sunphotometer.

A sunphotometer is a filter spectroradiometer with a few narrow bandpass filters with center wavelengths (peak transmission) at the center of absorption or scattering features in the solar spectrum (such as the 942 nm water vapor absorption band, and the ozone absorption band at 362 nm) and a complementary set of filters in nearby

atmospheric transmission windows (such as 862 nm and 380 nm) with little absorption. The ratio of the signals at absorption centers to signals in transparent regions are indicators of the relative amounts of absorbers and scattering centers or turbidity of the atmosphere, and are used to estimate the solar spectral distribution. Angstrom (1961) described the power dependence of turbidity on wavelength:

$$\tau = \beta \cdot \lambda^{-\alpha} \tag{9}$$

where β is Angstrom's turbidity coefficient, representing an index of the amount of aerosols in the atmosphere. β varies from 0 to 0.5 as the amount of aerosols increases from a clear to a turbid condition. α is related to the size distribution of the aerosols, and varies from 0 for particles much larger than λ, to -4 for very small particles. Angstrom computed an average value of -1.3 for β. α and β can be determined experimentally by measurements at two different wavelengths, generally 380 nm and 500 nm, where molecular absorption is minimal.

Filter sunphotometers generate a signal proportional to the irradiance at the wavelength of interest. It is generally the case that atmospheric extinction of the extraterrestrial irradiance, I_o, increases exponentially with air mass, M, resulting in the irradiance at the ground, I_g, given as $I_g=I_o e^{-\tau M}$. This expression is known as Beer's or Bouger's law.

Plotting the logarithm of the ratio of the single wavelength signal (irradiance) to the extraterrestrial irradiance at that wavelength as a function of the air mass (amount of absorber) generally results in a straight line (known as a "Langley plot", after S. P. Langley) as long as atmospheric conditions are stable during the period of varying air mass. The clear day zero-air-mass-intercept of the line from least squares regression fit to the data results in the extraterrestrial irradiance, and the negative of the slope of the fitted line results in τ for the wavelength. Frohlich and Shaw (1980) give an overview of the techniques and analysis.

In addition to aerosols, there are other important absorbers and scattering centers in the atmosphere such as water vapor and ozone (as well as molecular scattering, not treated by NASA) not included in the above discussion, but obtainable from sunphotometer data as described above. These constituted the parameters defining spectral conditions.

NASA conducted outdoor measurements under "clear" skies (no clouds within 15° of the sun) with solar direct beam irradiance between 750 watt/m² and 900 watt/m² optical air mass between 1.0 and 2.0 atmospheric turbidity less than 0.25, cell temperatures at 28 °C ± 2 °C. Cell current was to be stable within ±0.5% over a 30-second period, and measured across a 0.1% precision shunt resistor, with a voltage of less than 20 millivolts across the cell.

Measurements were then adjusted to Standard Reporting Conditions (SRC) using equations developed by Sandstrom (1967). A direct normal spectral distribution for use in "theoretical calculations" related to these calibrations was provided, derived by Thekaekara (1973), based on the Labs and Neckel AM0, assuming the following parameters (NASA, 1976):

Precipitable Water (total column cm) 2.00
Turbidity (@ 500 nm 0.12
        Angstrom alpha coefficient 1.30
        Angstrom beta coefficient 0.12
Air Mass 1.50
Ozone (total column cm) 0.34

Indoor PV cell calibration techniques were described in the NASA procedures, but always with comparison to reference PV cells calibrated outdoors, and with reference cells representative of the test cell technology. Only the total irradiance from 3 allowable types of solar simulators (short-arc Xenon lamps, long-arc pulsed xenon

31

lamps, and dichroic filtered incandescent lamps of American National Standards Institute ([ANSI] type ELH), as indicated by the short-circuit current of PV reference cells, were specified. No spectral information or measurements were required of the illumination sources.

4.2.2 The NREL Direct Normal Method

In 1984, responsibility for calibrating and maintaining reference cells for the terrestrial PV community was assigned to the Solar Energy Research Institute (SERI), now NREL. Researchers from NASA, NREL, and the PV industry devised more detailed and rigorous outdoor and indoor calibration techniques with the goal of 1) reducing measurement uncertainties, and 2) developing procedures that were site independent. These efforts eventually contributed significantly to the consensus standards developed for terrestrial PV reference cell calibrations and measurements. Osterwald, et al. (1990) describe the NREL method.

PV reference cells are mounted on a temperature-controlled plate, maintained at 25°C ±0.5°C., measured with a 4-wire, platinum resistance thermometer. View-limiting tubes restrict the field of view (FOV) of the cells to a solid angle of 5°, to match the FOV of an absolute-cavity radiometer for broadband direct normal irradiance measurement, and the FOV of a scanning spectroradiometer with a view-limiting tube mounted over the optical input. Short-circuit currents are measured with a 4-terminal technique across precision 1.0 Ω resistors with individual calibrated values known to 10-20 parts per million (ppm). All measurements, including I_{sc}, total direct normal irradiance, spectral irradiance, and temperatures are accomplished during a 30-second measurement period with an automated data acquisition system. Figure 4.3 is a block diagram of the measurement system, adapted from Osterwald, et al. (1990).
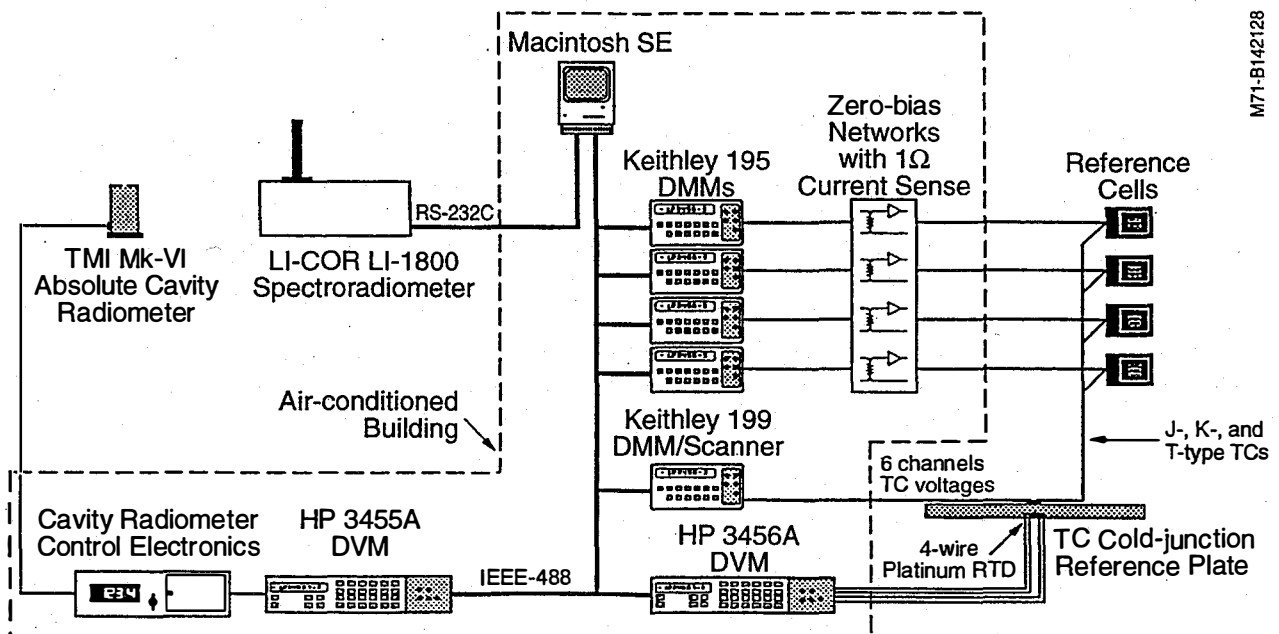
Figure 4.3. Block diagram of NREL reference cell calibration measurement system

32

Stringent criteria are used to accept or reject calibration data. The standard deviation of the derived calibration numbers (after modelled extension of the 300 nm to 1100 nm measured spectrum to 4000 nm and spectral mismatch correction) must be less than the standard deviation of the measured I_{sc}. The range of short-circuit currents should be less than 0.3% of the mean value of the I_{sc}, and the variation in the measured direct normal (cavity radiometer) direct beam must be less than 750 ppm (or 0.75 watts/m²). The integral of the extended spectrum is checked against the cavity pyrheliometer measurement of the total direct beam measurement.

Spectral responses are measured as described in ASTM E-1021, *Standard Test Method for Measuring Spectral Response of Photovoltaic Cells*, and in general by Field (1995). Cell temperature responses are measured under a solar simulator while varying the temperature of a plate with large thermal mass to which the cell is mounted. Detailed procedures for measuring electrical parameters can be found in ASTM E-948, *Standard Test Methods for Electrical Performance of Non-Concentrator Terrestrial Photovoltaic Cells using Reference Cells*. A typical NREL spectral response report is shown in Figure 4.4.

Sample: ARCO 150576   Temperature = 25.0° C
May 23, 1995 11:11 AM   Device Area = 100.0 cm²

NREL Filter QE System

Light Bias = 100.000 mA
bias Voltage = 0.00 V
RS-08 w/expanded beam corrected @ vacuum plate
J_{sc} = 34.97 mA/cm² for ASTME 892 Global (1000 W/m²)
Spectrum)
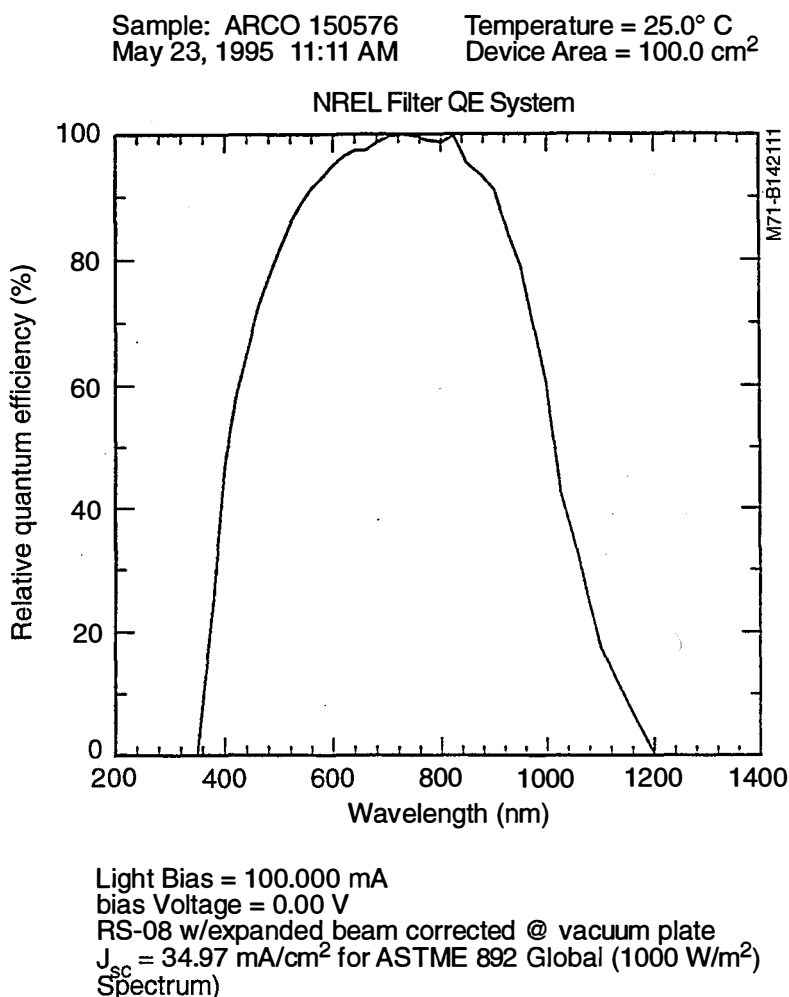
Figure 4.4. NREL sample spectral response report

Several efforts at uncertainty analysis for this technique have resulted in total uncertainty estimates of 0.5% bias and 0.3% random sources of error for a total uncertainty of $\pm 1.0\%$ in the tabular calibration method (Emery et al., 1989; Emery and Osterwald, 1989). Calibration checks of NASA Lewis Air Mass Zero (AM0) reference cells (calibrated through aircraft and balloon flights, using a Langley plot technique evaluating the variation of I_{sc} vs. air mass) against NREL terrestrial techniques resulted in agreement of better than 0.7% (Emery et al., 1988). A study of the sources of error and uncertainty in the spectral mismatch correction factor itself (which contains errors in spectral response and spectral distribution data) is discussed in Field and Emery (1993). They conclude that this element in the NREL process contributes about 0.33% to the total uncertainty in an outdoor PV reference cell calibration.

4.2.3 Sandia Laboratory Method

An alternative method of calibrating PV reference cells developed by Sandia National Laboratories in conjunction with the National Institute of Standards and Technology is based on using incandescent lamps with well-characterized spectral distributions as the test source illuminating the reference cell. The method, along with an uncertainty analysis, is described in King, Hansen, and Jackson (1993). Figure 4.5 schematically illustrates the setup using a standard spectral irradiance source to illuminate the reference cell being calibrated.

Some of the issues associated with this method include the determination of the correct "calibration distance" between the device and the lamp. An error of only 1 mm out of the 500-mm calibration distance can result in irradiance errors of 0.4% in the irradiance. The glass-to-cell distance is typically of this magnitude, as is the thickness of the cover glass (approximately 1.3 mm). In addition, the index of refraction, assumed to be approximately 1.46, should be known in order to correct the I_{sc} to the measured value to arrive at the final value.
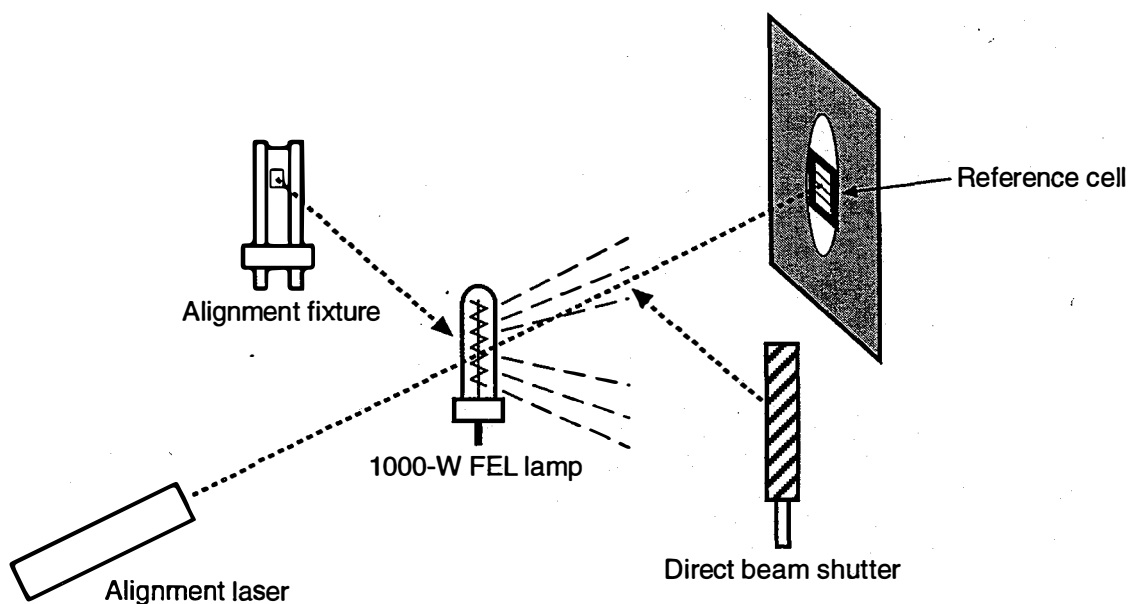
Figure 4.5. Schematic of equipment used for Sandia/NIST calibration procedure

This method relies on the accuracy of the irradiance standard lamp spectral distribution, and mismatch calculations, again involving spectral response functions for the reference cell, to compute the calibration number for the PV reference cells. One assumption made in the process is that the "calibration spectrum is itself a standard and known accurately." Even though a standard reference artifact itself, the lamp's spectrum *has uncertainty associated with it that results in uncertainty in the computed total irradiance*, as well as the uncertainty associated with the spectral data used in the mismatch computation.

If a primary spectral irradiance standard lamp, usually used by NIST only to transfer spectral irradiance scales to test lamps provided to customers, is used to illuminate the reference cell, the uncertainties associated strictly with the lamp spectrum are 1.06% at 350 nm, 1.01% at 900 nm, and 0.99% at 1300 nm. These are the root-sum-square of the quadrature sum of errors associated with the integrating sphere source spectral radiance standard and the transfer from radiance to primary irradiance standard. Thus, the uncertainty in the irradiance alone over the response range of a typical material could be on the order of 1.0%, about twice the uncertainty in the direct beam measurement made in the outdoor method described above.

If a typical NIST Spectral Irradiance Standard Lamp, the result of a transfer from the primary standards, is used, the uncertainty grows to 1.1% at 350 nm and 900 nm, and 1.2% at 900 nm. This results in slightly larger (1.1% versus 1.0%) total irradiance uncertainty. Further, assumptions must be made about the extension of the (smooth, pseudo-black body) distribution curve beyond 2400 nm (the spectral limit of NIST data for these lamps) out to 4000 nm.

The NREL and Sandia methods are comparable, but the spectral distribution uncertainty source contributions are made in different ways. Wavelength-dependent errors in the outdoor method are in the spectral distribution measurement and model extension. Those in the indoor method are in the spectral uncertainties in the lamp distribution, which propagate to the lamp total irradiance. Comparing results using the two methods, King, Hansen, and Jackson (1993) show I_{sc} values for various cell technologies as in Table 4.1.

The parenthetical 1 and 2 refer to repeated measurements (across the top) or different cells (down the first column). Differences between the results of the two methods are less than 1.0%, and 1.0% error bars about each value means the two methods are statistically the same, and impossible to differentiate.

Table 4.1. Comparison of Sandia and NREL Method Calibration Number Results

Material	SNL (1)	SNL (2)	NREL (1)	NREL (2)	MEAN SNL/NREL
Crystalline Silicon (1)	118.6	118.3	118.1	117.7	0.40%
Crystalline Silicon (2)	120.3	121.0	121.7	-----	0.87%
Gallium Arsenide	24.83	-----	24.72	-----	0.45%

4.2.4 Global (Outdoor) Method

A third method for calibrating PV reference cells that has been investigated during round-robin intercomparisons of laboratory results using different calibration techniques is the use of global, rather than direct, radiation to calibrate reference cells and modules (Emery, et al., 1988, 1989a, 1989b). In this case, essentially the same procedures are carried out as in the NREL outdoor method; however, no view-limiting geometry is used, and a

pyranometer is used to measure the global irradiance. The method is detailed in ASTM E-1039, *Standard Test Method for Calibration of Silicon Non-Concentrator Photovoltaic Primary Reference Cells Under Global Irradiation*. However, the E-1039 standard test method does not include or address spectral measurements or instrumentation. The impact of neglecting the spectral information is discussed qualitatively in the "Precision and Bias" section of the method.

A detailed uncertainty analysis for this approach, which includes spectral measurement instrumentation, measurements, and corrections (Emery et al., 1989a, 1989b), shows the limit of uncertainty for this method to be about 4.25%, even when including spectral information, as compared with the 1.0% associated with the two previously described methods. The expanded uncertainty is due to the problems associated with pyranometer calibrations (described in detail in Section 5, below) and the alignment, or accurate knowledge of, the plane of measurement (and thus the incident angles) for the pyranometer and the cell, module, or PV device under test.

The problems with the pyranometer calibration can be eliminated by using the direct beam measurement of an absolute-cavity radiometer and a shading disk mounted above a pyranometer to measure the diffuse sky and ground-reflected radiation while tracking the sun with all devices. The resulting uncertainty in the global irradiance seen by the device under test is still 3.25%.

Table 4.2, based on Emery et al., 1989a, compares various indoor and outdoor PV reference device calibration techniques with regard to uncertainty.

Table 4.2. PV Reference Cell Calibration Method Accuracies

Method	Total Irradiance Instrumentation	Total Uncertainty
Global, Fix Tilt	Pyranometer	4.3%
Global, Fix Tilt	Cavity+ Diffuse	3.2%
Global, Track	Pyranometer	3.7%
Global, Track	Cavity+Diffuse	2.5%
Direct Normal	Cavity Pyrhel.	0.7%
X25 Simulator	PV Ref. Cell	1.1%
Pulse Simulator	PV Ref. Cell	3.0%
AM0 Balloon	Langley Plot	0.7%
AM0 Aircraft	Langley Plot	1.0%

4.3 Standardized Measurements of PV Performance vs. PV Reference Cells

The preceding sections described the application of spectral measurements and instrumentation to the development of primary photovoltaic reference cells. The reference cells are calibrated in terms of short-circuit current per (reference solar) watt per square meter irradiance, essentially at the standard irradiance of 1000 watts per square meter. We judiciously include the words "reference solar" to emphasize that the *calibration is with respect to a defined solar spectral distribution, namely the terrestrial, extraterrestrial, global, or direct normal spectrum at air mass 1.5, under certain specified atmospheric conditions.*

Since either the extraterrestrial (air mass zero: ASTM E-490), terrestrial direct (ASTM E-891) or terrestrial global (ASTM E-892) spectrum could be used as a reference spectrum ("the standard spectrum"), it is important to be clear about which specific reference spectrum the primary reference cell is being used to represent. The typical difference between a "direct" and "global" reference cell output (I_{sc}) observed at NREL is on the order of 2% for crystalline Silicon, or 3%-4% for gallium arsenide, cadmium telluride, or copper indium diselenide technologies. Most often, newly developed or production PV cells are evaluated against primary or secondary reference PV cells, either outdoors in natural sunlight, or indoors using simulated sunlight, as summarized below.

4.3.1 PV Cell Performance versus PV Reference Cells

Primary and secondary photovoltaic reference cells are the "standards" for test (prototype, or research and development, new manufacturing process) cell performance. The reference cell is used to set the source irradiance (based on the reference cell I_{sc} and CN), the test cell is substituted, and its output recorded. For the very best accuracy, the radiometric techniques described above need to be applied to such comparisons, especially with respect to (1) the specific spectrum used as the reference spectrum, (2) the spectral response of the test cell, and (3) the spectral distribution of the light source under which the tests are performed.

ASTM E-948 *Standard Test Methods for Electrical Performance of Non-Concentrator Terrestrial Photovoltaic Cells using Reference Cells* details the measurement procedures used to obtain the electrical parameters and report results. The "global calibration number" (spectral mismatch correction to I_{sc}) for a reference cell under a certain simulator (implying the spectral distribution of the simulator has been measured), can be used to set the simulator irradiance level to the standard value of 1000 watts per square meter, representing the global spectrum.

Alternatively, the reference cell is used to measure (estimate) the prevailing natural outdoor irradiance level and spectral distribution. The electrical parameter data are taken as prescribed by E-948 for the test cell (current-voltage curves, I_{sc}, V_{oc}, etc.), and reported with respect to the global reference spectrum.

Secondary reference cells for monitoring and testing newly developed PV cells may be derived by comparison with primary reference cells as described in ASTM E-1362 *Standard Test Method for the Calibration of Non-Concentrator Photovoltaic Secondary Reference Cells*. Similar measurement techniques are used to generate secondary reference cells and to evaluate the performance of cells under test.

As the PV reference cell is the radiometric reference for most of the measurements, it is critical that the user keep in mind the characteristics and limitations of these devices. Limited spectral response range, non-uniform spectral response, and source spectral distribution variations in absorption and emission features in natural, continuous, and pulsed Xenon and Mercury Xenon lamps, and the smooth, high infrared content incandescent lamp and filter combinations can lead to significant errors. The reference cells and their calibration numbers *carry information relating to the specific reference spectrum used to evaluate the test device performance.*

The procedures allow tests to be performed under either natural or simulated sunlight. However, *only in the case of the secondary reference cell (E-1362) is a measurement of the "test" spectral distribution required.* Note that without information about the spectral distribution of the test source, changes in the test spectral distribution (and therefore the total incident radiation) that occur outside the spectral response region of the reference and/or test cell will NOT be observed and will contribute a nonstatistical component to the uncertainty in the reported results. This may be important for absolute measurements, but less so for relative performance measurements (since reference and test device see the same spectrum in any case). Appendix D contains a typical NREL test cell performance report.

If the test and reference cells respond similarly over the same spectral region, these errors are minimized. But even slight differences in spectral response in regions where the slope of either the distribution or the response functions is large, contribute to the uncertainty in both relative and absolute performance data.

4.3.2 PV Module Performance versus PV Reference Cells

The measurement techniques described in the previous section are useful in evaluating PV module performance. There are issues associated with modules that make direct application of these techniques difficult. These include the determination of a module spectral response, determination of the appropriate area, spatial uniformity of the module's active and encapsulant components, consistency of module cell electrical performance (shunt resistances, etc.), defining an effective and accurate "module temperature," evaluating the impact of differing cell and module field-of-view geometry, and definition and alignment of effective cell and module receiver planes.

ASTM E-1036, *Standard Test Methods for Electrical Performance of Nonconcentrator Terrestrial Photovoltaic Modules and Arrays Using Reference Cells*, describes essentially the same procedures and test methods as ASTM standards for evaluating PV cell performance. The issue of module spectral response is resolved by requiring a "representative" cell" from the module or array, packaged to produce the same optical properties in the cell and module, for which spectral response information is determined. The reference cell to be used as the radiometric reference must have a spectral mismatch correction factor within 2% ($0.98 <$ CN < 1.02) of the representative cell, and for the selected reference (global or direct) and test (outdoor, or simulator) spectra.

NREL operates a Standardized Outdoor Measurement System (SOMS) following these procedures; however, in addition, spectral measurements of the natural outdoor global solar spectrum are made using a Li-Cor LI-1800 spectroradiometer to verify that the spectral restrictions are met, or can be accounted for.

The most important consideration in the nature of PV performance measurements is the restricted spectral region utilized by the technology being tested, and the relationship of the cell or module response to the test spectrum. Therefore, the need for spectral measurement instrumentation and measurements. Those measurements provide the link to specific reference spectral conditions as a common denominator for the technologies, and the reference devices (primary and secondary PV reference cells) which carry within their (global, direct) calibration numbers the reference spectra.

When making PV-related measurements with respect to a broadband radiometer, pyranometer, or pyrheliometer, *there is no link or information with respect to the reference spectrum, as occurs when a reference cell is used.* Nevertheless, broadband radiometers have their place in both PV performance and solar resource assessment monitoring, as described in the next section.

5.0 PV APPLICATIONS FOR BROADBAND RADIOMETRIC INSTRUMENTATION

The most common applications of broadband radiometry are the monitoring of incoming solar radiation to evaluate the solar resource available to various energy conversion technologies, and the monitoring of the performance of conversion systems once deployed. The sensing and recording of the solar resource during such endeavors involves selecting, calibrating, installing, monitoring, and maintaining radiometric sensors of adequate accuracy and suitable configuration to meet the engineering needs of the test or measurement. This section addresses these concerns with respect to PV engineering applications.

5.1 Review of Broadband Radiation Terminology

Recall from our discussion of broadband concepts in Section 2.2 that the solar radiation reaching the top of the atmosphere is collimated radiation, or a beam of parallel rays, the direct beam (**B**) radiation, from the solar disk. The disk of the sun subtends a plane angle of about $0.5°$ in the sky, and the rays fill a cone (the base being the solar disk) with half angle of divergence of $0.25°$. Pyrheliometers capture radiation within a small, well-defined solid angle of $5°$ to $6°$ on the sky dome centered on the solar disk. The pyrheliometer measures the direct beam, and a small amount of circumsolar radiation from the sky near the sun. The angle of incidence, **i**, of the direct beam on a given surface is the angle between the normal to the surface and the direction of the direct beam.

As the direct beam traverses the atmosphere, photons are scattered out of the direct beam by gas molecules and aerosols, contributing to the sky brightness and color. The radiation reaching the ground from all the sky dome except the solar disk is the diffuse radiation, **D**.

Most of the radiation reaching the earth's surface is absorbed, but some is reflected back into the sky, contributing to the diffuse sky radiation. The total or global radiation, **G**, is the combination of direct, reflected, and diffuse radiation on a horizontal or tilted surface. Pyranometers measure total, or global, radiation at a surface. They have a large field of view, or solid angle of acceptance near $180°$, or 2-pi steradians. Reflected and diffuse radiation are not collimated, but consist of rays from random directions, which cannot be focused or concentrated like the collimated beam radiation.

On a horizontal surface (a plane parallel to the local tangent plane at the earth's surface) the global radiation **G** can be computed from beam, **B**, and diffuse, **D**, radiation using Equation 1:

$$G = B \cdot \cos(i) + D$$

where **D**, the diffuse radiation, includes both sky and reflected radiation seen by the surface.

A perfect radiometer which generates a signal s_0 from a collimated beam of light of constant irradiance **I** at normal incidence, would produce a signal **s** in accordance with the cosine of the incidence angle, **i**, as **i** varies from normal incidence ($0°$) to tangent ($90°$), using Equation 2:

$$s = s_0 \cdot \cos(i)$$

as mentioned several times in preceding sections. The radiometric detectors in general use today demonstrate some measure of deviation from perfect cosine law response by significant (5% or more) amounts. Only careful calibration and characterization of radiometers can lead to a knowledge of the magnitudes of these deviations, and possible corrections for them.

5.2 Broadband Radiometer Characteristics and Calibrations

5.2.1 Detector Elements

Pyrheliometers, which sense the direct beam, collimated radiation, are generally constructed using thermal (thermopile) detectors. Because of the large spectral shifts that occur in the direct beam as a result of the wide range of air masses through which the beam traverses (red sunrises and sunsets), solid-state photodetectors with their restricted spectral response regimes are not suitable for simple, accurate direct beam measurements. The fundamental calibration standard for solar radiometry, the World Radiometric Reference, or WRR, is derived from a set of very-well-characterized, carefully maintained absolute-cavity pyrheliometers calibrated using broadband thermal detectors (thermopiles) and electrical substitution techniques. (See 5.2.2 on calibrations, below.)

Pyranometers are manufactured with either solid-state (photodiode, as in the Li-Cor, Inc., detector series) or thermal (thermopile or resistance temperature detector [RTD]) detectors. Thin-film platinum resistance temperature detectors (PtRTD) are used by Yankee Environmental Systems, Inc. The RTD approach requires excitation voltages, since changes in resistance are being sensed, usually as changes in voltage drop across the sensor element.

Photodiode detectors are more acceptable for measuring global radiation because the spectral shifts in the global radiation are not as large as those in the direct beam radiation. The radiation scattered out of the direct beam is returned through the diffuse, which contributes to the total, or global, radiation. However, the accuracy of the photodiode pyranometers degrades, by about a factor of two, versus the best thermal detectors due to both the limited spectral response range as well as sensitivity to temperature.

5.2.2 Radiometer Calibration Standards

5.2.2.1 Absolute Cavity Pyrheliometer Standards

There is no U.S. current national analog to the NIST standards of spectral irradiance for the solar radiometric instrumentation used in PV testing applications or solar radiation monitoring in general. For the history of solar radiometric scales, see Coulson (1979) and Iqbal (1983).

The solar radiation community has developed an international solar radiometric scale through the World Meteorological Organization, Commission for Instrumentation and Methods of Observation (CIMO). The current solar radiometric reference scale is called the World Radiometric Reference, or WRR. The WRR was established in 1977 through special intercomparisons of 15 absolute (electrical substitution calibrated) cavity pyrheliometers of 9 different designs. (WMO, 1983)

Absolute-cavity radiometers rely on careful construction and characterization of a light-trapping cavity of silver, painted black (to approximate a black body absorber), with a view-limiting aperture known to high accuracy. The cavity is in good thermal contact with a thermopile generating an electrical signal as the incident radiation is trapped and heats the cavity. Descriptions of design, characterization, and operation of these instruments can be found in Kendall, 1969; Kendall and Behrdahl, 1970; Willson, 1973; and Zerlaut, 1986.

Cavity calibration results from joule heating supplied by an electrical current to heat the cavity and generate a temperature rise equivalent to that seen during the exposure to radiation. Accounting for (measuring or estimating) the losses due to re-radiation, non-equivalence of the electrical and radiometric heating, nonperfect absorption properties of the black coatings, and physical dimensional measurements of the area of the limiting aperture, and measurement of the values of current, voltage, and resistance results in an absolute measurement of radiometric power. Figure 5.1 is a sketch of a typical cavity radiometer design.
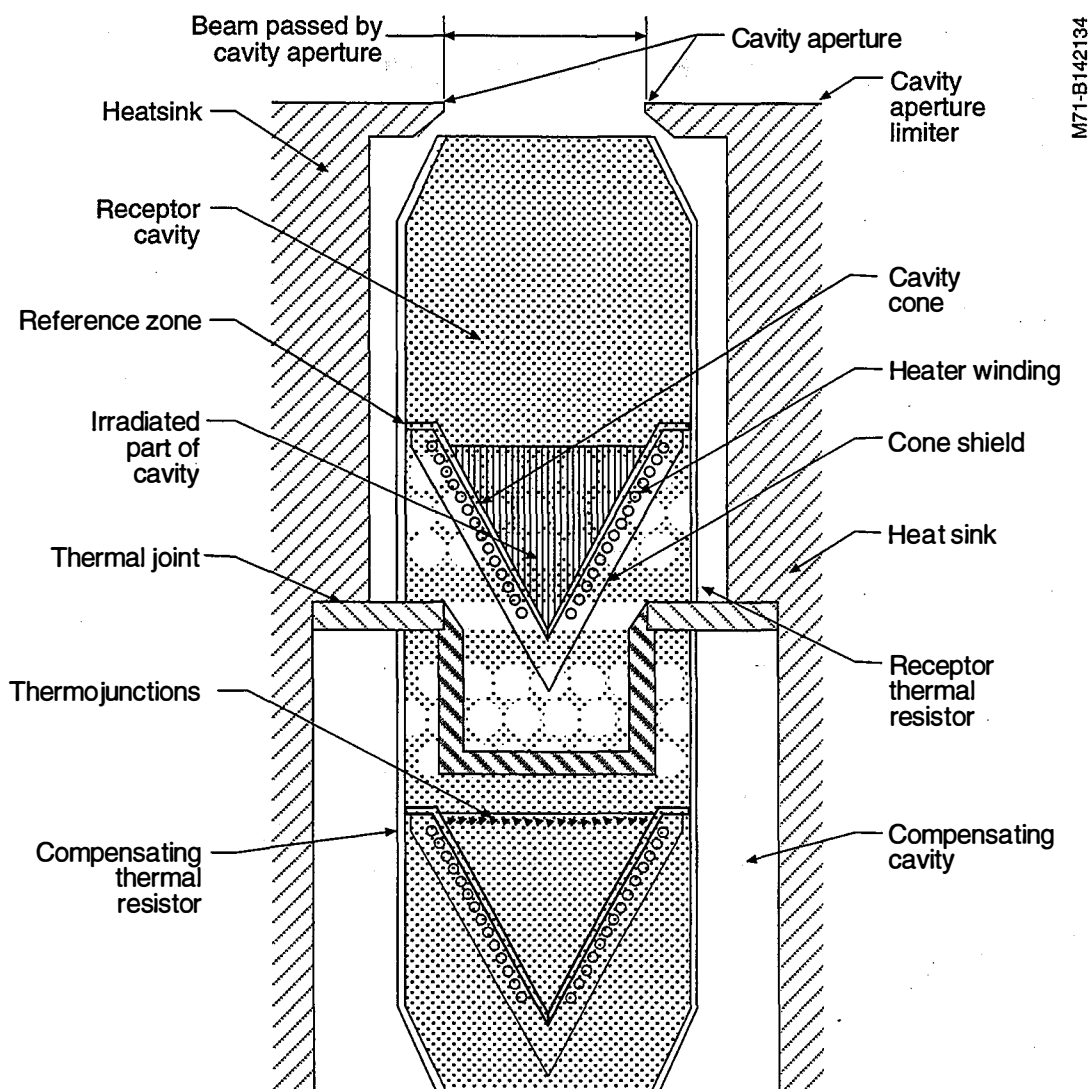
Figure 5.1. Typical absolute-cavity radiometer design

Stability, accuracy, and precision of the WRR is embodied and maintained by a World Standard Group (WSG) of seven absolute-cavity radiometers (three from the U.S, four from Europe). Four of the WSG were part of the original, defining group of 15 instruments. The instruments (and thus the WRR) are in the care of the Physicalish Meteorologishes Observatorium, Davos, World Radiation Center (PMOD/WRC), where they are regularly intercompared. Every 5 years from 1975 to 1995, international pyrheliometric intercomparisons (IPCs) are sponsored by WMO/PMOD/WRC to allow comparison of national reference instruments to WRR for the purpose of transferring the WRR (through a correction factor) to the various national reference instruments. The technical report of Reda (1995) describes the IPC process and data processing in detail.

The National Oceanic and Atmospheric Administration (NOAA) Solar Radiation Facility in Boulder, Colorado, NREL, and the primary U.S. manufacturer of commercially available absolute-cavity radiometers (the Eppley Laboratory) participate jointly in the IPCs, representing the meteorological, renewable energy, and manufacturing operations in the U.S. NREL has participated in the last four IPCs, and contributed one of the U.S. (NREL) radiometers to the WSG.

Uncertainty quoted in WMO, 1983, Section 9.1.3.1, for the WRR is ±0.3% (three sigma) of full scale (1000 W/m^2) or 3 watts/m^2. Absolute-cavity radiometers participating in the intercomparisons have a stated

uncertainty (off the shelf) of about 0.5%. The intercomparison process results in mean correction factors to agree with the WRR that have standard deviations (one sigma) of 0.1% or less, and values between 0.995 and 1.005. Thus, the claimed accuracies are confirmed, but direct intercomparison with WRR lowers the uncertainty in the absolute measurement of the direct beam to only slightly more than that of WRR itself. The national reference unit's readings, corrected to agree with WRR, become the references for calibrating solar pyrheliometers and pyranometers.

An intercomparison process permits the identification of gross (more than 0.3%) changes in reference instrument performance or sensitivity that may be identified and corrected. These usually involve contamination of some sort, or physical damage to apertures and coatings, or failures in the electronics that might not be apparent in stand-alone operation.

Both before and after WRR correction factors are determined for a particular IPC, NREL performs local intercomparisons among its own group of absolute-cavity radiometers. A minimum of three units (and usually more, invited from NOAA and other institutions) are intercompared, to permit the identification of which specific unit has a problem, in the event discrepancies arise. These are usually performed at the NREL Solar Radiation Research Laboratory (SRRL), using protocols emulating those at the IPCs. Time series plots of the results of the national and international comparisons (with respect to a reference instrument or group of instruments) indicate that the stability or precision of the NREL absolute solar radiometric reference is itself ±0.25% (Reda, 1996). These units become the reference standards against which all other pyranometers and pyrheliometers are calibrated. The procedures followed address the following protocol issues (Nelson, et al., 1987):

1) A data sheet requesting participating instrument particulars is filled out, with such relevant information as manufacturer, model, serial number, correction factors applied, WRR correction factor (if known), readout instrumentation, and special processing applied routinely by the user.

2) The reference instrument, or (weighted mean of) group of instruments must be assigned by the consensus of the participants. All other instrument signals will be ratioed to (divided by) the reference instrument to evaluate the stability and biases of each with respect to the reference.

3) A 30-minute warm-up is required after all power-off situations.

4) An initial 15-minute electrical check and calibration will be allowed after warm-up, but prior to the first data run.

5) Each experimental run will consist of at least 21 instantaneous readings taken over a period of 10 minutes, commencing at time T-0 (T-zero).

6) T-3 (minus 3) minutes will be announced and 3 minutes allowed for pre-run calibrations and checks. Time announcements will be made for T-2, T-1, T-30 seconds, T-15 sec, T-0, T+30 sec, T+ 1 min, and every succeeding 30 seconds until and including T+10 minutes.

7) If the interval between runs is less than or equal to 15 minutes, only one pre-run calibration will be allowed, but if the interval between runs exceeds 15 minutes, a pre-run calibration will be required.

8) Mean and standard deviation of the 21 reported irradiance values will be computed and reported after each run, to assist in determining the quality of the atmospheric conditions and to assist in identifying gross instrumental errors.

9) At least 5 runs, and preferably 10 (the more the better) of 21 readings (105 valid intercomparison points) are required for evaluating the precision, accuracy, and adequacy of the intercomparison data.

Agreement is generally required between all participants as to the handling of data interruptions, flagging of instrument problems, and inclusion of runs with missing data or instruments. Data processing consists of computing the statistical properties of the distribution of individual ratios of test cavity radiometers to the reference radiometer or mean of a group of reference radiometers, as described by Reda (1996), and assigning a correction factor and uncertainty to the test units.

5.2.2.2 Pyrheliometer Calibrations

The responsivity of a radiometric sensor is the proportionality constant relating the sensor signal to the magnitude of the stimulus. Pyrheliometer and pyranometer primary calibrations traceable to the WRR are performed outdoors under clear skies using absolute-cavity pyrheliometers as the reference instrument that monitors the magnitude of the radiation stimulus during calibration. Monitoring of ambient temperature conditions is recommended to provide data for temperature response characterization.

Secondary calibrations may be performed using a reference radiometer (itself traceable to WRR) other than a cavity pyrheliometer. Pyrheliometer millivolt signals are divided by irradiance values obtained from the absolute-cavity radiometer (usually at 30-second intervals) to give the responsivity (microvolts per watt per square meter) of the pyrheliometer. A sample size of 200 to 2000 data points, distributed over all periods of the day (covering different air masses and a wide range of irradiance levels), and over several (at least two) days, is required to fully characterize the accuracy and precision of the pyrheliometer calibration process.

The data are plotted in time series and/or versus ambient temperature to evaluate systematic errors, such as tracking and pointing errors, and temperature effects. Structure in the scatter plots will reveal systematic errors, and statistical mean and standard deviation of the responsivities provide calibration factors and uncertainty estimates. Figure 5.2 illustrates typical pyrheliometer calibration factors as a function of time of day for several days. Note that the spread in the data at a particular time of day (typically 0.5%) represents the inherent noise in the calibration process (test instrument, reference instrument, data logging equipment, and atmospheric stability) while the overall diurnal pattern of the calibration factors may represent tracking and alignment problems, changing atmospheric conditions (i.e., variation in circumsolar radiation), etc. Typical "good" pyrheliometer results vary by less than 1% through a day.

5.2.2.3 Pyranometer Calibrations

The reference instrument for pyranometer calibrations, as well as the pyrheliometer calibrations, is the absolute-cavity pyrheliometer. As the pyranometer should not respond to radiation at incidence angles of $90°$ (parallel to the plane of the sensor), we can say the pyranometer effectively responds to only the vertical component of the radiation field. The radiometer responsivity is the change in signal with respect to the change in the vertical component of the radiation. By recording the signal from a pyranometer monitoring the global radiation, then blocking the solar direct beam from a pyranometer sensor and recording the change in signal, while continuously monitoring the direct beam with an absolute-cavity radiometer, the pyranometer responsivity can be determined. See Myers, 1988, 1989a, 1989b, 1990, and Myers et al., 1989 for descriptions and detailed uncertainty analysis of these NREL methods.

The difference between the pyranometer signal when unshaded (Vu) and shaded (Vs) from the solar direct beam (by a disk which subtends the same solid angle, usually $5°$, as that accepted by the cavity radiometer) is proportional to the vertical component of the direct beam, D, namely B * cos (Z), being present, then absent. The ratio $(Vu-Vs)/(B *\cos(Z))$ is the responsivity of the pyranometer (volts per watt per square meter), and the reciprocal of this ratio is the calibration factor (watts per square meter per volt) for the instrument. Figure 5.3 is a plot of the signal from a pyranometer as it is shaded and unshaded.
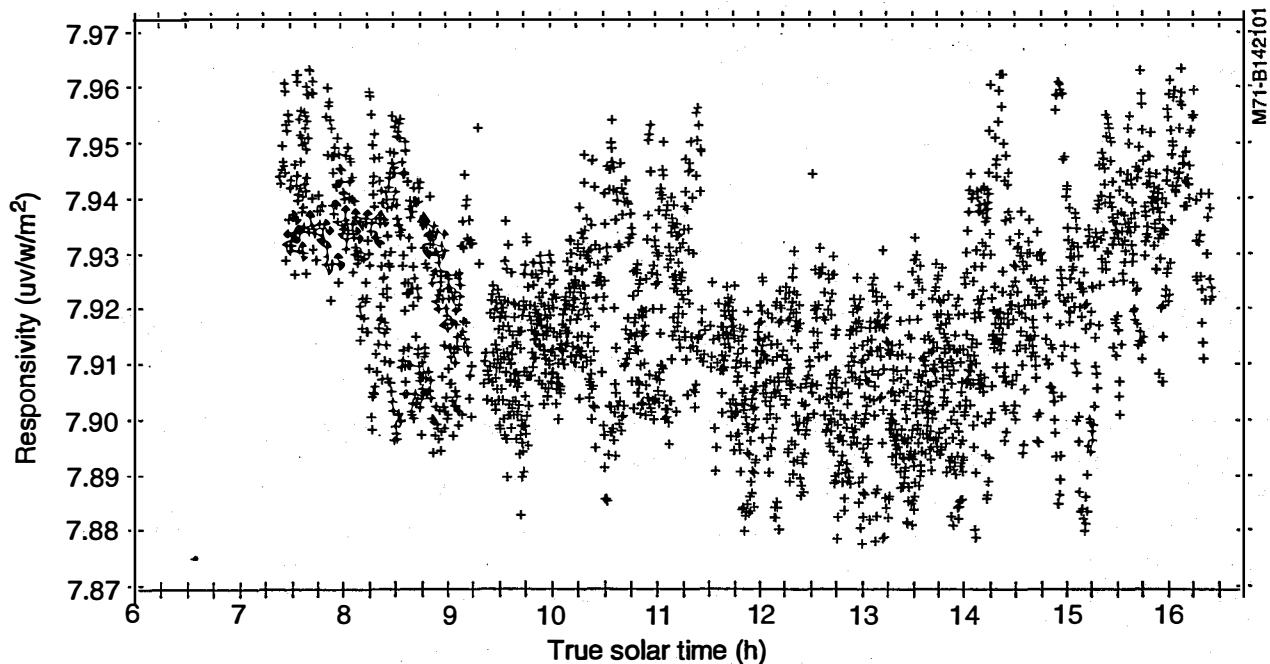
Figure 5.2. Typical pyrheliometer responsivity versus absolute-cavity reference. Note 1.2% variation in responsivity through the day.

The shade-unshade technique requires accurate timekeeping, location (latitude and longitude) information, stable atmospheric conditions and direct radiation levels, and slowly changing zenith angles for highest accuracy. The B * cos(z) term is computed as the average of the vertical components measured in the shaded and unshaded configurations. Accuracy of the results is also affected by the time constant of the pyranometer and that of the absolute-cavity radiometer.

Duration of the shade and unshade periods is typically a minute for thermopile sensors with time constants on the order of several seconds, while shorter periods are acceptable for solid-state sensors with much shorter time constants. Voltage signals are usually measured at the end of each measurement period. Figure 5.3 is similar to the illustration for a typical calibration measurement sequence, as prescribed in ASTM E-941, *Standard Practice for Calibrating Pyranometers by Shade Unshade.*

In practice, at least 20 shade/unshade cycles are performed, with a corresponding number of responsivities, which are then averaged to produce the responsivity and calibration factor. Plotting the responsivities as a function of zenith angle (which is the incidence angle for horizontal sensors) will provide information on the cosine response, or departure from Lambert's cosine law, if the range of zenith angles is large.

This method is also applicable to pyranometers mounted in tilted configurations, as long as the component of the direct beam normal to the sensor is computed from B * cos (i), where i is the incidence angle of the direct beam (angle between normal to the sensor and the beam).

44
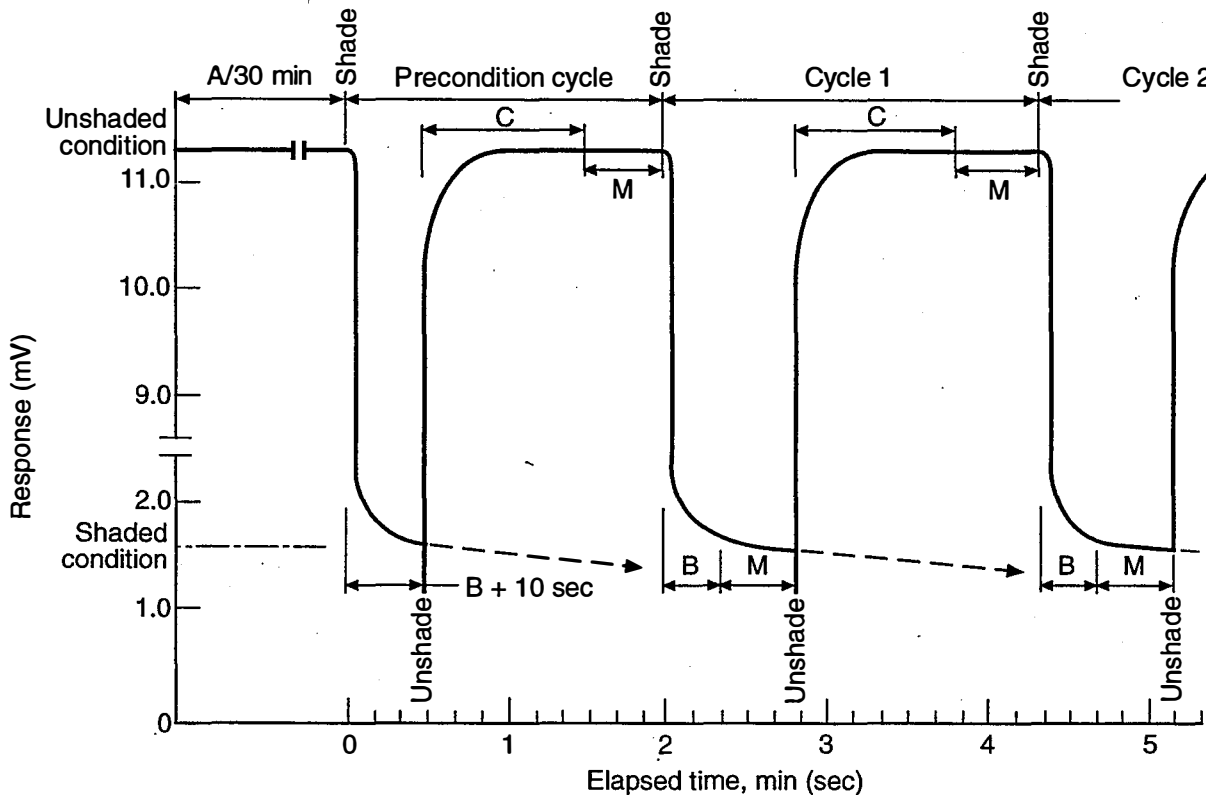
Figure 5.3. Shade-unshade pyranometer calibration time series of signal

The shade/unshade method is labor intensive, and expensive to implement if automated. But, since the global radiation is the sum of the vertical component of the direct, B * cos(Z), and the diffuse (sky radiation), D, a calibration can be performed using continuous direct and diffuse measurements, and computing the global radiation from the radiation component equation (Eq. 1). An absolute-cavity radiometer is used for the direct beam measurement. For the diffuse measurement it is necessary to use a pyranometer calibrated using the shade/unshade technique, which is continuously shaded by a tracking disk (subtending the same solid angle as the cavity radiometer accepts) to block the direct beam. We refer to this technique as the "component summation technique." Figure 5.4 is a schematic diagram of the setup for a typical component summation calibration.

NREL relies on the component summation calibration technique, with a shade/unshade calibrated pyranometer, shaded by a tracking disk subtending a 5° solid angle, measuring diffuse radiation, and one of our working complement of absolute-cavity radiometers measuring the direct beam. Millivolt, radiation, and temperature data are recorded at 30-second intervals on at least two, and preferably three, clear days. Plots of the reference irradiance(s), responsivity versus time of day, zenith angle, and temperature data are used to evaluate calibration conditions and individual instrument responsivity. Appendix F contains a sample NREL broadband radiometer calibration report.

Calibrations of pyranometers can also be accomplished indoors, inside a large integrating sphere illuminated with an artificial source, and comparing signals with a reference pyranometer. The reference pyranometer is calibrated

45

using either the shade/unshade or component summation techniques. NREL observes a 0.5% to 3% difference between indoor sphere/comparison-based calibrations and outdoor calibrations, with the outdoor results showing greater responsivity.

Checks of pyranometer calibration stability can be performed using a temporally stable artificial light source and statistically evaluating large sample sizes over short periods of time, to reduce random components of uncertainty due to noise (random variations) in lamp output (see Michalsky, et al., 1992).

Component summation is helpful for mapping out the cosine response of pyranometers over incidence angles encountered at the time of the calibration event; *however, neither technique (shade/unshade or component summation) completely characterizes the geometrical response of a pyranometer because the extensive range of solar incidence angles throughout the year is not encountered.* The uncertainties in the component summation technique is slightly larger, because of the added component of uncertainty in the diffuse pyranometer calibration uncertainty.

5.2.3 Radiometer Characteristics

5.2.3.1 Geometrical Response

Physical imperfections in the manufacture of pyranometers, and variations in the absorption, transmission, and reflectance of sensor and window materials result in detectors which do not perform with a uniform (cosine-law-related) response as the direction of the beam radiation changes. The change in a pyranometer signal as a function of the incidence angle and azimuth angle of collimated radiation is referred to as the geometrical response of the radiometer.
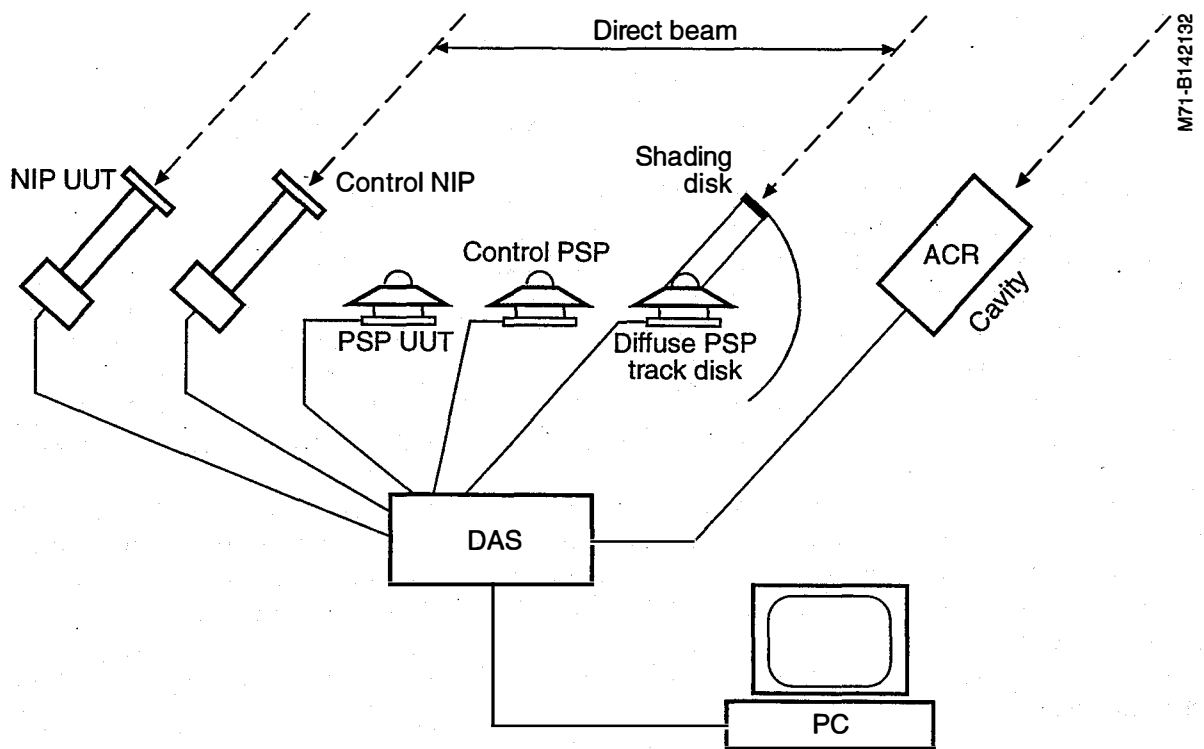
Figure 5.4. Schematic of component summation calibration for pyranometers

46

The variations observed, as shown in Figures 5.5 and 5.6 and shown in Stoffel, 1996, can be the result of many contributing factors. These include agreement between the sensor plane and the bubble level, reflections from instrument surfaces at various solar geometries, contamination and/or deformation of the absorbing disk surface, and variations in the thermal contact between the thermopile and the absorbing surface.

Note that there are NO specific representative or characteristic curves for families of pyranometers, because each radiometer has been found to have its own distinctive signature. Thus, Figures 5.5 and 5.6 cannot be used to characterize two different models of pyranometers. In fact, the curves are both for a single model of pyranometer. The following sections discuss the factors influencing variations in responsivity in greater detail.

With many radiometers deployed in a relatively small field, NREL has been able to examine the precision of the calibration process by comparing radiometric data from several systems. Without correction for individual instrument geometrical (or temperature) response characteristics, the radiometric data show the typical 2%-5% disagreement typically quoted for pyranometer data.

The large number of mechanisms (field of view, foreground reflections, mounting schemes and accuracy, thermal environment, as well as the condition of the absorbing surfaces) make it almost impossible to separate out the causes of the variations seen. The responses discussed above are probably responsible for about 80% of the variation seen.
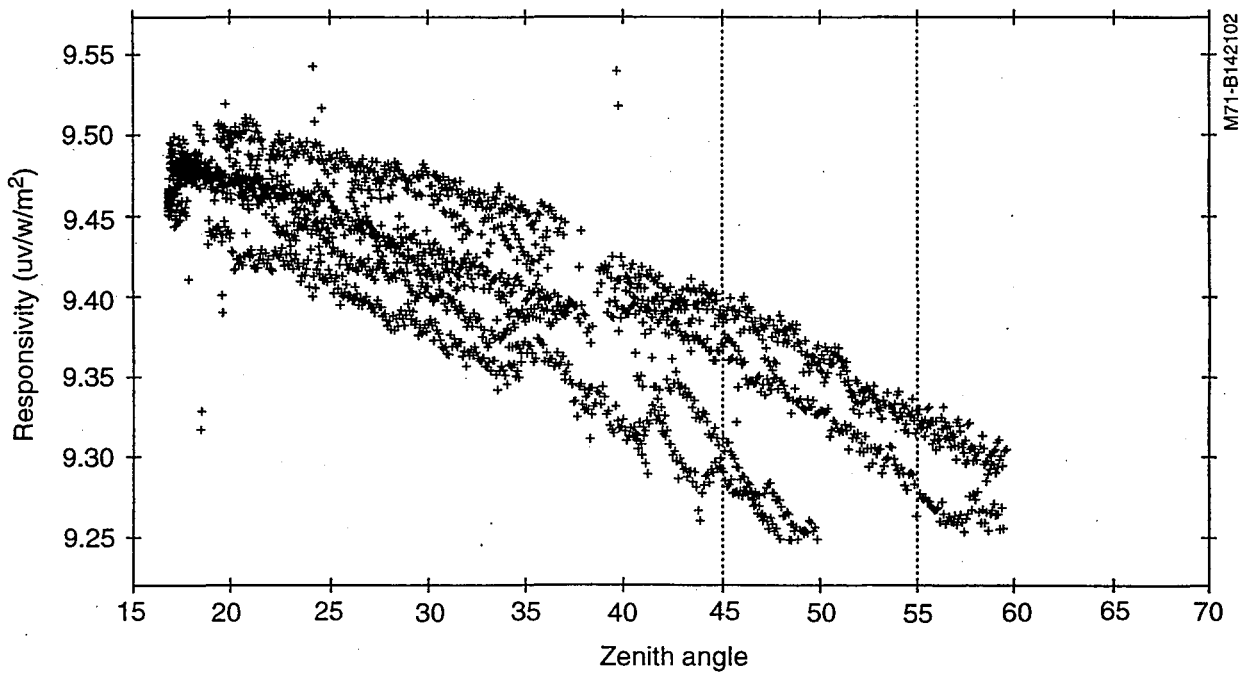
Figure 5.5 Typical pyranometer responsivity response vs zenith angle
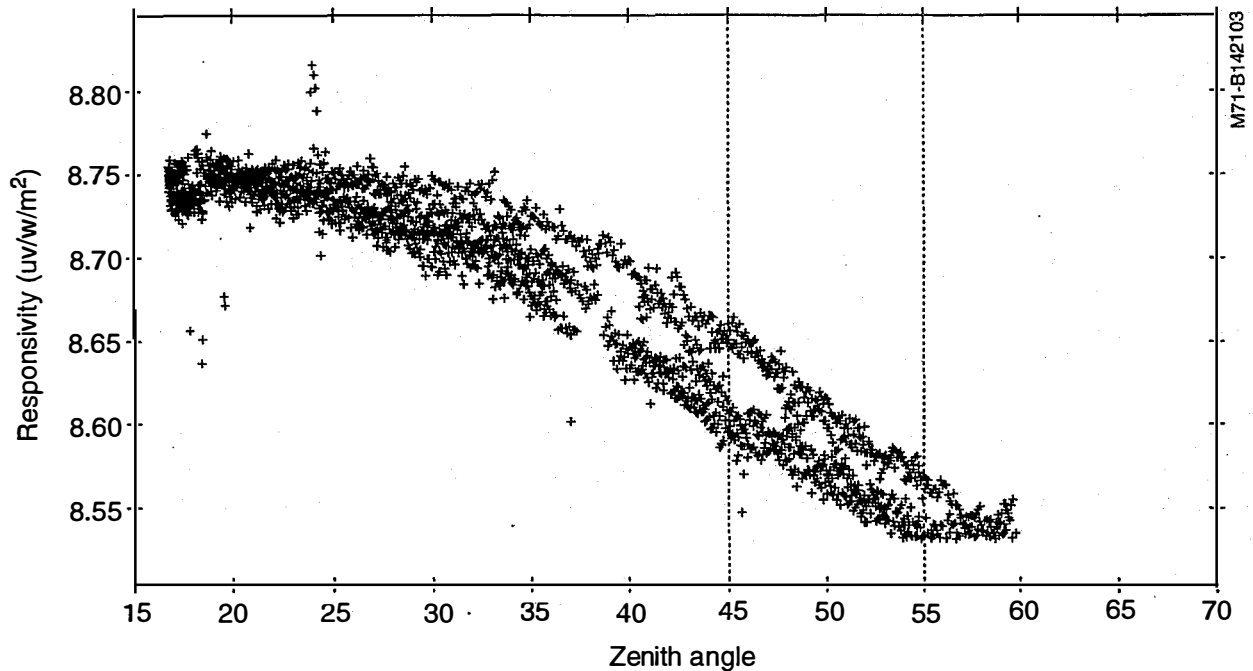
Figure 5.6. Responsivity vs zenith angle for same model pyranometer as Fig. 5.5

Figure 5.7 is a plot of the ratio of each of three NREL PV system radiometers to a reference pyranometer for clear sky conditions for two days in each of the four seasons.

One clear day from a month representing each of the four seasons (February, April, July, October) was chosen, and the ratios of the performance radiometers to the reference radiometer 15-minute averaged data were plotted. Thus, there are four different days worth of ratios plotted for each test radiometer.

The patterns of morning and evening departures from agreement, and about 3% spread in departures between 9 a.m. and 3 p.m., illustrate instrument-to-instrument variations, including the impact of variables mentioned in the paragraph above that constitute the instrument environment as well as sensor characteristics.

Figure 5.8 is a similar plot for partly cloudy conditions. Note the wider range of ratios, however, as well as the much more random and "flatter" diurnal pattern to the ratios.

Figure 5.9 displays the same type of data but for overcast conditions, showing the maximum spread in the ratios (instrument variability).

One reason for the increasing spread in the distribution of the ratios as cloudiness increases is that the values being compared are decreasing in absolute value. Any *fixed* bias (say 10 watts, or in terms of signal, 0.1 mV or 100 uV) becomes an increasingly larger proportion of the ratio or percent of reading, uncertainty.

1.20

1.15

1.10

1.05

Ratio to RMIS

1.00

0.95

0.90

0.85

0.80

Clear Sky Conditions OTF Pyranometers
15 min avg. versus RMIS 15 min avg. 1995

M71-B142104

• Roof

O CIS

x ASE

4:45 5:45 6:45 7:45 8:45 9:45 10:45 11:45 12:45 13:45 14:45 15:45 16:45 17:45 18:45

Time (h)
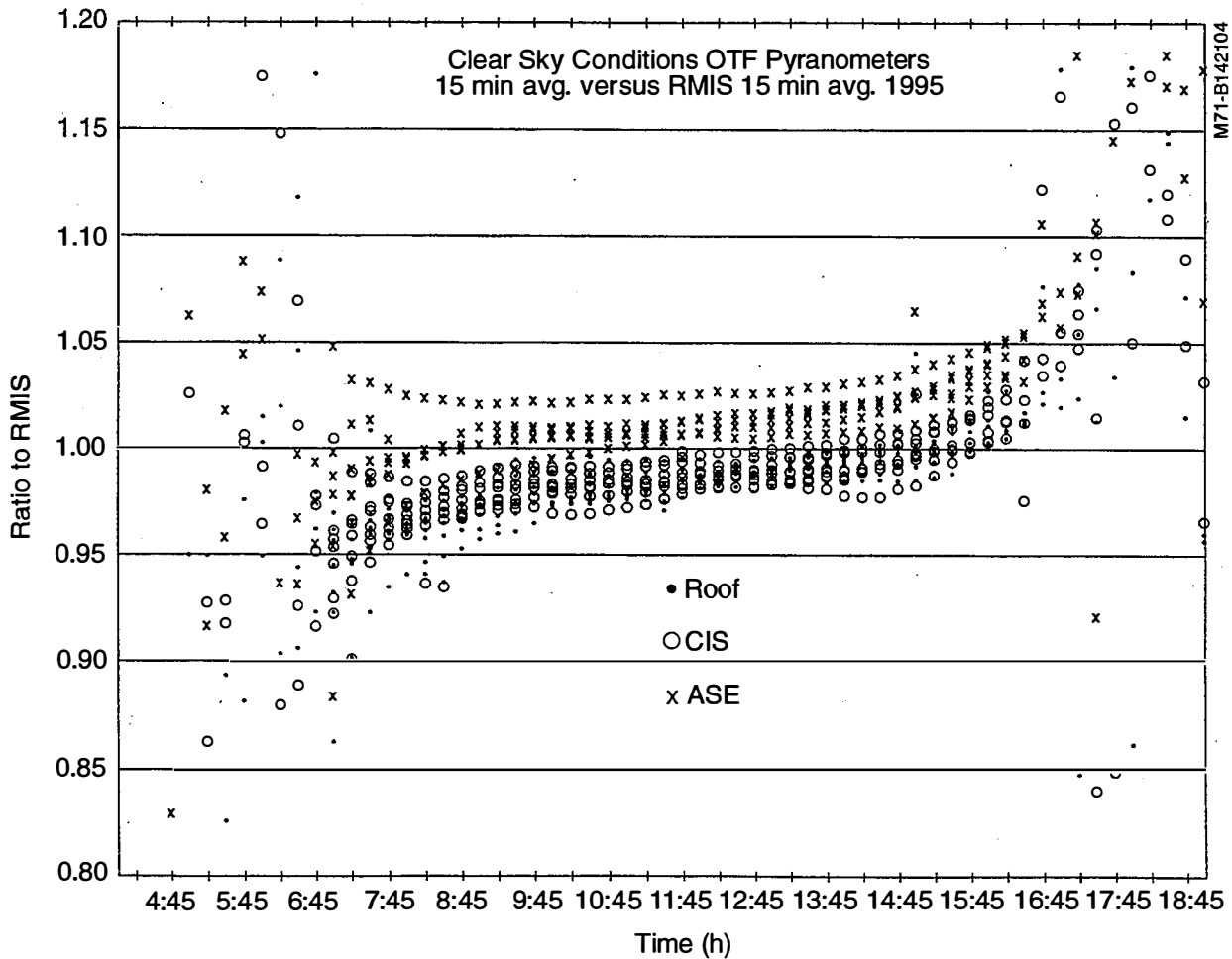
Figure 5.7.   Ratios of three latitude tilt NREL PV system pyranometers to a latitude tilt reference pyranometer for clear skies in each of the four seasons

The distribution of radiation inside an integrating sphere is homogeneous and nearly isotropic, in contrast to outdoor conditions where there is the strong directionality of the direct beam and the anisotropic distribution of the diffuse radiation from the sky dome. As a result, the directional response of the pyranometers calibrated inside integrating spheres is averaged out; whereas under direct beam illumination outdoors, some of the directional response information can be *mapped* out. This is demonstrated in the more random appearance of the ratios as cloudiness increases in Figures 5.8 and 5.9 above.

Using a clear sky model (for relative computations) or a pyrheliometer to measure the direct beam, and measurements or estimates of the diffuse component, techniques used in pyranometer calibration procedures can be applied to PV performance radiometric data on any clear day throughout the year, to generate a map of instrument response as a function of solar elevation (zenith angle) and azimuth. The technique is described in the section on "synthetic calibration" in Maxwell et al., 1995, the final technical report on NSRDB. A typical azimuth-elevation response map for an NREL radiometer has been performed, and the result is seen in Figure 5.10.

Such a map of a radiometer's response as a function of azimuth and elevation (or zenith) angle allows corrections (in this case up to 12%) to be applied in real time, or in post-processing.

49
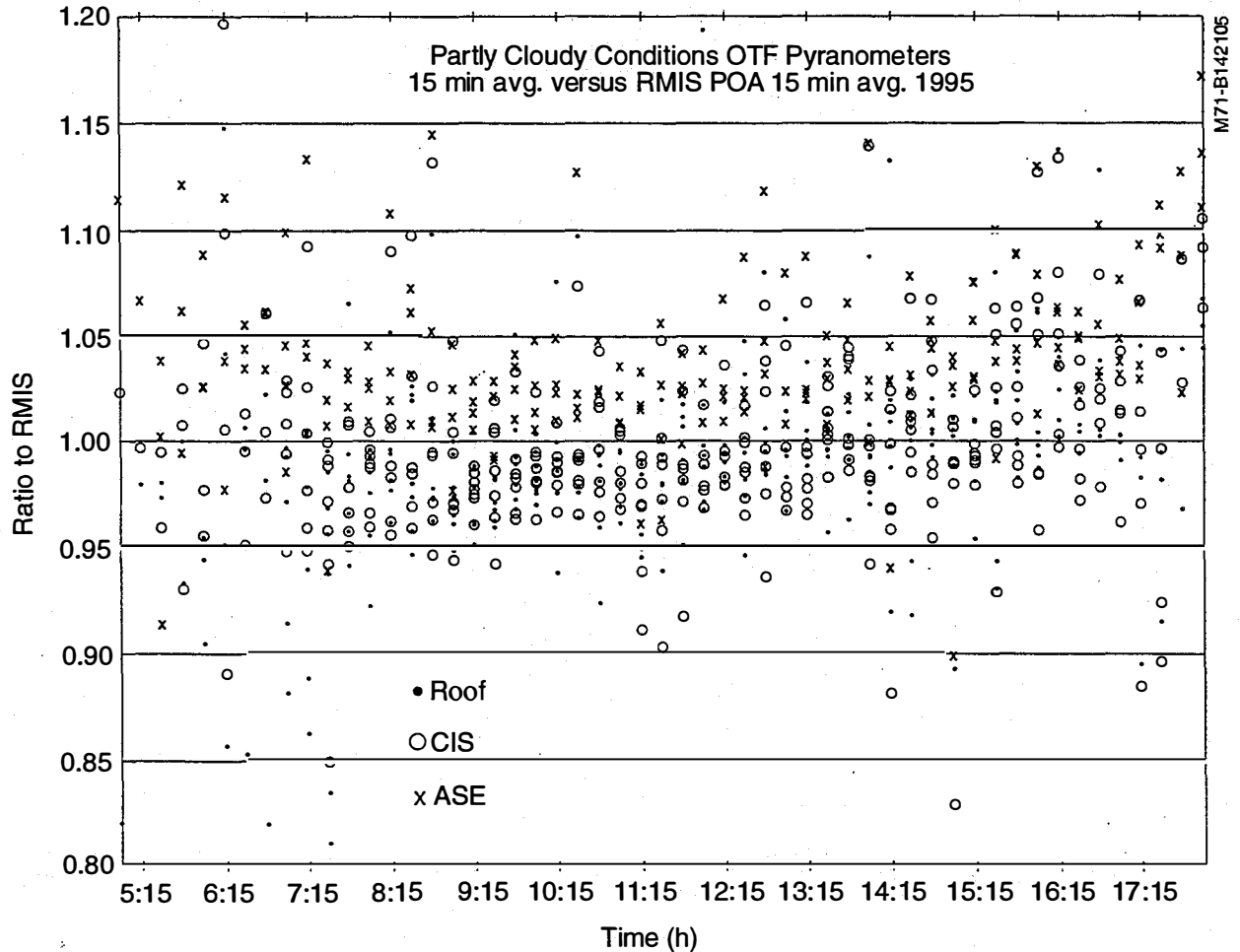
Figure 5.8. Similar to Figure 5.7, but for partly cloudy conditions

5.2.3.2 Temperature Response

The most common radiometric thermal detector is the copper-constantan (type-"T" thermocouple material) thermopile. The thermopiles are constructed in wire-wound (Eppley Laboratories) or thin-film (Kipp and Zonen) configurations. The thermopiles generate a voltage proportional to the temperature rise in an absorbing receiver, or "hot" junctions, relative to a "cold" reference junction, usually the instrument body. It is therefore important that great attention be paid to the thermal environment (thermal pathways) of the body of the instrument and that the mechanical mounting scheme be the same in the application as in the calibration of the radiometer.

For example, a pyranometer is calibrated with a clearance space under the body (the preferred method, using standoffs), or with a thermal insulator between the body of the instrument and the mounting platform. If the instrument is mounted in the field flush to an aluminum plate which absorbs radiation, heats up, and conducts heat to the body of the radiometer (in full sun), or conducts heat away from the body (in cold weather) in the application, the thermal environment of the cold reference junctions will be significantly different in the application versus the calibration. Effectively, the mounting plate has become part of the radiometer that was not included in the calibration. Significant systematic errors (of several percent) will be introduced into the radiometric data in such an installation.

50
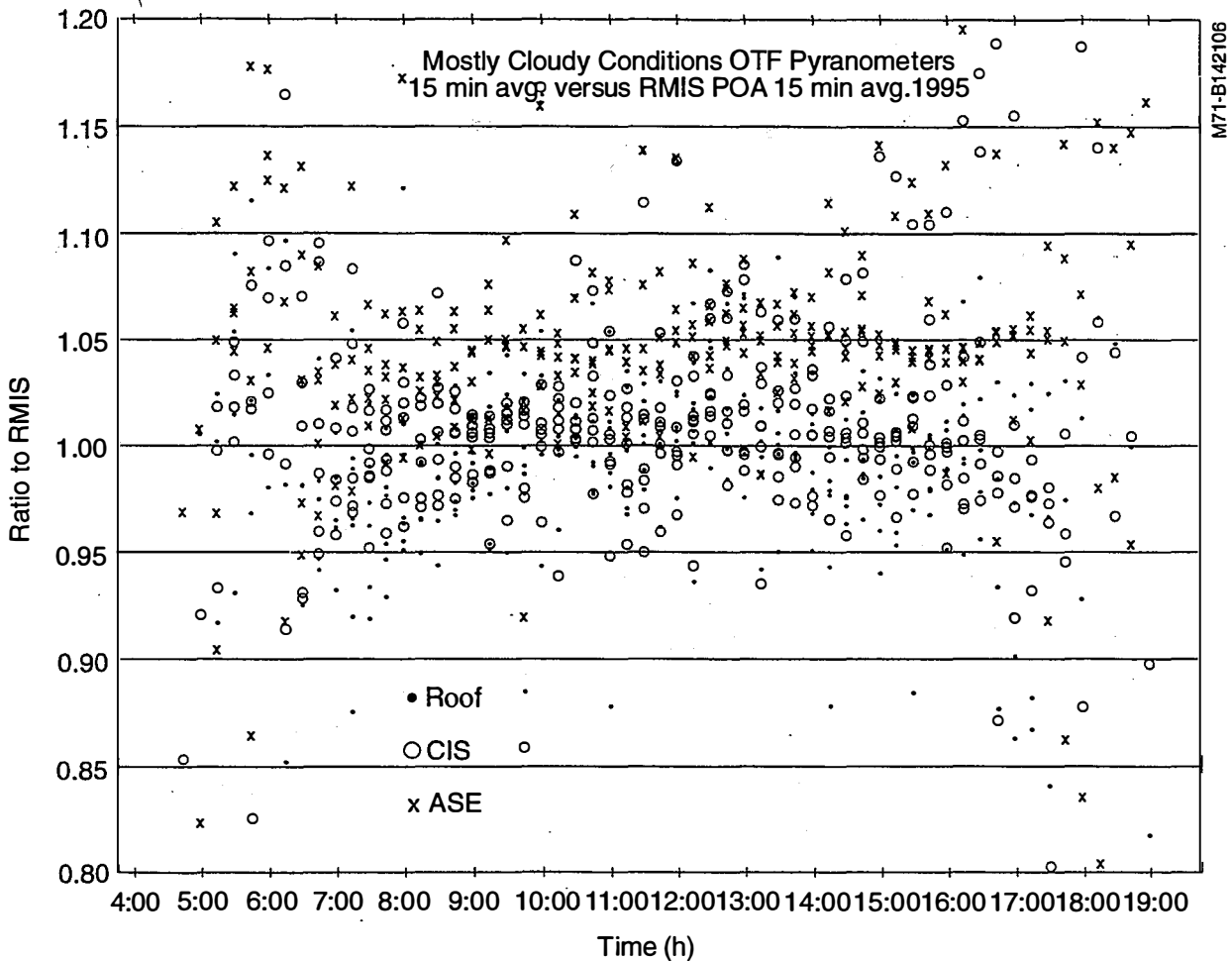
Figure 5.9. Similar to Figures 5.7 and 5.8, except for overcase conditions

The thermopiles are separate from the absorbing surface, but in intimate thermal contact with it. Type-T thermocouple material has a temperature coefficient of about 40 microvolts per °C temperature difference, but this response is NOT linear, even over the limited range of temperatures (-40°C to 40°C) seen by the detectors. (Hammond and Mason, 1971).

In the case of the Eppley PSP thermopiles, under 1000 watts/m², a signal of about 10 millivolts may be generated. If there are about 50 junctions (typical) in the thermopile, then the average contribution to the signal from each junction is 200 microvolts. Thus, an approximate temperature difference of 5°C is being sensed between the cold and hot junctions.

In Table 5.1 are shown (1) the temperature of the measuring junction, (2) the signal from a single type-T thermocouple (in microvolts) when the reference junction is at 0°C, (3) the temperature coefficient (slope) of response, and (4) the signal a 5°C temperature difference would generate (e.g., at 1000 watts per square meter) at each temperature.

Figure 5.11 is a plot of the relative change in temperature response, normalized to that at 25°C, for the thermocouple material.

51
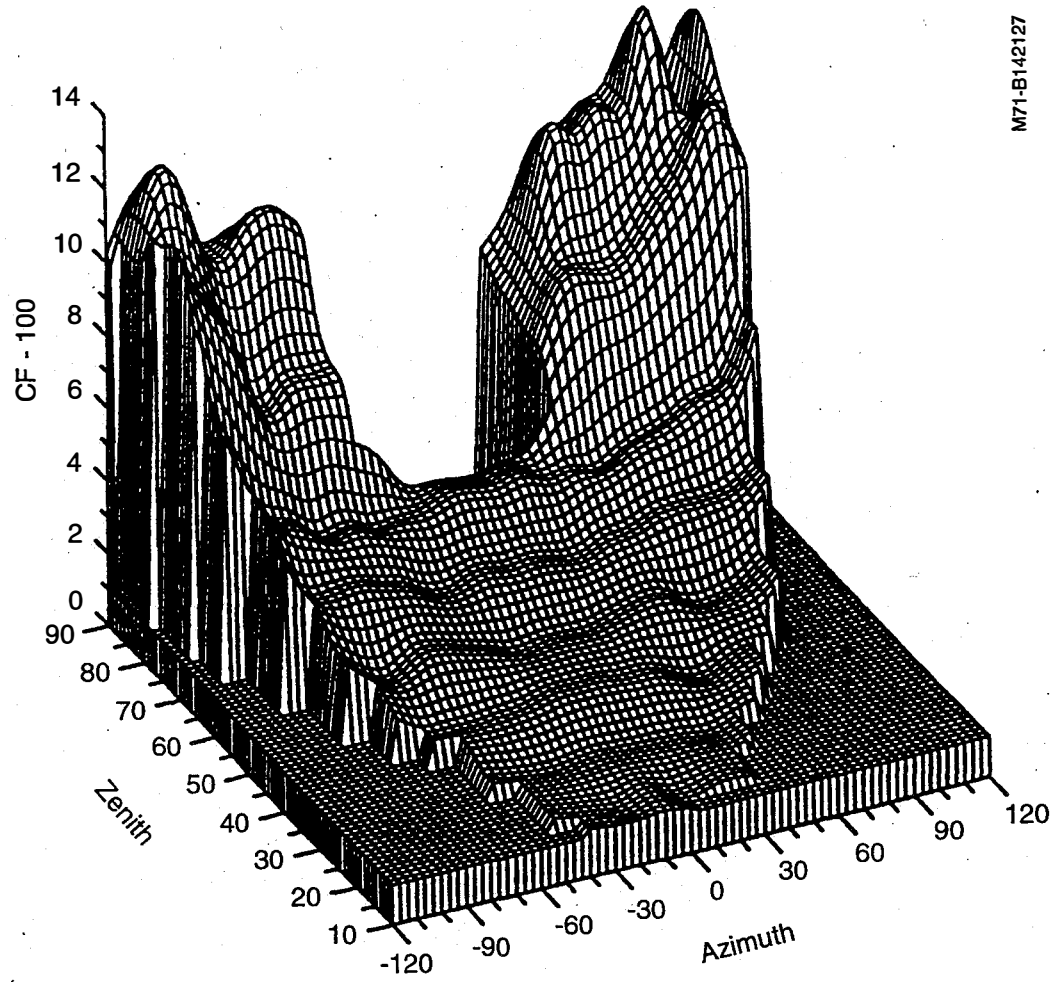
Figure 5.10. Azimuth-elevation response map for an NREL pyranometer generated from clear sky component summation (pyrheliometer/diffuse) data.

The table and plot show that raw thermopile voltages result in a -16% to +5% change in the response of the thermocouple over the -40°C to +50°C range. Some form of correction for the nonlinear temperature response is needed.

A sketch of a temperature compensation circuit is shown in Figure 5.12. The network employs a thermistor (negative, logarithmic temperature coefficient) in a series/parallel network with the detector to reduce the voltage drop across the network in a fashion that linearizes the radiometer response (see Figure 5.12). A "compensated" thermopile response generated using such a scheme is shown for comparison purposes in Figure 5.11.

Note that even with compensation, there are still deviations in the temperature response of up to 5%. This is reflected in the temperature response data typically provided by a manufacturer, such as Eppley or Kipp and Zonen, shown in Figure 5.13.

Despite the fact that these deviations from a uniform temperature response are measurable, we also note that the uncertainty in the corrections can be as large as the corrections themselves. Figure 5.14 shows that repeated temperature response tests in the laboratory only repeat to within 2% at -30°C, and 1% up to 40°C. The value

Table 5.1 Temperature Dependence of Uncompensated Thermocouple Response

Measuring Junction T °C (Ref. 0°C)	T-Type Thermocouple uV	dV/dT uV/°C	50-Junction Thermopile mV @ 1 kW
-40	-1474	34.9	8.664
-30	-1120	35.9	8.914
-20	-756	36.9	9.160
-10	-382	37.9	9.403
0	0	38.6	9.631
10	390	39.4	9.815
20	789	40.2	10.01
30	1196	41.1	10.23
40	1611	41.9	10.44
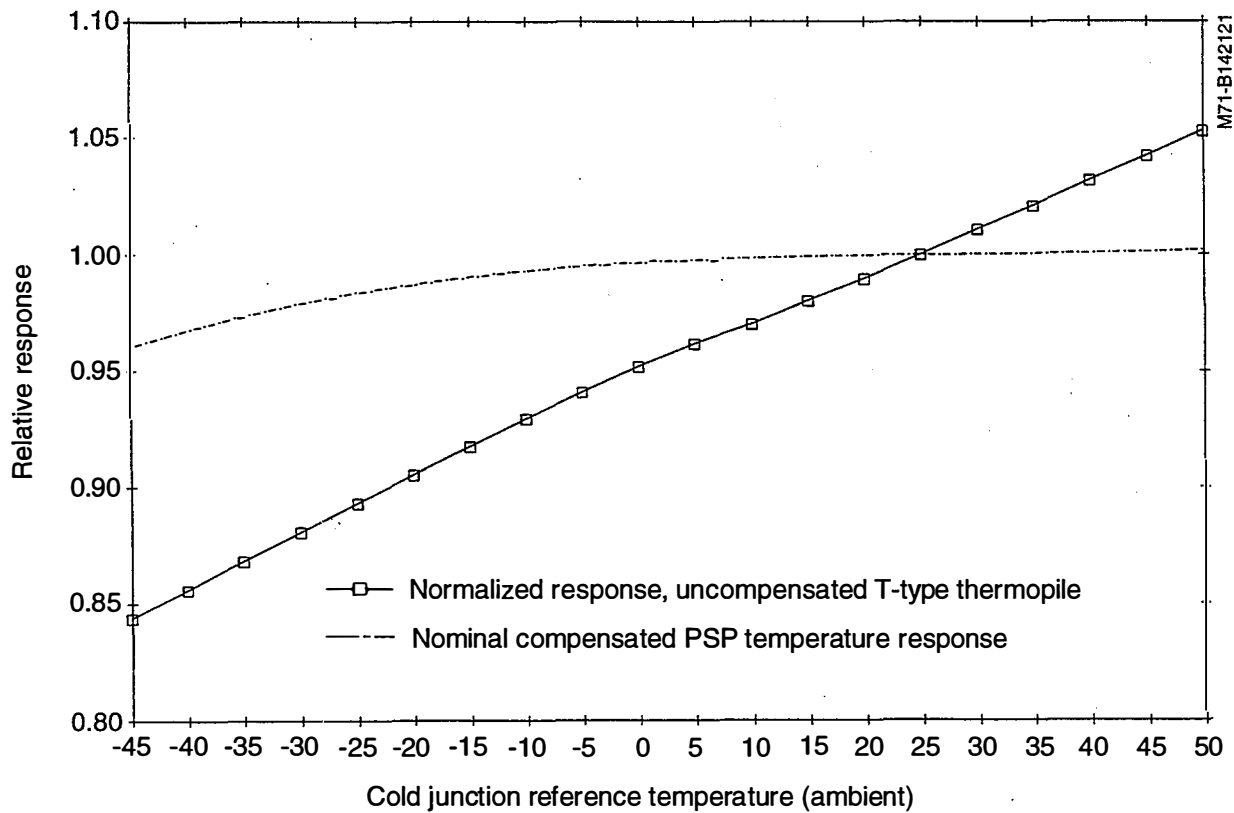
Figure 5.11.   Temperature response nonlinearity of an uncompensated, 50-junction T-type thermocouple. Response with a compensation network is also shown.

Internal Wiring
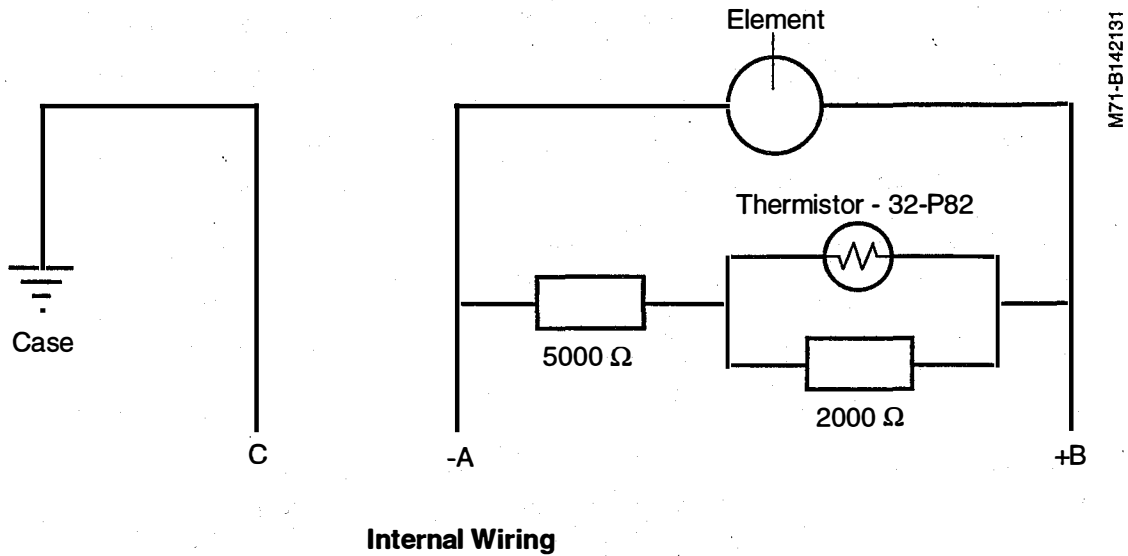
Figure 5.12. Sketch of Eppley Laboratories temperature compensation network
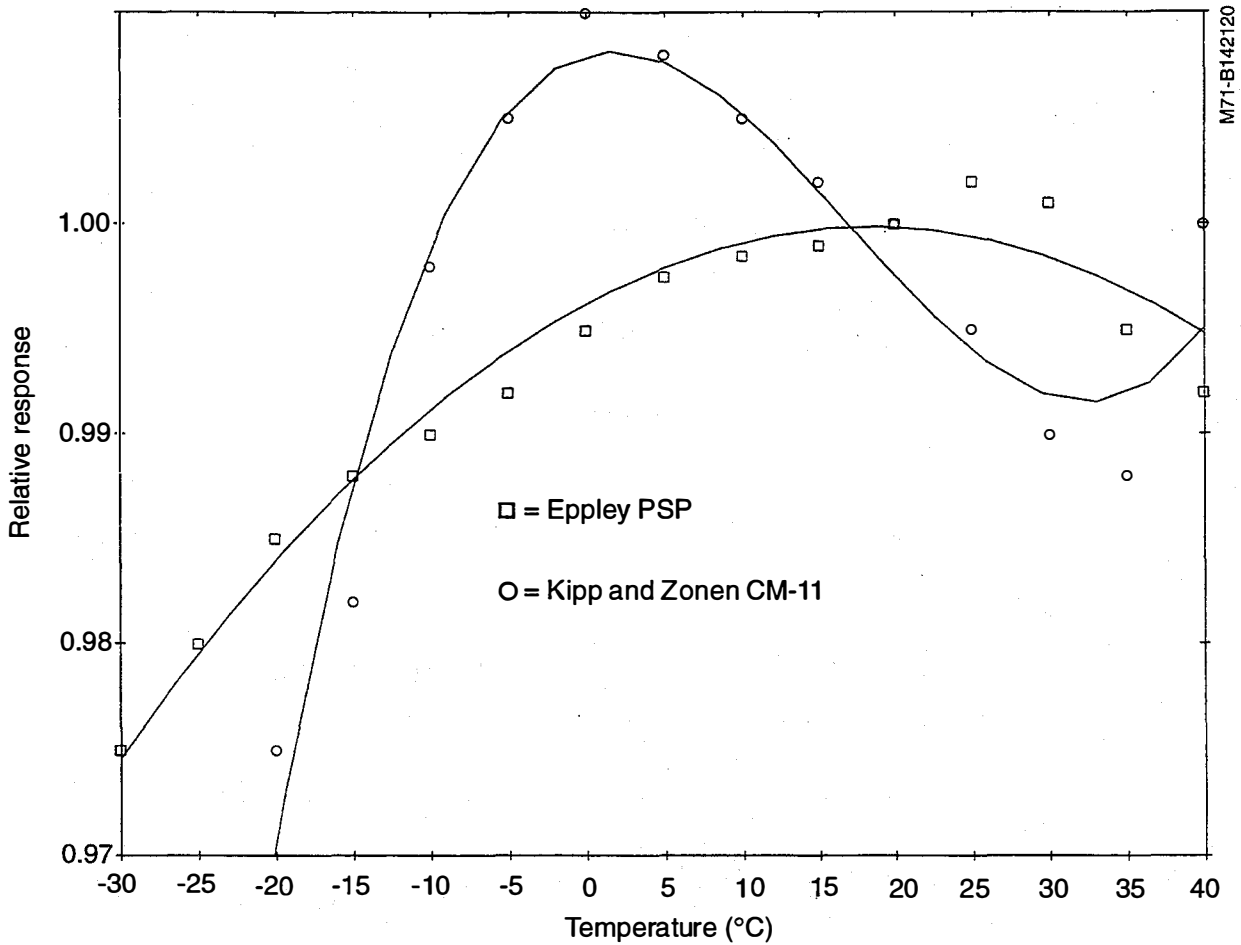
Figure 5.13. Typical Eppley PSP and Kipp and Zonen temperature response data

of applying a single temperature response correction is questionable, but can be informative, as long as the uncertainty in the correction is noted as well.

This section has introduced the most important characteristics of radiometers, which can have a significant impact on the uncertainty associated with radiometric performance in field-test data. The composite of geometrical and thermal responses, embodied to different degrees in separate instruments, often leads to confusing and incommensurate testing results by two (or more) parties on the same artifact (cell, module). These effects can result in apparent diurnal and seasonal patterns in PV performance, when in fact it is seasonal and diurnal radiometer performance that is being observed. In the next section we address the installation and operation of radiometric instrumentation in typical PV performance applications, with emphasis on how radiometer characteristics can affect data collection and interpretation.

5.2.4 Applications of Pyranometer Characterization Data

There are two applications for the characterization of pyranometers: (1) to develop an appropriate uncertainty statement for the radiometer based on the known characteristics, and those which are and are not accounted for, and (2) to correct pyranometer data to account for known (bias, type B, or systematic) error sources.
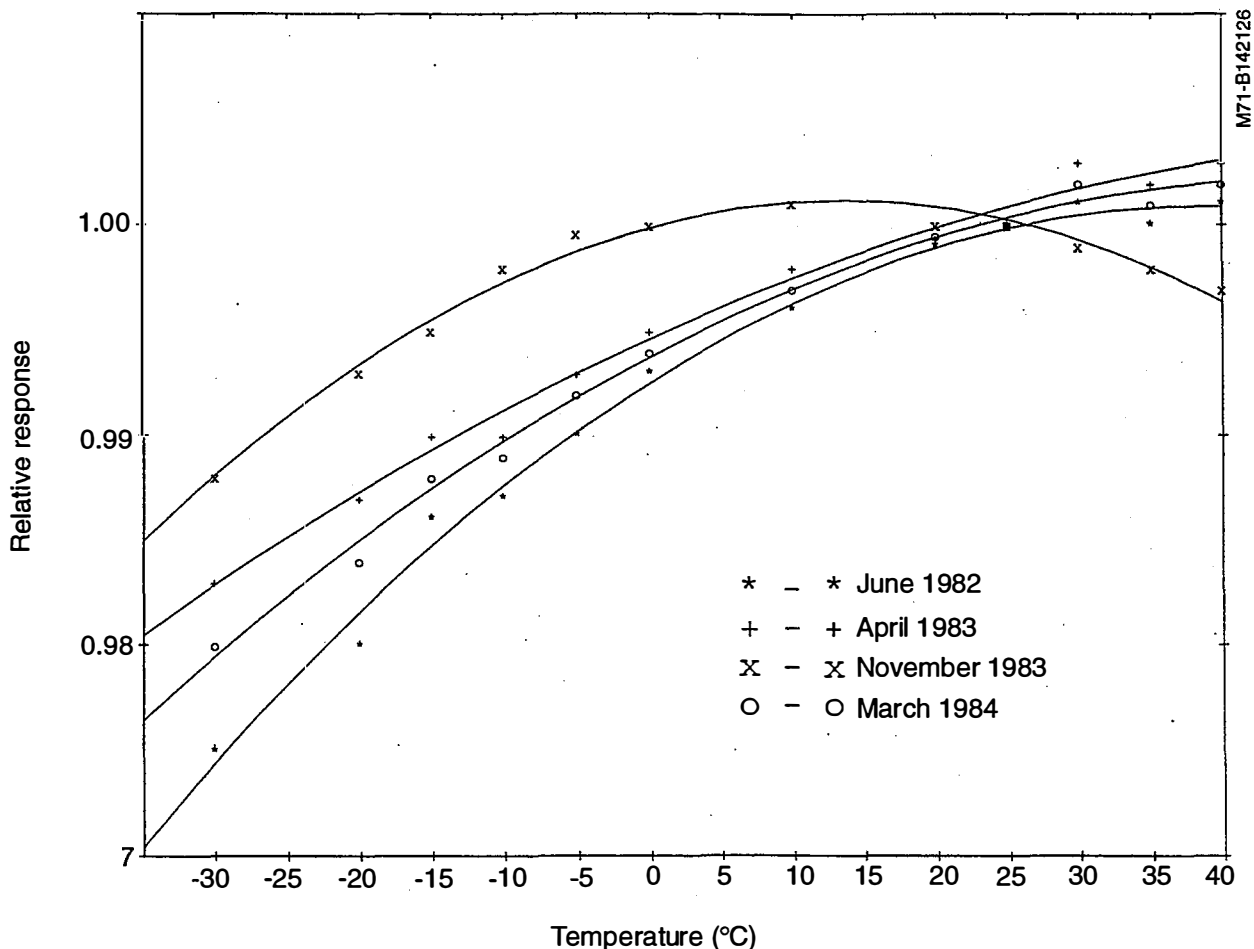
Figure 5.14. Repeated temperature response results for single pyranometer

55

In either case, the researcher or engineer must determine the required level of uncertainty to meet the objective of the measurements. The uncertainty statement determines the need to map out response characteristics of the pyranometer. The uncertainty envelope for a given sensor is based on environmental and installation parameters, as well as instrument responses. The uncertainty statement should identify both random (normally distributed, Gaussian) and systematic sources of error in the calibration, characterization, and measurement processes. These are usually seen as a small (0.5% or less) band of responsivity about some much larger distinct pattern of systematic variation(s) throughout an hour, day, month, year, etc., as seen in Figures 5.5 and 5.6 above.

In deciding what responsivity to use, the engineer and researcher has to answer several questions:

"What uncertainty envelope covers the testing conditions if a single responsivity is used?"

Looking at the total range (minimum to maximum) of responsivities for "reasonable" test conditions defined by the engineer, say, for restricted ranges of incidence angles, ambient temperatures, etc., will assist the engineer in computing this number.

If a single responsivity is used, what criteria are used to select it from the possible range of responsivities?"

Restricted test ranges mentioned above can be used to reduce uncertainty, but the selection criteria and rationale must be documented and reported. Table 5.2 displays how the responsivity of a pyranometer at tilt varies with incidence angle, along with the empirical random (standard deviation) uncertainty in the responsivity.

The overall mean responsivity for the 2735 data points is 8.824 uV/W/m^2 with a range of 5.7%. The distribution of the responsivities is not Gaussian. Overall uncertainty in the computation of **each individual data point** is 1.5% (due to the cavity, data logger, and incidence angle computation uncertainty). The range of variation within each 10 degree bin is about 2%, or half the uncertainty in using the mean response.

"If I apply correction factors and functions, will the uncertainty be reduced?"

Table 5.2. Typical Incidence Angle Dependence of Pyranometer Responsivity

Incidence Angle Bin Center (degrees)	Mean Responsivity uV/W/m^2	Range of Responsivity uV/W/m^2	Range as a Percent of Mean	Sample Size N
5	8.907	0.18	2.0	491
15	8.930	0.19	2.1	493
25	8.902	0.19	2.1	386
35	8.849	0.25	2.8	415
45	8.791	0.26	2.9	337
55	8.660	0.16	1.8	322
65	8.588	0.28	3.2	276
75	8.603	0.51	5.9	15

The characterization data must be examined to determine the uncertainty in the correction factors and or functions. If the uncertainty in the characterization factor/function is of the order of magnitude of the correction, applying the correction increases (by a factor of 2) rather than reduces the uncertainty in the radiometric data. This is the single most important reason that a cosine correction curve generated from a few days of calibration data is not recommended.

Especially if the geometrical response shows strong variation (greater than 2% over the course of a day) it is probable that the variation in the geometrical response through the year will be at least as great, if not greater, than that seen during the calibration period. Therefore, any correction applied will be accurate only for the conditions of calibration, and an additional bias error will be introduced under all other conditions.

The solution to this dilemma is complete characterization data relating the response of the radiometer to all solar geometry conditions to be encountered, including normal (or near normal) incidence (at latitude tilt, at noon true solar time, on those days when the solar declination is at or near zero), with an adequate uncertainty analysis to establish that the uncertainty in the correction factors needed is at least an order of magnitude less than the correction factor itself. That is:

> "Is the characterization of data uncertainty adequate to perform corrections that will reduce the uncertainty?"

As for techniques for applying corrections, either in the data collection, or post-collection data processing, classical methods of curve fitting, lookup-tables, and response function mapping may be used, as long as there are adequate resources to accomplish the corrections, and the techniques are well documented. For instance, the "look-up table" technique, in conjunction with linear regression on long-term drift data, was used in the synthetic calibration process for the 1961-1990 National Solar Radiation Data Base (NCDC, 1992; Maxwell, et al., 1995) to identify, quantify, and correct sometimes grievous (greater than 10%) cosine response and sensitivity changes embedded in the radiometric data from individual radiometers.

6. BROADBAND RADIOMETRY APPLICATIONS TO PV PERFORMANCE TESTING

This section addresses particular applications of solar spectral and broadband radiometry to activities usually engaged in during routine NREL PV indoor and outdoor PV module and system testing and monitoring activities.

6.1 Standardized Outdoor PV Module Performance

The NREL Standardized Outdoor Measurement System (SOMS) operated by the NREL Measurements and Characterization Center is designed to acquire PV performance data under conditions nearly equivalent to Standard Reporting Conditions described in the ASTM standards described earlier. The equipment and setup are similar to those in the Primary PV Reference Cell Calibration System, except testing is done with modules normal to the sun, with solar radiation measured by a pyranometer as shown in Figure 6.1. Radiometrically, the total and spectral irradiance are measured during each module test or test run using a complement of broadband radiometers and a Li-Cor LI-1800 spectroradiometer to scan the wavelength region from 300 nm to 1100 nm. The broadband instrumentation consists of a pyranometer for global irradiance, mounted as co-planar as practicable with the module under test.

From a Reference Meteorological and Irradiance Station (RMIS, described in Myers, 1993), direct normal irradiance measured by an Eppley Laboratories Hickey Frieden Absolute-Cavity Radiometer is monitored on a 5-second interval during the tests. Meteorological information such as relative humidity, barometric pressure, ambient temperature, wind speed, and wind direction are also recorded at the 5-second time resolution.
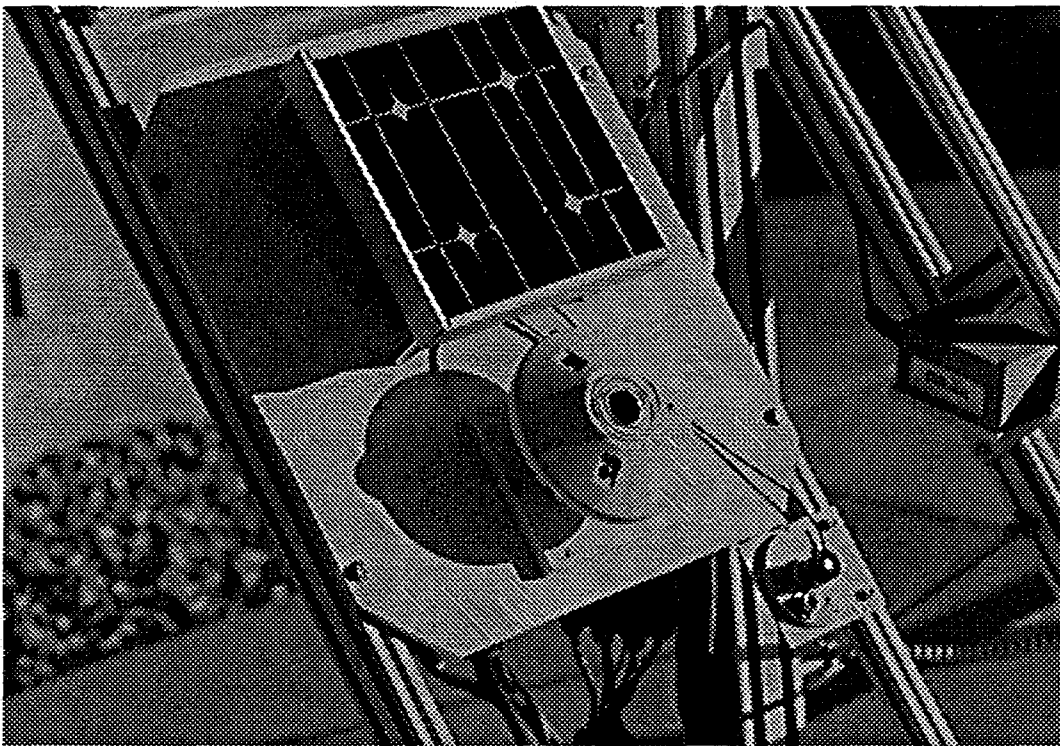
Figure 6.1. Pyranometer mount for NREL Standardized Outdoor Measurement System for PV Module Performance Testing

58

The module, spectroradiometer, and co-planar pyranometer are mounted on a platform that can be tilted and rotated in azimuth to obtain normal incidence radiation during the tests. The spectroradiometer is calibrated on a 6-month interval as described in the sections on spectral calibration above. Spectral data is extended to 4 micrometers using the techniques described in Osterwald (1988) and spectral mismatch with the ASTM standard global spectrum is computed, and the mismatch value is reported, but not applied to the data.

The pyranometer is calibrated at near normal incidence using the component summation technique, and a responsivity and uncertainty (generally about 1.5%) for that measurement configuration. The near-normal incidence responsivity can be used for off-normal measurements, with an expanded uncertainty range (approaching 3% for incidence angles greater than 50 degrees). A typical SOMS data report is shown in Appendix G.

These data are compared with indoor module performance data, obtained under controlled laboratory conditions using solar simulators that have had their spectral distributions characterized by the spectroradiometer systems described above. A typical indoor characterization report is shown in Appendix H.

6.2 PV System Performance Applications

Long-term PV system performance is carried out by monitoring both electrical performance parameters and the solar radiation resource used by the system. It is a challenge to the test engineer to identify and reduce the effects of measurement instrumentation variations in the observed data, so as to identify real changes in PV module and system performance.

One or more pyranometers monitors the solar radiation resource, which serves as the fuel for the PV system. The important issues of calibration and installation have been discussed above, but bear repeating here.

Seasonal variation in PV system performance can be highly correlated with temperature and changes in the solar geometry through the year. Therefore, accurate knowledge of radiometer geometrical response is required, so that instrumental effect can be removed, or accounted for (perhaps in an uncertainty error bar). If the sensor and module/system planes are not accurately aligned (or defined), significant errors may occur (greater than 5% for a 2 degree misalignment between planes) in the irradiance indicated by the radiometer and that seen and used by the modules, as shown in Emery et al., 1989b, and Myers et al., 1994. Misalignments such as this will appear as asymmetrical diurnal patterns of power production and or efficiency in clear day data, accounting properly for the azimuth of the system, if necessary.

Proper stand-off mounting distances to ensure good ambient air circulation and reduce the conduction of thermal energy to the body (reference junction) of the radiometer is important. It is important to employ the radiation shields or shades to shade the body of the pyranometer, and reduce temperature fluctuations in the body. It is advisable to provide shading "collars" to the bodies of radiometers installed at tilt, so that morning and afternoon sun does not induce large thermal gradients or transients in the body of the pyranometer.

The best mounting location of pyranometers with respect to large systems is an open question. It would be desirable to mount several radiometers at various locations to determine if there are any gross fluctuations or gradients across a large-area field. However, given the uncertainty envelopes demonstrated in Figures 5.7 to 5.9 above, on the order of 3%-5% agreement (between several radiometers within 50 to 100 feet of each other), it is clear that radiation differences of 5% or more would be needed to ensure a real difference was being observed. Convenient mounting locations on the edges or corners of the array, at least 6 feet or more above ground level, are generally used. Mounting tilted radiometers any lower would not be representative of the majority of the array elements, unless that is the way the array is constructed. The photos in Figure 6.2 show various mounting schemes used at the NREL PV Outdoor Test Facility.
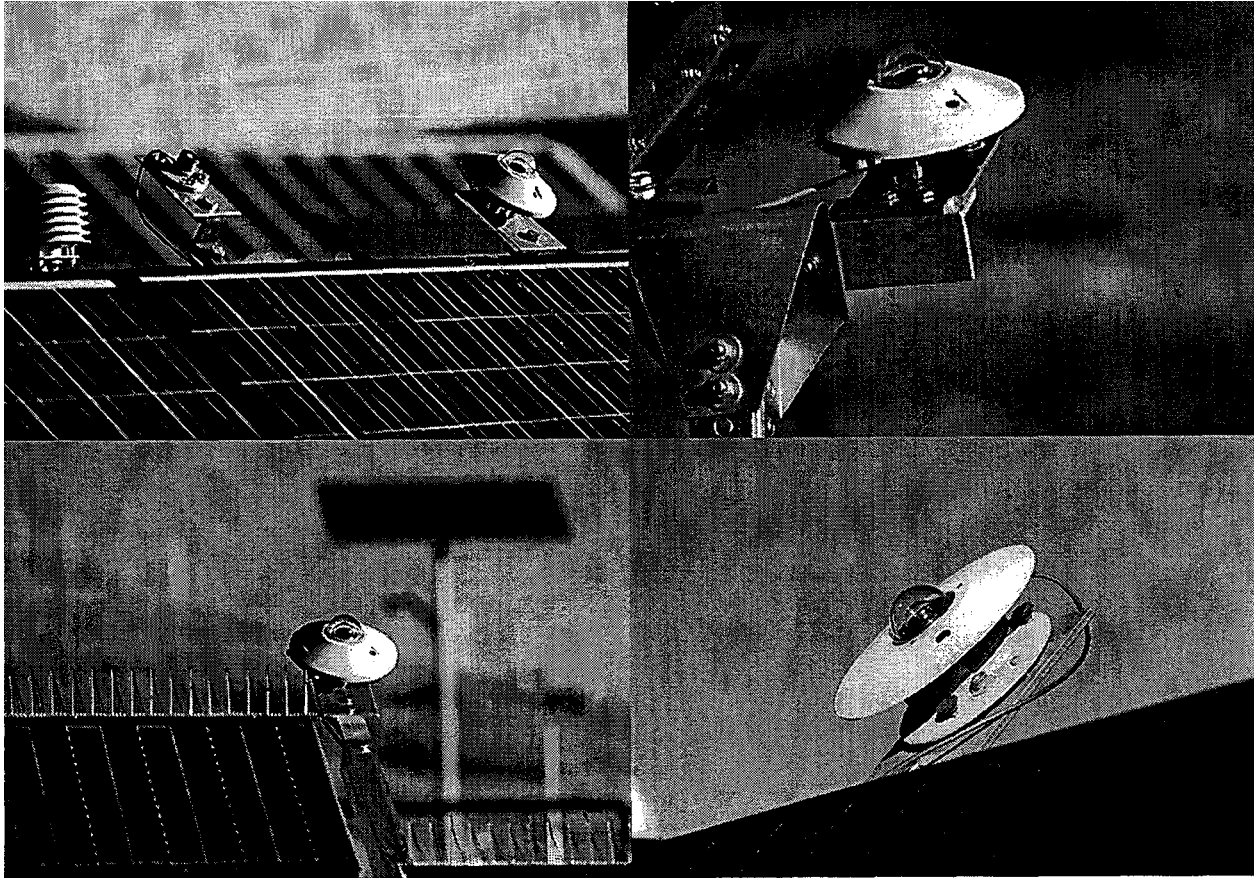
Figure 6.2. Pyranometer mounting schemes used at NREL Outdoor Test Facility

The accuracy of pyranometer data when processed using a single responsivity factor and without corrections for temperature and or geometrical response is typically 3% to 5%, and often exceeds 5% at incidence angles greater than 60 to 70 degrees, as shown in Figures 5.5 to 5.10 and Table 5.2 above.

For the highest accuracy, it is best to measure the direct beam irradiance and the diffuse irradiance on the plane of the array of system with a tilted pyranometer and shading disk arrangement. Using this approach, clear sky performance data can be as accurate as 2%, or 20 watts per square meter at standard reporting conditions of 1000 watts per square meter. The largest component is the probable 10% uncertainty in the diffuse measurements, which may range from 50 watts per square meter to 200 watts per square meter, or 5 watts per square meter to 20 watts per square meter absolute, while the direct beam error could be as small as 0.5% (5 watts per square meter) for a cavity pyrheliometer, or 1% (10 watts per square meter) for a thermopile pyrheliometer.

Accuracy for overcast days will be limited by the diffuse measurement also, but on the order of 10% at irradiance levels of about 200 watts per square meter, or an absolute error of 20 watts per square meter. Under partly cloudy conditions, the accuracy will be somewhere between these extremes, mainly due to the time constants of the radiometers with respect to both solar irradiance levels, and temperature fluctuations.

6.3 Module and System Energy Rating

The means of determining how much energy a module or system will generate when installed at a specific location has been at issue for the life of the terrestrial PV program. It is well known that PV modules and systems

60

performance at standard reporting conditions (SRC) is always higher than that experienced in the field. The PV design engineer has often used rules of thumb such as "de-rate to 80% of SRC," or "15% will be lost due to interconnect and Balance of System losses." But these rules of thumb apply to older conventional PV systems (crystal silicon, mainly), and appropriate experience with the newer emerging thin-film technology systems (Cadmium Telluride, Cadmium Indium Diselenide, etc.) and improved balance of system components (such as integral module and DC to AC conversion devices) is lacking.

The utility and consumer industries prefer a rating more representative of real-world performance, based on the variations in climate and solar resources at the locations of intended use. This means some standardized procedures, similar to those developed for PV performance testing at SRC, are needed. Radiometric data and measurements are an important component of developing, testing, and eventually implementing such a methodology. These components are highlighted in the diagram below, which illustrates all of the steps required to establish a projected energy output, say, in kilowatt-hours per day, for selected "solar climates." See Kroposki, 1996, for the details of the methodology. The scope of this guide covers the measurement instrumentation, calibration, and use needed to validate the methodology outlined in Figure 6.3.

6.4 Resource Assessment and Design Data

The designer of PV power systems often begins with a need for the amount of solar radiation available at the proposed system location. Depending on the application, the designer may be interested in various levels of time-resolved data, from historical hourly data to monthly mean daily totals, long-term averages or particular climatic patterns, such as morning and afternoon cloudiness. Obtaining the specific data required, assessing the quality of the data, and playing the data against the design parameters are beyond the scope of this manual. In the paragraphs below, we will discuss some available sources of data and models.
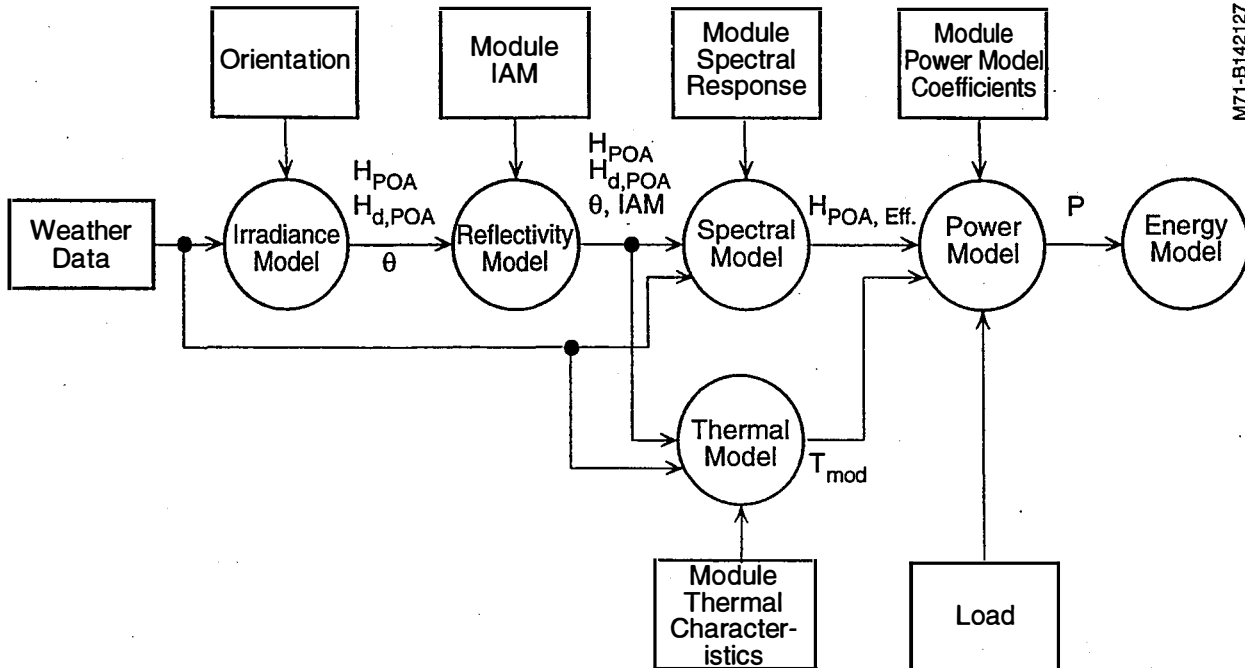
Figure 6.3. Flowchart of proposed methodology for rating PV modules for energy production

61

Figure 6.4 is an example of monthly and hourly average data typically recorded at a solar radiation monitoring station. Because of the simplicity of the measurements, the most common solar radiometric data available is global horizontal radiation. Maxwell (1988) developed a model for deriving direct normal irradiance from global horizontal data. Models for converting global and direct data to tilted surfaces have been developed by Perez, et al., (1990) (see Appendix K) and incorporated into PV system performance modelling routines, such as PVFORM (Menicucci and Fernandez, 1988). However, Maxwell (1990) and Marion (1995) have described the evaluation and generation of 30-year hourly solar meteorological data bases, sources of radiometric and meteorological data, and statistical summaries of so-called "typical" solar and meteorological data reflecting the most often requested system design data aids.

Figure 6.5 is an annotated example of the radiometric and meteorological data available in the 1961-1990 National Solar Radiation Data Base (NCDC, 1992) containing 30 years of hourly data for 239 U.S. sites. Many common statistical formats of radiometric data were computed at the same time that the NSRDB was assembled. These include "hourly statistics" (monthly hourly averages for each of the months in each of the 30 years and the entire 30-year period) and "daily statistics" (monthly daily totals for each month in the 30 years, and for the entire 30-year period) as well as persistence and quality statistics files.

The 30-year hourly data base is available on three CD-ROMs (as the Solar and Meteorological Surface Observation Network, SAMSON, data set) from the National Climatic Data Center (NCDC), 151 Patton Avenue, Asheville, NC, 28801-5001. (Customer Inquiries, 704-271-4800). The pre-computed statistical summaries (hourly, daily, persistence, and quality statistics), as well as custom-processed data files, are also available from the NCDC. Electronic versions of the NSRDB summary statistics files, as well as maps and other products (including some described below) are available over the Internet World Wide Web through the links appearing on the NREL Internet (World Wide Web) home page at **http://nrel.gov/**.

The NREL *Solar Radiation Data Manual for Flat-Plate and Concentrating Collectors* (Marion and Wilcox, 1994) provides the designer with summaries of the NSRDB data in the most commonly requested formats. Figure 6.6 is a sample page from that document. It depicts radiation resources from 1961 to 1990 for 15 different PV collector configurations. The hardcopy manual as well as magnetic media copies of the data are available from the NREL Document Distribution Center.

"Typical," "representative," or "average" years of hourly data for each of the 239 NSRDB sites have been derived from the NSRDB hourly data (Marion, 1995). These data are useful in modeling system design and relative performance comparisons for different systems.

The "typical" data sets are designated Typical Meteorological Year two (TMY2) data to differentiate them from earlier TMY data sets developed from older (1952-1976) Solar and Meteorological (SOLMET) data. TMY2 is available on a single CD-ROM disk from the NREL Document Distribution Center, or through the NREL Internet World Wide Web page mentioned above.

As there is never enough good-quality data, measured at the place of interest, for a long enough period of time, current efforts at generating solar radiation data on a 40-km grid are under way at the time of this writing (1997). Combining earth-orbiting satellite and ground observations, the techniques developed should be applicable to developing regional, national, and international maps and data sets for design engineers.

For simple modelling of the spectral distribution of natural sunlight, the clear sky model of Bird (Bird, 1982, Bird, 1984, Bird and Riordan, 1986), SPCTRL2, is often used for studying spectral effects. Glatefelter et al., 1987, used SPCTRL2 in conjunction with NSRDB data to evaluate spectral "climatic" impacts on thin-film PV performance. The SPCTRL2 spectral model was integrated into a spectral model addressing non-clear sky conditions by Nann and Riordan (1991), which is the spectral model component of the energy rating methodology

STATION: MONTE CRISTI, DOMINICAN REPUBLIC

May 1986

19.83 N Latitude   71.67 W Longitude   0. Meters AMSL   Time Zone   -4.0

GLOBAL SOLAR RADIATION ON A HORIZONTAL SURFACE
HOURLY INTEGRATED AND DAILY TOTALS
WATT-HOURS PER SQUARE METER

HOUR DAY	1	2	3	4	5	6	7	8	9	10	11	12	13	14	15	16	17	18	19	20	21	22	23	24	DAILY
1	1	1	1	1	1	1	26	194	419	501	840	974	958	863	840	729	377	192	58	1	0	1	1	2	6982
2	2	2	2	2	2	2	18	92	261	447	659	328	974	972	864	708	525	333	61	1	0	0	0	1	6257
3	2	2	2	2	2	2	14	111	237	491	692	576	978	947	863	717	452	369	121	1	0	0	0	0	6581
4	2	2	2	2	1	1	13	113	402	517	536	743	860	720	717	640	375	240	78	1	0	1	1	2	5967
5	2	2	2	2	2	2	19	165	330	413	589	877	759	674	415	425	433	122	37	0	0	0	1	2	5272
6	2	2	2	1	1	1	7	102	307	667	535	608	931	964	881	750	487	162	122	1	0	0	0	1	6533
7	1	1	1	1	1	2	31	201	390	666	842	944	1011	988	885	727	537	313	90	3	0	0	0	1	7634
8	2	2	2	2	2	1	28	198	423	479	806	937	993	974	885	736	538	216	76	1	0	0	0	0	7297
9	1	1	1	1	1	1	30	199	414	556	580	937	985	979	886	696	550	265	78	3	0	0	0	0	7165
10	0	1	1	1	1	1	21	171	405	623	798	935	983	966	922	526	367	312	79	1	0	0	0	0	7113
11	0	1	1	1	1	2	31	197	414	629	803	924	986	966	880	730	531	302	68	3	0	0	0	1	7467
12	1	1	1	2	2	2	12	87	158	217	337	619	673	967	839	712	493	229	77	1	0	0	0	0	5427
13	0	1	1	1	1	1	14	85	273	318	205	472	920	579	444	145	68	188	47	2	0	0	0	0	3764
14	1	1	1	1	1	1	30	248?	439?	622	630	926	928	975	883	722	525	258	129	1	0	0	0	0	7321-?
15	1	1	1	1	2	1	24	159	424	616	620	872	989	970	897	729	370	105	24	2	0	0	1	1	6809
16	1	1	1	2	2	2	35	122	316	344	478	324	623	953	865	660	520	250	80	3	0	0	0	0	5581
17	1	1	1	1	1	1	19	170	230	382	625	523	680	720	137	42	55	96	47	1	0	0	0	1	3733
18	1	1	1	1	1	1	10	196	145	169	496	944	980	744	644	567	519	287	71	5	0	0	1	1	5785
19	1	1	1	1	1	1	24	182	417	621	806	677	980	929	868	716	532	205	76	0	0	0	0	0	7037
20	0	0	0	0	0	0	32	194	414	565	817	802	979	942	861	697	486	291	41	1	0	0	0	0	7122
21	0	0	1	1	1	1	43	183	378	517	611	587	699	615	714	639	318	208	52	2	0	0	0	0	5568
22	0	1	1	1	0	1	26	200	411	580	585	890	755	949	832	668	431	166	58	1	0	0	0	0	6556
23	0	0	0	0	0	0	24	108	285	616	650	931	877	934	847	692	360	245	80	2	0	0	0	0	6651
24	0	0	0	0	0	0	17	162	341	588	766	795	866	804	697	612	497	247	53	1	0	0	0	0	6447
25	0	0	0	0	0	0	23	127	280	375	429	316	662	828	490	347	190	112	26	1	0	0	0	0	4206
26	0	0	1	1	1	1	13	50	151	297	264	307	257	235	290	136	97	58	23	1	0	0	0	0	2184
27	0	1	1	0	1	0	24	194	421	596	782	820	713	899	684	512	510	292	99	3	0	0	0	0	6551
28	0	0	0	0	0	0	32	195	413	583	496	269	404	317	883	655	531	312	99	3	0	0	0	0	5192
29	0	0	0	0	0	0	32	207	419	622	478	907	951	945	853	718	531	313	111	5	0	0	0	0	7091
30	0	1	1	1	1	0	30	207	423	586	669	MISS	MISS	950	868	721	529	214	42	1	0	0	0	0	5244-M
31	0	0	0	0	1	0	32	193	306	273	477	591	604	864	703	510	267	172	42	1	0	0	0	0	5037
AVG	1	1	1	1	1	1	24	162	343	499	610	712	832	843	753	599	419	228	69	2	0	0	0	0	6078
S D	1	1	1	1	1	1	9	48	90	139	168	234	190	191	198	191	146	78	29	1	0	0	0	1	1293
S/A	0	0	0	0	0	0	0.36	0.30	0.26	0.28	0.28	0.33	0.23	0.23	0.26	0.32	0.35	0.34	0.42	0.75	0	0	0	0	0.21
MIN	0	0	0	0	0	0	7	50	145	169	205	269	257	235	137	42	55	58	23	0	0	0	0	0	2184
MAX	2	2	2	2	2	2	43	248	439	667	842	974	1011	988	922	750	550	369	129	5	0	1	1	2	7634

Data Recovery: < 1% missing; < 1% exceeded the 15% QC threshold -- total 5-minute measurements, 8928.

NOTES: (1) "HOUR" means ending hour local standard time
    (2) "MISS" means more than 2 five-minute samples missing; NOT used in further summaries.
    (3) "M" means daily total is missing one or more hours; NOT used in monthly summary.
    (4) "N/A" means Not Applicable, since there are insufficient valid data available.
    (5) "?" means more than 2 five-minute samples failed the 15% QC threshold; USED in monthly summary.

Instrument: Eppley PSP   Serial Number: 25816F3
Calibration Constant: 9.800uV/Wm-2   Calibration Date: April, 1985

Figure 6.4. Sample monthly hourly average data report for radiometric data

Figure 6.5. Annotated sample of NSRDB hourly data format

Header Elements (For First Record of File)

Diagonal header labels: WBAN Number | City | State | Time Zone | Latitude | Longitude | Elevation

WBAN Number	City	State	Time Zone	Latitude	Longitude	Elevation
14920	LA CROSSE	WI	-6	N43 52	W091 15	205

Year	Month	Day	Hour	Extraterrestrial Horizontal Radiation	Extraterrestrial Normal Radiation	Global Horizontal Radiation	Source and Uncertainty Flags	Direct Normal Radiation	Source and Uncertainty Flags	Diffuse Horizontal Radiation	Source and Uncertainty Flags	Total Sky Cover	Opaque Sky cover	Dry Bulb Temperature	Dew Point Temperature	Relative Humidity	Atmospheric Pressure	Wind Direction	Wind Speed	Visibility	Ceiling Height	Present Weather	Precipitable Water	Broadband Aerosol Optical Depth	Snow Depth	Days Since Last Snowfall
61	1	1	1	0	0	0	?0	0	?0	0	?0	99	99	-4.4	-6.1	88	993	290	2.6	11.3	4000	0999999999	8	-9.999	0	0
61	1	1	2	0	0	0	?0	0	?0	0	?0	99	99	-5.0	-6.7	88	993	250	4.1	11.3	4000	0999999999	7	-9.999	0	0
61	1	1	3	0	0	0	?0	0	?0	0	?0	99	99	-5.0	-6.7	88	993	0	0.0	11.3	4030	0999999999	7	-9.999	0	0
61	1	1	4	0	0	0	?0	0	?0	0	?0	99	99	-5.0	-6.7	88	994	0	3.6	11.3	6050	0999999999	7	-9.999	0	0
61	1	1	5	0	0	0	?0	0	?0	0	?0	99	99	-4.4	-6.7	85	993	0	0.0	11.3	5020	0999999999	7	-9.999	0	0
61	1	1	6	0	0	0	?0	0	?0	0	?0	10	10	-5.0	-6.7	88	993	0	0.0	12.9	6050	0999999999	7	-9.999	0	0
61	1	1	7	0	0	0	?0	0	?0	0	?0	10	10	-5.6	-7.2	88	994	0	0.0	12.9	6010	0999999999	7	-9.999	0	0
61	1	1	8	36	354	7	G5	10	G4	6	G5	10	10	-5.0	-6.7	88	995	180	2.6	12.9	6010	0999999999	7	0.031	0	0
61	1	1	9	164	1415	40	G5	4	G4	40	G5	10	10	-4.4	-6.7	85	996	180	3.1	16.1	6010	0999999999	7	0.031	0	0
61	1	1	10	342	1415	85	G5	5	G4	84	G5	10	10	-3.9	-6.7	81	996	180	3.1	16.1	6010	0999999999	7	0.031	0	0
61	1	1	11	471	1415	167	G4	7	G4	165	G5	10	10	-3.3	-8.3	69	996	230	2.1	16.1	6010	0999999999	7	0.031	0	0
61	1	1	12	543	1415	171	G4	5	G4	169	G5	10	10	-3.3	-8.9	66	996	270	3.1	19.3	6010	0999999999	7	0.031	0	0
61	1	1	13	551	1415	155	G4	4	G4	153	G5	10	10	-3.3	-8.9	66	996	250	2.1	19.3	6010	0999999999	7	0.031	0	0.
61	1	1	14	496	1415	148	G4	4	G4	147	G5	10	10	-2.8	-7.2	72	996	290	3.6	19.3	6010	0999999999	7	0.031	0	0
61	1	1	15	381	1415	123	G4	4	G4	122	G5	10	10	-2.8	-7.2	72	996	0	0.0	19.3	6010	0999999999	7	0.031	0	0
61	1	1	16	215	1415	65	G5	2	G4	64	G5	10	10	-2.8	-7.2	72	996	180	2.1	19.3	6050	0999999999	7	0.031	0	0
61	1	1	17	66	731	15	G5	0	G4	15	G5	10	10	-2.8	-6.7	75	996	0	0.0	16.1	6050	0999999999	7	0.031	0	0
61	1	1	18	0	0	0	?0	0	?0	0	?0	10	10	-3.3	-6.1	81	996	0	0.0	16.1	6010	0999999999	8	-9.999	0	0
61	1	1	19	0	0	0	?0	0	?0	0	?0	10	10	-3.3	-6.1	81	996	0	0.0	8.0	6050	0999099999	8	-9.999	0	0
61	1	1	20	0	0	0	?0	0	?0	0	?0	10	10	-3.3	-5.6	85	996	180	2.1	4.0	7070	0999099999	8	-9.999	0	0
61	1	1	21	0	0	0	?0	0	?0	0	?0	10	10	-3.9	-4.4	96	997	180	2.1	3.2	5060	0999099999	8	-9.999	0	0
61	1	1	22	0	0	0	?0	0	?0	0	?0	99	99	-3.9	-4.4	96	997	180	1.5	3.2	5060	0999099999	8	-9.999	0	0
61	1	1	23	0	0	0	?0	0	?0	0	?0	99	99	-4.4	-4.4	100	997	0	0.0	3.2	4070	0999099999	8	-9.999	0	0
61	1	1	24	0	0	0	?0	0	?0	0	?0	99	99	-4.4	-4.4	100	997	0	0.0	3.2	4070	0999099999	8	-9.999	0	0

Data Elements (For All Except the First Record of File)

M19-G0923202

Variability of Latitude Fixed-Tilt Radiation — Monthly Radiation (kWh/m²/day) — 1961-1990 Average
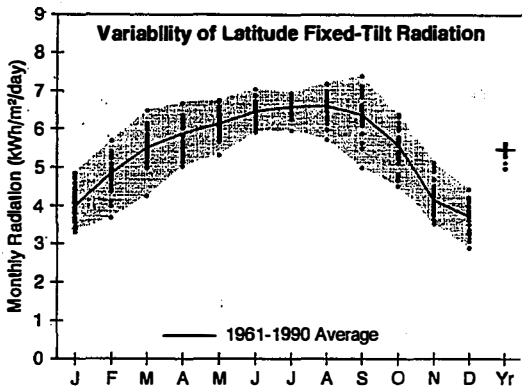
WBAN NO. 24027

LATITUDE: 41.60° N
LONGITUDE: 109.07° W
ELEVATION: 2056 meters
MEAN PRESSURE: 794 millibars

STATION TYPE: Secondary

Solar Radiation for Flat-Plate Collectors Facing South at a Fixed Tilt (kWh/m²/day), Uncertainty ±9%

Tilt (°)		Jan	Feb	Mar	Apr	May	June	July	Aug	Sept	Oct	Nov	Dec	Year
0	Average													
	Min/Max													
Latitude -15	Average	3.5	4.4	5.3	6.0	6.5	7.0	7.1	6.9	6.3	5.2	3.7	3.2	5.4
	Min/Max	2.9/4.1	3.4/5.1	4.2/6.1	5.2/6.8	5.7/7.2	6.4/7.7	6.4/7.5	5.9/7.5	5.0/7.2	4.2/5.9	3.2/4.4	2.6/3.8	5.0/5.7
Latitude	Average													
	Min/Max													
Latitude +15	Average	4.3	5.1	5.5	5.5	5.4	5.5	5.7	6.0	6.1	5.7	4.4	4.1	5.3
	Min/Max	3.5/5.3	3.7/6.0	4.1/6.5	4.6/6.2	4.7/5.9	5.1/6.0	5.2/6.0	5.2/6.5	4.8/7.1	4.6/6.5	3.7/5.4	3.1/4.8	4.8/5.6
90	Average													
	Min/Max													

Solar Radiation for 1-Axis Tracking Flat-Plate Collectors with a North-South Axis (kWh/m²/day), Uncertainty ±9%

Axis Tilt (°)		Jan	Feb	Mar	Apr	May	June	July	Aug	Sept	Oct	Nov	Dec	Year
0	Average													
	Min/Max													
Latitude -15	Average	4.3	5.6	6.9	8.0	9.0	10.0	10.1	9.6	8.5	6.8	4.6	3.9	7.3
	Min/Max	3.5/5.3	4.2/6.6	5.0/8.3	6.6/9.4	7.3/10.3	8.6/11.4	8.9/11.1	7.8/10.7	6.3/10.2	5.3/8.0	3.8/5.7	2.9/4.7	6.4/7.7
Latitude	Average													
	Min/Max													
Latitude +15	Average	5.0	6.1	7.0	7.7	8.2	9.0	9.2	9.0	8.5	7.2	5.1	4.6	7.2
	Min/Max	4.0/6.2	4.5/7.3	4.9/8.6	6.2/9.0	6.7/9.5	7.8/10.3	8.1/10.1	7.3/10.1	6.1/10.2	5.5/8.4	4.2/6.5	3.4/5.6	6.3/7.8

Solar Radiation for 2-Axis Tracking Flat-Plate Collectors (kWh/m²/day), Uncertainty ±9%

Tracker		Jan	Feb	Mar	Apr	May	June	July	Aug	Sept	Oct	Nov	Dec	Year
2-Axis	Average													
	Min/Max													

Direct Beam Solar Radiation for Concentrating Collectors (kWh/m²/day), Uncertainty ±8%

Tracker		Jan	Feb	Mar	Apr	May	June	July	Aug	Sept	Oct	Nov	Dec	Year
1-Axis, N-S Horiz Axis	Average	2.1	3.0	4.0	5.0	5.9	7.2	7.3	6.7	5.8	4.2	2.4	1.9	4.6
	Min/Max	1.5/3.0	2.1/3.9	2.2/5.1	3.4/6.4	4.0/7.6	5.3/8.9	6.0/8.6	4.7/8.2	3.5/7.7	2.8/5.5	1.7/3.3	0.9/2.6	3.6/5.2
1-Axis, N-S Tilt=Latitude	Average													
	Min/Max													
2-Axis	Average	3.5	4.2	4.8	5.4	6.1	7.4	7.5	7.1	6.6	5.5	3.7	3.3	5.4
	Min/Max	2.5/4.9	2.8/5.4	2.7/6.1	3.7/6.9	4.2/7.9	5.4/9.2	6.2/8.9	5.0/8.6	3.9/8.7	3.6/7.0	2.6/5.2	1.7/4.6	4.2/6.0

Average Climatic Conditions

Element	Jan	Feb	Mar	Apr	May	June	July	Aug	Sept	Oct	Nov	Dec	Year
Temperature (°C)													
Daily Minimum Temp	-11.6	-9.8	-6.3	-2.0	2.7	7.6	11.6	10.4	5.0	-0.4	-6.7	-11.2	-0.9
Daily Maximum Temp	-1.4	1.3	5.4	11.5	17.6	23.7	28.4	27.1	21.1	14.0	4.8	-0.7	12.7
Record Minimum Temp													
Record Maximum Temp													
HDD, Base 18.3°C	768	633	581	407	253	103	12	37	168	357	577	751	4647
CDD, Base 18.3°C	0	0	0	0	0	23	64	51	10	0	0	0	148
Relative Humidity (%)													
Wind Speed (m/s)													

245

Figure 6.6. Sample data summary page from *Solar Radiation Data Manual for Flat-Plate and Concentrating Collectors*

described in Section 6.3 above. A detailed description of the operation and use of these models is beyond the scope of this guide. However, we provide a QuickBasic© source code listing for SPCTRL2 in Appendix J.

6.5 Ultraviolet Radiometry for Module Reliability and Durability

Accelerated testing of photovoltaic modules for reliability and durability has resulted in the development of standardized test procedures (JPL, 1981, DeBlasio, Mrig, and Waddington, 1990) and consensus standards (IEEE, 1996) for evaluating the susceptibility of PV modules to known failure mechanisms. Such tests involve a sequence of physical and electrical stresses being placed on representative sample modules. These include high humidity, freeze/heat cycling, insulation (hi-potential) testing for leakage currents in wet and dry conditions, thermal cycling, dynamic and static load testing, hot-spot, bypass diode, and hail impact testing.

In addition to the above mechanical tests, electrical performance testing is required (to the requirements of ASTM E-1036, *Methods of Testing Electrical Performance on Nonconcentrator Terrestrial Photovoltaic Modules and Arrays using Reference Cells*. That standard requires the verification of so-called "standard reporting conditions" of 1000 watts per square meter, Air Mass 1.5 global reference spectrum (ASTM E-892), and module temperature of 25 °C. Whether performed indoors or outdoors, assurance of or translation to the required spectral test conditions requires accurate measurements of the spectral distribution of the natural or artificial (solar simulator) source used.

In addition to the mechanical stresses encountered in PV module field operations, there are the issues of material reliability, durability, degradation, and ultimate service lifetime related to the effects of damaging ultraviolet solar radiation in the natural environment. Accelerated testing of materials with respect to environmental parameters such as ultraviolet radiation, high ambient temperatures, extremes of climatic conditions, etc., have long been preformed by the materials and consumer product testing community (Nelson, 1990, Wineburg, 1992, Putman, 1993, Jorgenson, 1995 and 1996). Of particular interest is the synergism between ultraviolet radiation and other environmental stresses, as described by Czanderna (1990), Faiman (1994), and Czanderna and Pern (1996), on encapsulant materials and the layered structure of laminated and multijunction PV devices.

As of this writing (1997), the PV community is investigating the proper approach to accelerated ultraviolet testing of PV modules. National (ASTM) and international (ISO) consensus standards organizations are drafting and attempting to verify proposed testing procedures. Many of the approaches are based on similar testing procedures used in materials testing for other consumer products. Examples are ASTM G-7, *Practice for Atmospheric Environmental Exposure Testing of Non-Metallic Materials*, ASTM G-90, *Practice for Performing Accelerated Outdoor Weathering of Nonmetallic Materials using Concentrated Natural Sunlight*, as well as photovoltaic-specific standards such as ASTM E-1596 *Test Methods for Solar Radiation Weathering of Photovoltaic Modules*.

The issues being addressed in the development of these test methods and procedures that relate to ultraviolet radiation measurements include:

- What instruments are available to measure natural and artificial sources of UV radiation?

- What is the accuracy, stability, and dynamic range of UV-measuring radiometers?

- What is the variation in the natural UV radiation environment?

- What are the differences between natural and artificial UV radiation distributions?

- What are the correlations between artificial, accelerated UV exposure and natural solar UV exposure?

66

Typically, ultraviolet radiometers are designed as relatively broadband (20 nm to 200 nm bandwidths) filtered detector radiometers. The instruments require excellent blocking of longer wavelength radiation to avoid artificially high signals; temperature and temporal stability of filter transmission and bandwidth; and linearity, temperature, and temporal stability of detector responsivity. Appendix E list manufacturers of broadband radiometers that include UV radiometers of various designs.

The major source of uncertainty in accuracy of the UV radiometers in use today (above and beyond the geometrical and temperature effects as described for pyranometers above) is the variability in the terrestrial solar UV spectrum itself, as well as the variability in the spectral distributions of the artificial sources used. Figure 6.7 displays a plot of the variation in terrestrial UV spectral irradiance at various air masses along with a typical broadband (100 nm) UV radiometer spectral response.

It is clear that the calibration of the radiometer with spectral response shown in Figure 6.7 will vary with the spectral distribution used as a calibration source, and the distribution under which measurements are performed. In essence, there is spectral mismatch effect. Angstrom and Drummond (1962) describe how to account for this calibration issue in detail.
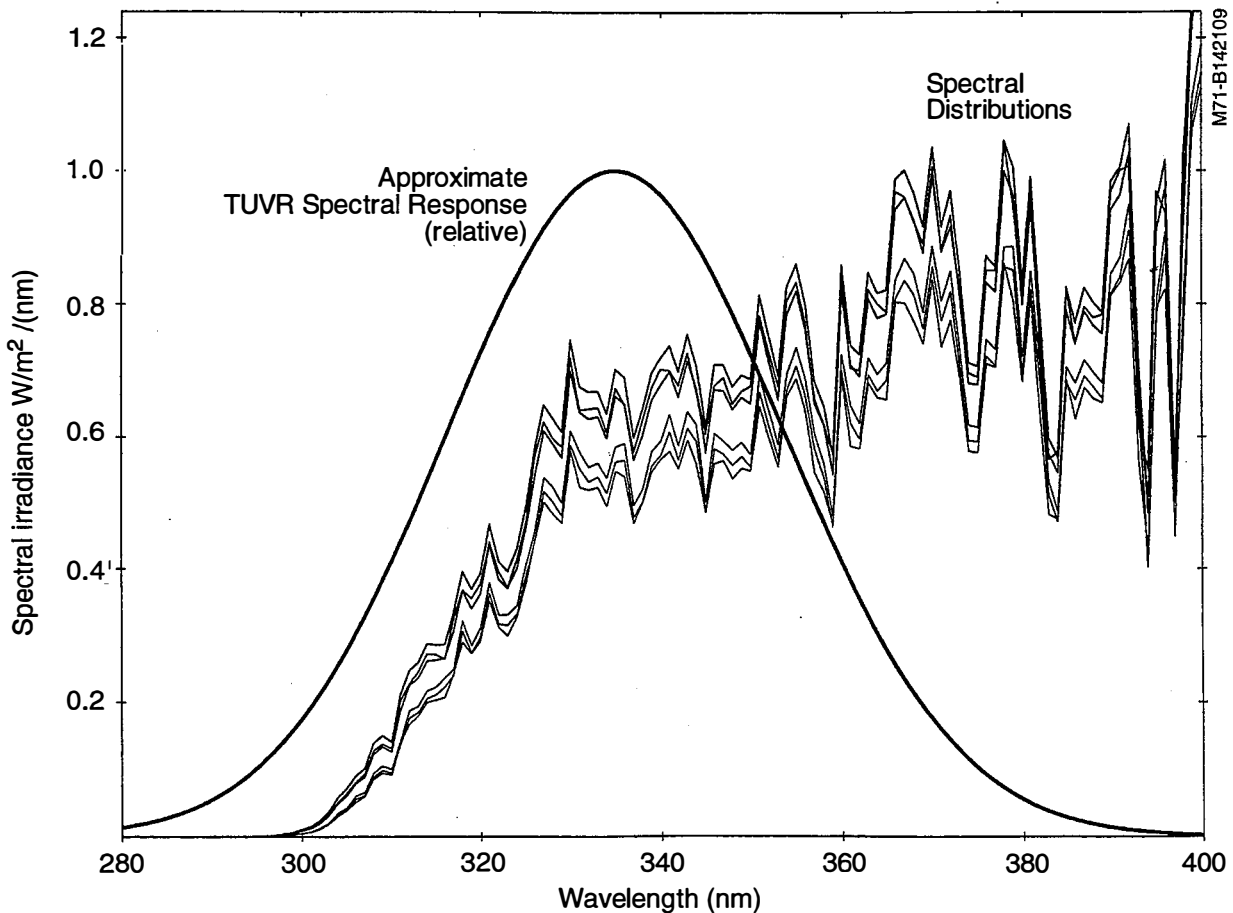
Figure 6.7. Variation in terrestrial solar UV spectral distribution as a function of changing air mass and a typical brandboad UV radiometer spectral response

At NREL, every attempt is made to calibrate such broadband instruments <u>using a source with a UV spectral</u> <u>distribution similar to that which the instrument is expected to measure.</u> We use our ultraviolet spectroradiometers to measure the absolute spectral distribution of the source (lamp or natural sunlight) and integrate the spectrum over the passband of the instrument to determine the irradiance magnitude. The output signal of the radiometer is then measured using the same source. The calibration factor is the integrated irradiance divided by the signal. A calibration of this sort for natural sunlight is the source of the curves shown in Figure 6.7.

There are the attendant uncertainties in the <u>spectral</u> measurements that contribute to uncertainty in the absolute spectral irradiance, especially where the slope of the solar UV curve is very steep, and small wavelength, spectroradiometer calibration source amplitude, and signal-to-noise problems can greatly amplify errors in the UV spectral measurement (see Stair, 1966, and Koskela, 1994).

Figure 6.8 displays a typical solar UV spectrum and UV lamp sources (UVB-313 and UVA, and a mixture of the two) used for accelerated UV weathering of materials. The same approach to calibrating UV radiometers for monitoring these sources as described above is recommended.
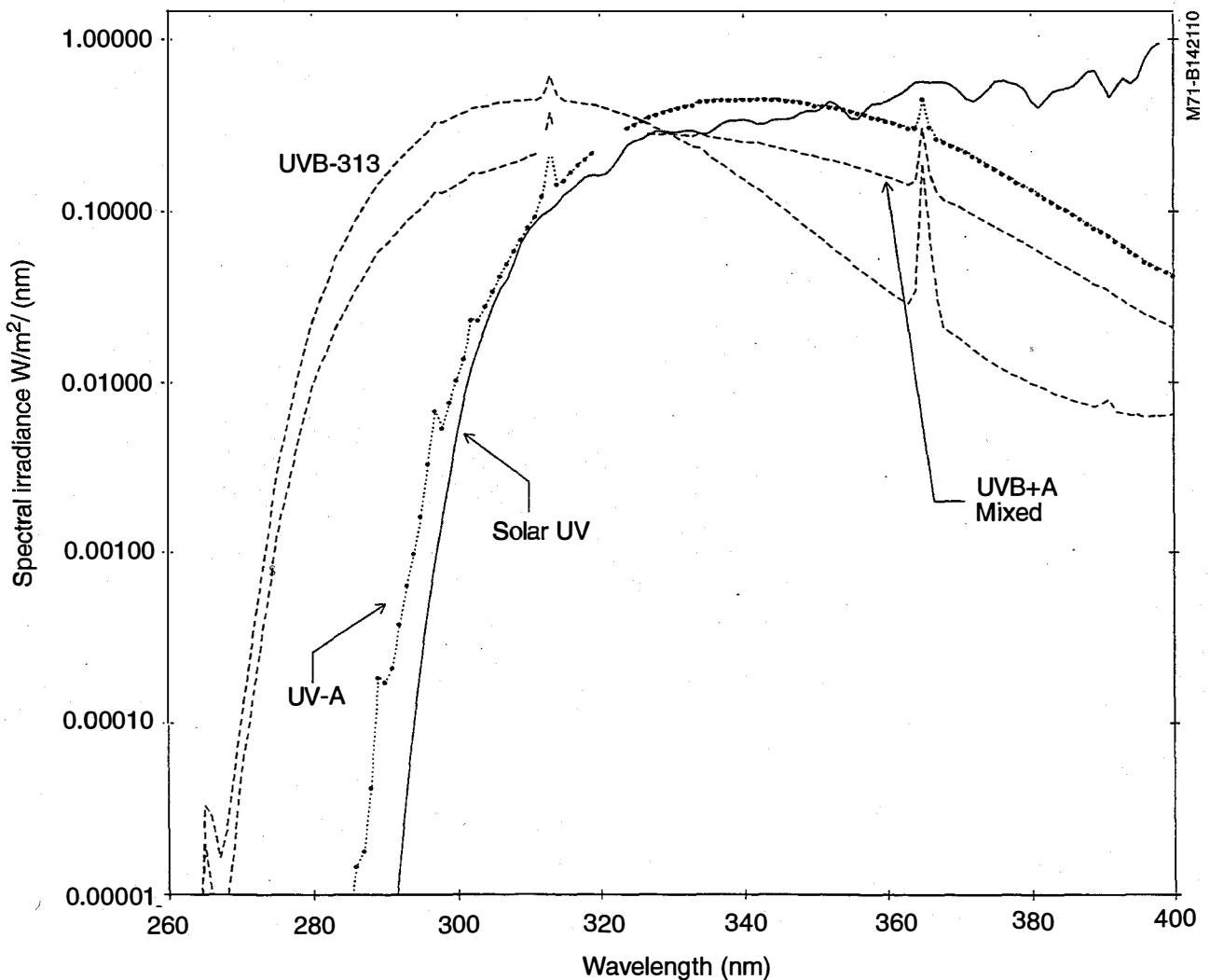
Figure 6.8. Typical solar terrestrial UV spectral distribution compared with several UV lamp sources used for accelerated UV exposure testing

Figure 6.8 also relates to the fourth and fifth bullets in the issues mentioned at the beginning of this section. As no UV photons are seen to reach the earth's surface below about 290 nm, the question arises: How meaningful is the exposure of materials to photons of shorter wavelength during artificial testing?

Secondly, as the spectral irradiance in the UV portion of the spectrum is such a strong function of wavelength, it is clear that the natural exposure time equivalent to the accelerated exposure will be a strong function of the wavelength as well. This is illustrated in Table 6.1, where an acceleration factor is shown for various 20 nm wavelength intervals when a UVB-313 lamp (spectral distribution peaking at 313 nm) is compared to a typical, clear, noontime solar terrestrial spectrum over similar wavelength intervals.

Note that the ratio of the two integrated spectral irradiances is about 0.5, indicating the total irradiance from the lamp is about half that of the natural irradiance over the range from 270 nm to 400 nm. However, the acceleration in the band from 270 to 320 nanometers is approximately ten to one over the natural exposure. Using only the total irradiance values, an error of 100*(10/0.5)= 2000% occurs in estimating the exposure acceleration at the shorter wavelengths.

How to correlate the degradation effects, the acceleration factors, and the predictions of material performance lifetime in these circumstances are current (1997) topics of research in the PV, as well as materials testing, community. The research and manufacturing communities are encouraged to participate, and remain aware of the latest results of these efforts.

Table 6.1. Wavelength Dependent Acceleration Factor of UVB-313 Lamp

Spectral Range (nanometers)	UVB-313 W/sq m (In Band)	Midday Sun W/sq m (in band)	Acceleration with Respect to Sun
270-320 (mostly 313)	12.3	1.3	9.5
320-340	9.3	6.7	1.4
340-360	2.3	10.0	0.23
360-380	1.0	13.0	0.07
380-400	0.1	16.0	0.06
TOTAL	25.0	46	0.5(*)

(*) The ratio of the lamp total to the natural irradiance total over the wavelength band from 270 nm to 400 nm

7.0 CONCLUSIONS AND ACKNOWLEDGEMENTS

We have discussed the fundamentals of optical radiometric measurements, instrumentation, and data that the photovoltaic research and engineering communities often ask NREL to explain, or describe. From the intricacies of spectral measurements to the installation of pyranometers and availability of solar resource data to the engineer, there will be continual improvements in the science of radiometry applied to PV research, development, and testing. We hope the interested researcher and engineer can use this document to further both the scientific understanding and economic viability of benign alternative energy systems that convert the sunlight that sustains all life on earth to meet the energy needs of our nation and civilization in the future.

8.0 REFERENCES AND BIBLIOGRAPHY

Angstrom, A., (1930), "On the Atmospheric Transmission of Sun Radiation II," *Geophysika Annaler,* Vol. 12, pp. 130-159.

Angstrom, A. K. and A. J. Drummond, (1962), "Fundamental Principles and Methods for the Calibration of Radiometers for Photometric Use," *Applied Optics*, Vol. 1, No. 4, July 1962.

Bird, R.E., (1982), "Terrestrial Solar Spectral Modeling," *Solar Cells*, Vol. 7, pp. 107-111.

Bird, R.E., (1984), "A Simple Spectral Model for Direct Normal and Diffuse Horizontal Irradiance," *Solar Energy*, Vol. 20, pp. 461-471.

Bird, R.E. and C. Riordan, (1986), "Simple Solar Spectral Model for Direct and Diffuse Irradiance on Horizontal and Tilted Planes at the Earth's Surface for Cloudless Atmospheres," *Journal of Climate and Applied Meteorology*, Vol. 22, pp. 87-97.

Cole, E.H. and L.G. Smeins, (1989), "Signal Processing Electronics for MAMA Detector Readout" In *Ultraviolet Technology III*, Proceedings of the Society of Photo-Optical Instrumentation Engineers, Vol. 1158.

Correll, D.L., C.O. Clark, B. Goldberg, V.R. Goodrich, D.R. Hayes, Jr., W.H. Klien, and W.P. Schecher, (1992), "Spectral Ultraviolet-B Radiation Fluxes at the Earth's Surface: Long Term Variations at $39°$ N $77°$ W," *Journal of Geophysical Research*, Vol. 97, No. D7, pp. 7579-7591, May 20, 1992.

Coulson, K., (1978), *Solar and Terrestrial Radiation*, Academic Press, New York, NY.

Czanderna, A.W., "Possible Causes of EVA Degradation in PV Modules," Photovoltaic Module Reliability Workshop, October 25-26, 1990, Lakewood, CO. SERI/CP-4079, National Renewable Energy Laboratory, Golden, CO.

Czanderna, A.W. and J. Pern, (September 1996), *Solar Energy Materials and Solar Cells*, Vol. 43.

DeBlasio, R., L. Mrig, and D. Waddington, January 1990, "Interim Qualification Tests and Procedures for Terrestrial Photovoltaic Thin-Film Flat-Plate Modules," SERI/TR-213-3624, National Renewable Energy Laboratory, Golden, CO.

Driscoll, W.G. and W. Vaughn (eds.), (1978), *Handbook of Optics*, sponsored by the Optical Society of America. McGraw Hill Book Company, New York, NY.

Drummond, A.J. and H.W. Greer, (1966), "An Integrating Hemisphere for the Calibration of Meteorological Pyranometers," *Solar Energy*, Vol. 10, No.4.

Emery, K. and C. Osterwald, (1987), "Measurement of Photovoltaic Device Current as a Function of Voltage, Temperature, Intensity and Spectrum," *Solar Cells*, 21, p. 313.

Emery, K.A., C.R. Osterwald, L.L. Kazmerski, and R.E. Hart, (1988), "Calibration of Primary Terrestrial Reference Cells When Compared with Primary AM0 Cells," Proceedings of 8th European Photovoltaic Conference, Florence, Italy, May 9-12, 1988, pp. 64-68.

Emery, K.A., C.R. Osterwald, T.W. Cannon, D.R. Myers, J. Burdick, T. Glatfelter, W. Czubatyj, and J. Yang, (1988), "Methods for Measuring Solar Cell Efficiency Independent of Reference Cell or Light Source," Proceedings of 18th IEEE Photovoltaic Specialists Conference, Las Vegas, Nevada, p. 623.

Emery, K. and C. Osterwald, (1989), "Solar Cell Calibration Methods," *Solar Cells,* 27, p. 445.

Emery, K.A., D. Waddington, S. Rummel, D.R. Myers, T.L. Stoffel, and C.R. Osterwald, (1989a), "SERI Results from the PEP 1987 Summit Round Robin and a Comparison of Photovoltaic Calibration Methods," SERI TR/213-3472, Solar Energy Research Institute, Golden, CO.

Emery, K.A., C.R. Osterwald, S. Rummel, D. R. Myers, T.L. Stoffel, and D. Waddington, (1989b), "A Comparison of Photovoltaic Calibration Methods," Proceedings of 9th European Photovoltaic Solar Energy Conference, Freiburg, FRG, September 1989.

Emery, K., C.V. Wells, and C.R. Osterwald, (1990), "Uncertainty Analysis of Photovoltaic Efficiency Measurements," Proceedings of 19th IEEE Photovoltaic Specialists Conference, May 1990, New Orleans, Louisiana, p. 153.

Emery, K.A. and C.R. Osterwald, (1990), "PV Performance Measurement Algorithms, Procedures, and Equipment," Proceedings of 21st IEEE Photovoltaic Specialists Conference, May 21-25, Orlando, Florida, pp.1068-1073

Estey, R. and C.H. Seaman, (1981), "Four Absolute Cavity Radiometer (Pyrheliometer) Intercomparisons at New River, AZ," JPL Publication 81-60, Jet Propulsion Laboratory, Pasadena, CA.

Faiman, D., (1994), "Efficiency Loss Associated with EVA Laminate Browning Observed in the Negev Desert," Photovoltaic Performance and Reliability Workshop, September 21-23, 1994, Lakewood, Colorado. NREL/CP-411-7414, National Renewable Energy Laboratory, Golden, CO.

Field, H., (1995), "Radiometry for Characterizing Photovoltaic Devices in the Laboratory," in PV Radiometric Workshop Proceedings, NREL CP/411-20008. National Renewable Energy Laboratory, Golden, CO.

Field, H. and K. Emery, (1993), "An Uncertainty Analysis of the Spectral Correction Factor," Proceedings of 23rd IEEE Photovoltaic Specialists Conference, Louisville, Kentucky, pp. 1180-1187.

Frohlich, C., (1985), "Radiometry at PMOD and the World Radiometric Reference," in *Advances in Absolute Radiometry,* Proceedings of an International Meeting, June 24-25, 1985. P. Foukal (ed.) Atmospheric and Environmental Research, Inc., Cambridge, MA.

Frohlich, C. and G.E. Shaw (1980), "New Determination of Rayleigh Scattering in the Terrestrial Atmosphere," *Applied Optics,* 19, p. 1773.

Glatfelter, T., J. Burdick, J. Fournier, and L. Boman, (1987), "Outdoor Performance Measurements Comparing Different Types of Multiple-Cell a-Si Alloy Photovoltaic Devices: Dependance on Spectral Context," Proceedings of 19th IEEE Photovoltaic Specialists Conference, May 1987, New Orleans, Louisiana, p. 194.

Hammond, H.K. III, and H.L. Mason, (1971), NBS Special Publication 300, Vol. 7, *Precision Measurement and Calibration Radiometry and Photometry.* National Bureau of Standards, Washington, D.C.

Hill, A.N., (1966), "Calibration of Solar Radiation Equipment in the U.S. Weather Bureau," *Solar Energy*, Vol. 10, No. 4, 1966.

Hutley, M.C., (1982), Diffraction Gratings, Academic Press, New York, NY.

IEEE, (1996), Institute of Electrical and Electronic Engineers, IEEE 1262, "IEEE Recommended Practice for Qualification of Photovoltaic (PV) Modules."

Iqbal, M., (1983), *An Introduction to Solar Radiation*, Academic Press, New York, NY.

Jorgenson, G., (1995), "An Overview of Service Lifetime Prediction (SLP)," Photovoltaic Performance and Reliability Workshop, September 7-8, 1995, Golden, Colorado. NREL/CP-411-20379, National Renewable Energy Laboratory, Golden, CO, November 1995.

Jorgenson, G., (October 1996), "Accelerated Environmental Testing for Screening and Lifetime Prediction," Photovoltaic Performance and Reliability Workshop, September 4-6, 1996, Golden, Colorado. NREL/TP-411-21760. National Renewable Energy Laboratory, Golden, CO.

JPL, (1981), "Block V Solar Cell Module Design and Test Specification for Intermediate Load Applications," JPL 5101-161. Jet Propulsion Laboratory, Pasadena, CA.

Kendall, J.M., (1969), "Primary Absolute Cavity Radiometer," NASA Technical Report 32-1376. National Aeronautics and Space Administration, Jet Propulsion Laboratory, Pasadena, CA.

Kendall, J.M. and C.M. Berhdahl, (1970), "Two Blackbody Radiometers of High Accuracy," *Applied Optics*, Vol. 12, pp. 1089-1091.

King, D.L., B.R. Hansen, and J.K. Jackson, (1993), "Sandia NIST Reference Cell Calibration Procedure," Proceedings of 23rd IEEE Photovoltaic Specialists Conference, Louisville, Kentucky, pp.1095-1101.

Koskela, T., (1994), "The Nordic Intercomparison of Ultraviolet and Total Ozone Instruments at Izana from 24 October to 5 November 1993. Final Report," Meteorological Publication No. 27, Finnish Meteorological Institute, Helsinki.

Lipson, S.G. and H. Lipson, (1969), *Optical Physics*, Cambridge at the University Press, New York, NY.

Marion, W., (1995), "New Typical Meteorological Years and Solar Radiation Data Manual," in PV Radiometric Workshop Proceedings, NREL CP/411-20008. National Renewable Energy Laboratory, Golden, CO.

Marion, W. and S. Wilcox, (1994), *Solar Radiation Data Manual for Flat-Plate and Concentrating Collectors*, NREL/TP-463-5607. National Renewable Energy Laboratory, Golden, CO.

Maxwell, E.L., (1987), "A Quasi-physical Model for Converting Hourly Global Horizontal to Direct Normal Insolation," Proceedings of 1987 Annual Conference of The American Solar Energy Society, Portland, Oregon, July 11-16, 1987, p. 35.

Maxwell, E.L., (1990), "Producing a 1961-1990 Solar Radiation Data Base for the United States," Proceedings of 1990 Annual Conference of the American Solar Energy Society, Austin, Texas, March 19-20, 1990, p. 165.

Maxwell, E.L., W.F. Marion, D.R. Myers, M.D. Rymes, and S.M. Wilcox, (1995), *NSRDB Volume 2, Final Technical Report National Solar Radiation Data Base (1961-1990)*, NREL/TP-463-5784. National Renewable Energy Laboratory, Golden, CO.

McCluney, R., (1994), *An Introduction to Radiometry and Photometry*, Artech House, Inc., Norwood, MA.

Michalsky, J.J., L.C. Harrison, and W.E. Berkheiser III, (1992), "Cosine Response Characteristics of Radiometric and Photometric Sensors," Solar '92, Proceedings of 1992 Annual Conference of the American Solar Energy Society, June 15-18, Cocoa Beach, Florida, pp. 335-339.

Myers, D.R., (1988), "Uncertainty Analysis for Thermopile Pyranometer and Pyrheliometer Calibrations Performed by SERI," SERI/TR-215-3294. Solar Energy Research Institute, Golden CO.

Myers, D.R., (1989a), "Estimates of Uncertainty for Measured Spectra in the SERI Spectral Solar Radiation Data Base," *Solar Energy*, Vol. 43, No. 6, 1989, pp. 347-353.

Myers, D.R., (1989b), "Application of a Standard Method of Uncertainty Analysis to Solar Radiometer Calibrations," Proceedings of 1989 Annual Conference of the American Solar Energy Society, Denver, Colorado, June 19-22, 1989, pp. 445-449.

Myers, D.R., (1990), "A Description of the Solar Radiometer Calibration (RADCAL) Process at SERI," Proceedings of 1990 Annual Conference of the American Solar Energy Society, Austin, Texas, March 19-22, 1990, p. 171.

Myers, D.R., (1992), "Solar Radiation Instrumentation and Measurement Methods for PV Performance Testing," Proceedings of the PV Reliability and Performance Workshop, Golden, Colorado, September 16-18, 1992. NREL CP/411-5184. National Renewable Energy Laboratory, Golden, CO.

Myers, D.R., (1995a), "SYNCAL: Synthetic Calibration of Solar Radiation Data," Chapter 7 of Volume II of National Solar Radiation Data Base Documentation, NREL/TP-463-5784. National Renewable Energy Laboratory, Golden, CO.

Myers, D.R., (1995b), "PV Solar Radiometric Issues and Needs," in Proceedings, Photovoltaic Performance and Reliability Workshop, NREL CP-411-20379. National Renewable Energy Laboratory, Golden, CO.

Myers, D. and T.W. Cannon, (1995c), "Photovoltaic Solar Radiometric Measurements and Evaluation," in 13th NREL Photovoltaics Program Review, Lakewood, Colorado, 1995. American Institute of Physics Conference Proceedings, Series No. 353, H. Ullal, E. Witt (ed.).

Myers, D.R., T.W. Cannon, and D. Trudell, (1993), "Radiometric Measurements for PV Performance Characterization," NREL/TP-411-5757, in Proceedings of PV Reliability and Performance Workshop, Golden, Colorado, September 8-10, 1993, NREL/CP-410-6033. National Renewable Energy Laboratory, Golden, CO.

Myers, D.R., T.W. Cannon, and D. Trudell, (1994), "Technical Overview of Photovoltaic Solar Radiation Research at NREL," 12th Annual NREL PV Program Review, Denver, Colorado, October 13-15, 1993. American Institute of Physics Conference Proceedings, Series No. 306, H. Ullal and E. Witt (ed.).

Myers, D.R., K. Emery, and T.L. Stoffel, (1989), "Uncertainty Estimates for Global Solar Irradiance Measurements Used to Evaluate PV Device Performance," *Solar Cells*, 27, 1989, p. 456.

Nann, S. and C.J. Riordan, (1991), "Solar Spectral Irradiance under Clear and Cloudy Skies: Measurements and a Semi-Empirical Model," *Journal of Applied Meteorology*, Vol. 30, No. 4, April 1991.

National Aeronautics and Space Administration, (1977), "Terrestrial Photovoltaic Measurement Procedures," ERDA/NASA/1022-77/16 TM 73702. NASA Lewis Research Center, Cleveland, Ohio.

National Climatic Data Center, (1992), *NSRDB Volume 1, Users Manual National Solar Radiation Data Base (1961-1990)*, National Climatic Data Center, Asheville, NC.

Nelson, D., R. Haas, J. Deluisi, and G. Zerlaut, (1987), "Results of the NRIP 7 Intercomparison 18-21 Nov 1985," NOAA Technical Memorandum ERL-ARL-161. National Oceanic and Atmospheric Administration, Environmental Research Laboratories, Air Resources Laboratory, Silver Spring, MD.

Nelson, W., (1990), *Accelerated Testing Statistical Models, Test Plans, and Data Analysis*, Wiley Series in Probability and Mathematical Statistics, John Wiley and Sons, New York, NY.

Nicodemus, F.E., (1976), "Self Study Manual on Optical Radiation Measurements, Part 1, Concepts, Chapters 1 to 3," NBS Technical Note 910-1. Optical Physics Division, National Bureau of Standards, Washington, D.C.

Nicodemus, F.E., (1977), "Self Study Manual on Optical Radiation Measurements, Part 1, Concepts, Chapter 6," NBS Technical Note 910-3. Optical Physics Division, National Bureau of Standards, Washington, D.C.

Nicodemus, F.E., (1978)," Self Study Manual on Optical Radiation Measurements, Part 1, Concepts, Chapters 4 and 5," NBS Technical Note 910-2. Optical Physics Division, National Bureau of Standards, Washington, D.C.

Nicodemus, F.E., (1979), "Self Study Manual on Optical Radiation Measurements, Part 1, Concepts, Chapters 7, 8, and 9," NBS Technical Note 910-4. Optical Physics Division, National Bureau of Standards, Washington, D.C.

Nicodemus, F.E., (1982), "Self Study Manual on Optical Radiation Measurements, Part III, Applications, Chapter 1," NBS Technical Note 910-5. Optical Physics Division, National Bureau of Standards, Washington, D.C.

Osterwald, C.R., (1992), "Results of 1992 ASTM Cell and Module Measurement Intercomparison," Proceedings of 23rd IEEE Photovoltaic Specialists Conference, Louisville, Kentucky, pp. 1102-1106.

Osterwald, C.R., K.A. Emery, D.R. Myers, and C.J. Riordan, (1988), "Extending the Range of Silicon-based Direct Beam Solar Spectral Radiometer Measurements," Proceedings of 20th IEEE Photovoltaic Specialists Conference, Las Vegas, Nevada, pp. 1246-1250.

Osterwald, C.R., K.A. Emery, D.R. Myers, and R.E. Hart, (1990), "Primary Reference Cell Calibrations at SERI, History and Methods," Proceedings of 21st IEEE Photovoltaic Specialists Conference, May 21-25, 1990, Orlando, Florida, pp. 1062-1067.

Putman, W., (1993), "Outdoor and Indoor UV Exposure Testing," Photovoltaic Performance and Reliability Workshop, September 8-10, 1993, NREL CP-410-6033, National Renewable Energy Laboratory, Golden, CO.

Reda, I., (1996), "Calibration of a Solar Absolute Cavity Radiometer with Traceability to the World Radiometric Reference," NREL TP/463-20619. National Renewable Energy Laboratory, Golden, CO.

Sandstrom, J.D., (1967), "A Method for Predicting Solar Cell Current-Voltage Characteristics as a Function of Incident Solar Intensity and Cell Temperature," Proceedings of 6th IEEE Photovoltaic Specialists Conference, Vol. II, pp. 199-208.

Sommerfeld, A., (no date), *Lectures on Theoretical Physics*, Volume IV, Optics. Academic Press, New York, NY.

Stair, R., (1966), "The Measurement of Solar Radiation with Principal Emphasis on the Ultraviolet Component," *Air and Water Pollution International Journal*, Vol. 10, pp. 665-688 (Reprinted in NBS SP-300).

Stoffel, T.L., (1996), "Radiometric Instrumentation for PV System Performance Monitoring," in PV Radiometric Workshop Proceedings, NREL/CP-411-20008. National Renewable Energy Laboratory, Golden, CO.

Thekaekara, M.P., (1973), "Extraterrestrial Solar Spectral Irradiance," in *The Extraterrestrial Solar Spectrum*, A.J. Drummond and M.P. Thekaekara (ed.), Institute of Environmental Sciences, Mount Prospect, IL.

Walker, J.H., R.D. Saunders, and A.D. Hattenburg, (1987), "Spectral Irradiance Calibrations," National Bureau of Standards (Now National Institute of Standards and Technology), Special Publication 250-20. National Institute of Standards and Technology, Gaithersburg, MD.

Walker, J.H, R.D. Saunders, J.K. Jackson, K.D. Mielenz, (1991), "Results of a CCPR Intercomparison of Spectral Irradiance Measurements by National Laboratories," *Journal of Research of the National Institute of Standards and Technology*, Vol. 96, No. 6, pp. 647-668.

Weinburg, J. (1992), "Can You Believe Lifetime Projections from Accelerated Life Testing?", Photovoltaic Performance and Reliability Workshop, September 16-18, 1992, Golden, Colorado. SERI/CP-411-5184, National Renewable Energy Laboratory, Golden, CO.

Wells, C.V., (1995), "Optical and Solar Radiometry Standards and Traceability," in PV Radiometric Workshop Proceedings, NREL CP/411-20008. National Renewable Energy Laboratory, Golden, CO.

Willson, R.C., (1973), "Active Cavity Radiometer," *Applied Optics*, Vol. 12, pp. 810-817.

World Meteorological Organization, (1983), *Guide to Meteorological Instruments and Methods of Observation WMO No. 8*, Secretariat of the World Meteorological Organization, Geneva, Switzerland.

Zerlaut, G.A., (1986), "Solar Radiometry Instrumentation, Calibration Techniques, and Standards," *Solar Cells*, Vol. 18, pp. 189-203.

Further Reading:

Bird, R., (1989), "Spectral Terrestrial Solar Radiation," in *Solar Resources*, R. Hulstrom (ed.). Massachusetts Institute of Technology, p. 309.

Bird, R.E., C.J. Riordan, and D.R. Myers, (1987), "Investigation of a Cloud Cover Modification to SPCTRL2, SERI's Simple Model for Cloudless Sky Spectral Solar Irradiance," SERI TR/215-3038. Solar Energy Research Institute, Golden, CO.

Cannon, T.W., (1988), "The Atmospheric Optical Calibration System," Proceedings of 20th Photovoltaic Specialists Conference, Las Vegas, Nevada, May 1988, p. 1258.

Cannon, T.W. and Roland L. Hulstrom, (1989), "A Multi-Channel Radiometer for Measurement of the Optical Properties of the Atmosphere," Society of Photo-Optical Instrumentation Engineers (SPIE), *Optical Radiation Measurements II*, Vol. 1109, p. 152.

DeBlasio, R., D. Waddington, and L. Mrig, (1987), "Outdoor Performance Stability Testing of Thin Film Devices," *Solar Cells*, 21, p. 343.

Emery, K.A., D.R. Myers, and S. Rummel, (1988), "Solar Simulation, Problems and Solutions," Proceedings of 20th IEEE Photovoltaic Specialists Conference, Las Vegas, Nevada, pp. 957-962.

Fabick, L.B., R. Rifai, K. Mitchell, T. Woolston, and J. Canale, (1987), "Outdoor Module Testing and Comparison of Photovoltaic Technologies," Proceedings of 19th IEEE Photovoltaic Specialists Conference, May 1987, New Orleans, Louisiana, p. 182.

Fernandez, J.P., (1987), "Techniques for Assuring Quality of Photovoltaic Performance Data," Proceedings of 1987 Annual Conference of the American Solar Energy Society, Portland, Oregon, July 11-16, 1987, p. 162.

Flowers, E., (1984), "An Open Letter on Pyranometer Calibration," Symposium Proceedings, Recent Advances in Pyranometry. SMHI Noorkoping, Sweden. IEA Task IX, Solar Radiation and Pyranometer Studies. Atmospheric Environment Service, Downsview, Ontario, January 1984.

Flowers, E.C., and N.F. Helfert, (1965), "Laboratory and Field Investigations of Eppley Radiation Sensors," *Monthly Weather Review*, Vol. 94, No. 4, pp. 259-264.

Flowers, E.C. and Maxwell, E.L., (1985), "Characteristics of Network Instruments," Proceedings of the Photovoltaics and Insolation Measurements Workshop, June 30-July 3, 1985, Vail, Colorado, SERI/CP-215-2773. Solar Energy Research Institute, Golden CO.

Gonzales, M.C. and J.J. Caroll, (1989), "Influence of Atmospheric Conditions on the Performance of Photovoltaic Systems," Proceedings of 1989 Annual Conference of the American Solar Energy Society, Denver, Colorado, June 19-22, 1989, p. 337.

Hoffman, J.E. and R. Yenemandra, (1987), "Construction Experience with a 300 kW Photovoltaic Plant in Austin, Texas," Proceedings of 1987 Annual Conference of the American Solar Energy Society, Portland, Oregon, July 11-16, 1987, p. 121.

Hoffman, J.E. and R Yenemandra, (1989), "Analysis of the 1989 Performance of Austin's 300 Kilowatt Photovoltaic Plant," Proceedings of 1989 Annual Conference of the American Solar Energy Society, Denver, Colorado, June 19-22, 1989, p. 48.

Hulstrom, R.L., (1986), "A Summary of the Photovoltaics and Insolation Measurements Workshop Panel Results," *Solar Cells*, 18, p. 393.

Hulstrom, R.L. and Theodore W. Cannon, (1987), "Atmospheric Optical Calibration System for Outdoor Photovoltaic Measurements," *Solar Cells*, 21, p. 329.

Hulstrom, R.L., C. Riordan, and T. Cannon, (1989), "Spectral Solar Radiation Data Base, Models, and Instrumentation," *Solar Cells*, 27, p. 279.

Jennings, C. and C. Whitaker, (1990), "PV Module Performance Outdoors at PG&E," Proceedings of 21st IEEE Photovoltaic Specialists Conference, May 1990, Orlando, Florida, p. 1023.

Latimer, J.R., (1966), "Calibration Program of the Meteorological Service," *Solar Energy*, Vol. 10, No. 4.

Liedquist, L., (1984), "Pyranometer Characterization Measurement Methods at the Statens Provingsanstalt, Boras, and Results from IEA Measurements in BORAS," Symposium Proceedings, Recent Advances in Pyranometry. SMHI Noorkoping, Sweden. IEA Task IX, Solar Radiation and Pyranometer Studies. Atmospheric Environment Service, Downsview, Ontario, January 1984.

Marion, W. and D.R. Myers, (1992), "A Comparison of Data from SOLMET/ERSATZ and the National Solar Radiation Data Base," NREL/TP-463-5118. National Renewable Energy Laboratory, Golden CO.

Mohr, A.J., D.A. Dahlberg, and I. Dirmhim, (1979), "Experiences with Tests and Calibrations of Pyranometers for a Mesoscale Solar Irradiance Network," *Solar Energy*, Vol. 22, pp. 197-203.

Mueller, R., (1987), The Calculated Influence of Atmospheric Conditions on Solar Cell I_{sc} Under Direct and Global Irradiances," Proceedings of 19th IEEE Photovoltaic Specialists Conference, May 1987, New Orleans, Louisiana, p. 166.

Nast, P.M., (1983), "Measurements on the Accuracy of Pyranometers," *Solar Energy*, Vol. 31, No. 3.

Perez, R., J. Doty, B. Bailey, and R. Stewart, (1992), "Experimental Evaluation of a Photovoltaic Simulation Program," Proceedings of 1992 Annual Conference of the American Solar Energy Society, Cocoa Beach, Florida, p. 46.

Randall, C.M., and R. Bird, (1989), "Insolation Models and Algorithms," in *Solar Resources*, R. Hulstrom (ed.). Massachusetts Institute of Technology, p. 61.

Riches, M.R., T.L. Stoffel, and C.V. Wells, (1981), *International Energy Agency Conference on Pyranometer Measurements*, March 16-29, 1981, Boulder, Colorado, SERI/TR-642-1156. Solar Energy Research Institute, Golden, CO.

Riordan, C., T. Cannon, and R. Hulstrom, (1987), "Spectral Solar Irradiance Data and Instrumentation for PV Device Measurements and Analysis," Proceedings of 19th IEEE Photovoltaic Specialists Conference, May 1987, New Orleans, Louisiana, p. 160.

Riordan, C.J., T.W. Cannon, D.R. Myers, and R.E. Bird, (1988), "Solar Irradiance Models, Data, and Instrumentation for PV Device Performance Analysis," Proceedings of 18th IEEE Photovoltaic Specialists Conference, Las Vegas, Nevada. p. 957.

Riordan, C., R. Hulstrom, T. Cannon, and D. Myers, (1991),"Solar Radiation Research for Photovoltaic Applications," *Solar Cells*, Vol. 30, p. 489.

Riordan, C.R., D.R. Myers, M.D. Rymes, R.L. Hulstrom, W. Marion, C. Jennings, C. Whitaker, (1989), "Spectral Solar Radiation Data Base at SERI," *Solar Energy*, Vol. 42, No. 1, pp. 67-79.

Riordan, C., D.R. Myers, and R. Hulstrom, (1990), "Solar Spectral Radiation Data Base Documentation and Users Manual," Vols. I and II, SERI/TR-215-3513A/B. Solar Energy Research Institute, Golden, CO.

Smith, Z.E. and S. Wagner, (1987), "Spectral Dependence of Performance in Multijunction Amorphous Silicon Solar Cells," 19th IEEE Photovoltaic Specialists Conference, May 1987, New Orleans, Louisiana, p. 204.

Stoffel, T., D. Myers, M. Rymes, S. Wilcox, (1991), "Solar Radiation Monitoring, and Overview," Proceedings of the 1991 International Solar Energy Society Conference, Denver, Colorado, October 1991.

Van Wely, F.L. and G.J. VandenBrink, (1984), "Presentation of Some IEA Instrument Characteristics," Symposium Proceedings, Recent Advances in Pyranometry. SMHI Noorkoping, Sweden. IEA Task IX, Solar Radiation and Pyranometer Studies. Atmospheric Environment Service, Downsview, Ontario.

Zerlaut, G., (1989), "Solar Radiation Instrumentation," in *Solar Resources*, R. Hulstrom, (ed.). Massachusetts Institute of Technology, p. 173.

Zerlaut, G.A., (1985), "Solar Radiometry Instrumentation, Calibration Techniques, and Standards," Proceedings of the Photovoltaics and Insolation Measurements Workshop, June 30-July 3, 1985, Vail, Colorado, SERI/CP-215-2773. Solar Energy Research Institute, Golden CO.

Zerlaut, G. and J.D. Maybee, (1984), "The Intercomparison of Pyranometers at Horizontal, 45 Degree Tilt, and Normal Incidence," Symposium Proceedings, Recent Advances in Pyranometry. SMHI Noorkoping, Sweden. IEA Task IX, Solar Radiation and Pyranometer Studies. Atmospheric Environment Service, Downsview, Ontario.

APPENDIX A
Manufacturers of Spectroradiometric Instrumentation

APPENDIX A
Manufacturers of Spectroradiometric Instrumentation

1. Li-Cor Incorporated
    P.O. Box 4425
    Lincoln, NE 68594
    Telephone 1-800-447-3576
    Fax (402) 467-2819

2. Optronic Laboratories
    4470 35th Street
    Orlando FL
    Telephone 1-800-899-3171
    Fax (407) 648-5412

3. Oriel Corporation
    250 Long Beach Boulevard
    PO Box 872
    Stratford, CT 06497
    Telephone (203) 377-8282
    Fax (203) 378-2457

4. Gamma Scientific
    8581 Aero Drive
    San Diego, CA 92123
    Telephone (619) 279-8034
    Fax (619) 576-9286

5. International Light, Inc.
    17 Graf Road
    Newburyport MA 01950
    Telephone (508) 465-5923
    Fax (508) 462-0759

6. Instruments SA, Inc.
    J-Y Optical Systems Division
    6 Olsen Avenue
    Edison, NJ 08820-2419
    Telephone (908) 494-8860
    Fax (908) 494-8796

7. Geophysical and Environemental
    Research Corporation
    1 Bennet Common
    Millbrook, NY 12545
    Telephone (914) 677-6100
    Fax (914) 677-6106

8. Acton Research Corporation
    525 Main Street
    P.O. Box 2215
    Acton MA 01720
    Telephone (508) 263-3584
    Fax (508) 263-5086

9. SPEX Industries, Incorporated
    3880 Park Avenue
    Edison, NJ 08820
    Telephone (908) 549-7144
    Fax (908) 549-5125

10. Analytical Spectral Devices, Inc.
    4760 Walnut Street
    Suite 105
    Boulder, CO 80301
    Telephone (303) 444-6522
    Fax (303) 444-6825

APPENDIX B
List of ASTM and ISO Photovoltaic-Related Standards

APPENDIX B
List of ASTM and ISO Photovoltaic-Related Standards

Designation	Title
E-927-91	Specification for Solar Simulation for Terrestrial Photovoltaic Testing
E-948-83	Test Methods for Electrical Performance of Non-Concentrator Terrestrial Photovoltaic Cells using Reference Cells
E-973-91	Test Method for Determination of the Spectral Mismatch Parameter Between a Photovoltaic Device and a Photovoltaic Reference Cell
E-1021-84	Methods for Measuring the Spectral Response of Photovoltaic Cells
E-1036-85	Methods of Testing Electrical Performance on Nonconcentrator Terrestrial Photovoltaic Modules and Arrays using Reference Cells
E-1038-93	Test Method for Determining Resistance of Photovoltaic Modules to Hail Impact with Propelled Ice Balls
E-1039-85	Method for Calibration and Characterization of Nonconcentator Terrestrial Photovoltaic Cells Under Global Irradiation
E-1040-93	Specification for Physical Characteristics of Non-Concentrator Terrestrial Photovoltaic Reference Cells
E-1125-86	Test Method for Calibration of Primary Non-Concentrator Terrestrial Photovoltaic Reference Cells Using a Tabular Spectrum
E-1143-87	Test Method for Determining the Linearity of a Photovoltaic Device with Respect to a Test Parameter
E-1171-93	Test Method for Photovoltaic Modules in Cyclic Temperature and Humidity Environments
E-1328-90	Terminology Relating to Photovoltaic Energy Conversion
E1362-90	Test Method for the Calibration of Nonconcentrator Terrestrial Photovoltaic Secondary Reference Cells
E-1462-94	Test Methods for Insulation Integrity and Ground Path Continuity of Photovoltaic Modules

List of ASTM and ISO Photovoltaic-Related Standards

Designation	Title
E-1524-93	Test Method for Saltwater Immersion and Corrosion Testing of Photovoltaic Modules for Marine Environments
E-1596-94	Test Methods for Solar Radiation Weathering of Photovoltaic Modules
E-1597-94	Test Method for Saltwater Pressure Immersion and Temperature Testing of Photovoltaic Modules for Marine Environments
E-842	Method for Transfer of Calibration from Reference to Field Radiometers
E-891-87	Terrestrial Direct Normal Spectral Irradiance Tables for Air Mass 1.5
E-892-87	Terrestrial Solar Spectral Irradiance Tables at Air Mass 1.5 for 37° Tilted Surface
(In Draft)	Standard Tables for Reference Solar Spectral Irradiance at Air Mass 1.5: Direct Normal and Hemispherical for a 37° Tilted Surface
E-941-	Method for Calibration of a Pyranometer Using a Pyrheliometer
E-490-73	Solar Constant and Air Mass Zero Solar Spectral Irradiance Tables
G-138-96	Standard Test Method for Calibration of a Spectroradiometer Using a Standard Source of Irradiance
ISO 9060	Solar energy-Specification of and classification of instruments for measuring hemispherical solar and direct solar radiation
ISO 9845	Solar energy-Reference solar spectral irradiance at the ground at different receiving conditions-Part I: Direct normal and hemispherical solar irradiance for air mass 1.5
ISO 9847	Solar energy-Calibration of field pyranometers by comparison to a reference pyranometer
ISO 9846	Solar energy-Calibration of a pyranometer using a pyrheliometer
ISO TR-9901	Technical Report:Solar energy-Field pyranometers-Recommended practice for use

APPENDIX C
Instructions for the Use of Standards of Spectral Irradiance

APPENDIX C
Instructions for the Use of Standards of Spectral Irradiance

General

These instructions cover the use of tungsten-filament quartz-halogen lamps issued as standards of total and spectral irradiance. The lamps employed are commercial G.E. type FEL 1000-watt lamps having a tungsten coiled-coil filament enclosed in a small quartz envelope. (Figure 1) The lamp bases have been converted to a medium bipost base which can be used with a kinematic lamp holder (see Figure 2), allowing the lamps to be removed and replaced repeatably in the same position.

Spectral irradiance values are given for the wavelength range of 0.25 to 2.5μm. The radiant intensity of the entire lamp as mounted in the manner prescribed below is measured and reported. The total irradiace of these lamps is based on the radiance of a blackbody as defined by the Stefan-Boltzman radiation law. The assigned values of total irradiance have estimated uncertainties of ±1%.

The spectral irradiance from these lamps over the wavelength range of 250nm to 1600nm is based on the National Bureau of Standards 1973 scale of spectral irradiance. The reported uncertainty in the NBS 1973 irradiance scale along with the uncertainty associated with the transfer from the NBS standard to the issued 1000-watt lamp standard are given below:

Wavelength (nm)	NBS Uncertainty (%)	Transfer Uncertainty (%)
250	2.5	1.0
350	1.4	0.7
450	1.2	0.4
555	1.0	0.4
655	0.75	0.4
800	0.9	0.5
1300	0.7	0.5
1600	0.7	0.5

Values of spectral irradiance from 1600nm to 2500nm are based on the NBS 1963 spectral irradiance scale. The 1963 scale has an uncertainty

of ±3% over the range of 1600 to 2500nm. The corresponding trans-
fer uncertainty to the 1000-watt standards is ±.5% over this wave-
length region.

Alignment and Orientation

The following procedure should be carefully followed when setting
up the standard for calibration purposes:

Required Lamp Position

1) The lamp should be positioned with its identification number
   facing away from the measuring instrument. The base pins
   shall be perpendicular to the optical axis of the measuring
   instrument and equidistant from the optical axis. The lower
   end of the base's positive post shall be 3.75 inches (appro-
   ximately 9.54cm) below the horizontal plane containing the
   optical axis. The plane tangent to the side of both posts
   facing the measuring instrument shall be set at 50cm away
   from the limiting aperture of the test instrument.

Discussion of Lamp Positioning

2) The lamp is aligned relative to the measuring instrument by
   defining the postion of the lamp base pins (not the filament)
   relative to the optical axis of the instrument. It is pos-
   sible for the center of the filament to be several millimeters
   off of the optical axis with the lamps correctly aligned.
   There can be many ways to accomplish this alignment of the
   lamp. The NBS alignment procedure is given in the following
   section as an example of one way to achieve a satisfactory
   alignment of the test lamp.

   ### The NBS   Procedure

3) Figure 4 shows a mock-up of the alignment equipment used at
   NBS, and indicates how the lamp holder is aligned. The first
   step in the alignment procedure is to define the optical axis
   of the measuring instrument. To define one point on the axis,
   a glass microscope slide containing a fiducial mark is attached
   to and the fiducial mark centered on the entrance aperture
   of an integrating sphere located in front of the entrance slit
   of the monochromator. A beam of light from a laser is directed
   onto the glass, and the direction of the beam is adjusted until
   the beam reflects from the glass back on itself while also inter-
   secting the fiducial mark on the glass. The laser beam then
   defines the instrument's axis and the laser is locked in place.
   The lamp holder is next aligned relative to the laser beam
   using an alignment jig designed at NBS and shown in a diagram
   in Figure 3 and in use in Figure 4. The alignment jig is
   made with two long rods potted into a base similar to the one
   used on the FEL lamps but with the rods extending up out of the
   epoxy block as well as below the block. A piece of glass has

been fitted between the parallel rods with one face in the plane
that is tangent to one side of the rods. This alignment jig is
placed in the lamp holder which is mounted on a milling table
with added vertical and tilt adjustments. One of the contacts
of the lamp holder is a concave V with the bottom end closed
to define the vertical position of the jig or lamp (see Figure 2).
When sighting along the optic axis from behind the lamp toward
the instrument, this V-block is on the left. A fiducial mark
on the front of the glass plate of the jig indicates the point
that is 3.75 inches above the bottom of the left hand pin and
half way between the rods. The lamp holder is adjusted so that
the laser beam along the optical axis reflects back on itself
off the jig's glass plate; and is centered on the fiducial mark.
The distance from the limiting aperture of the measuring instru-
ment to the glass surface of the alignment jug is then adjusted
to 50cm using a distance gauge.

Alignment Tolerances

There are six dimensional variables involved in the alignment of
a lamp relative to the instrument:

1. Distance from the lamp to the defining aperture of the
    instrument
2. Horizontal distance off the optical axis
3. Vertical distance off the optical axis
4. Pitch (tilt) ⎫
5. Yaw (rotation) ⎬   Lamp attitude
6. Roll   ⎭

Instruments will vary in their sensitivity to lamp misalignment.
Variation in the instrument's responses are due to the interaction
of a lamp's nonuniform irradiance field with an instrument's
geometrical detection sensitivity, along with a small component
due to error in the lamp to instrument distance. The alignment
tolerances required by each instrument must be determined by
the user. However from work which was reported in NBS Technical
Note 594-2 and from the present examination of lamp nonuniformity,
it is clear that good results will require very tight control of
lamp attitude and lamp to instrument distance. Angular positioning
of the lamp relative to the instrument's optical axis will need to be
to tenths of a degree and lamp to instrument and optical axis distances
must be made to 1/4-1/2 of a millimeter, if the systematic errors
due to physical positioning of the lamp are to be kept down in the
tenths of percent range. The alignment procedure used at NBS sa-
tisfies these requirements.

Current Setting

In order to realize the high accuracy assigned to the standard, the
current through the lamp should be set to precisely 8.00 amperes dc.
Setting of current is especially critical when using the standard for
calibration in the ultraviolet. For example, a 1% error in the current

setting results in a 12% error in the spectral irradiance at 250nm.

The following table gives the variation in the spectral irradiance at a number of wavelengths, the variation in the total irradiance, and the variation in the illumination for a 0.10% error in setting the lamp current.

Wavelength (nm)	Uncertainty Due to 0.10% Current Setting Error (%)
250	1.2
300	0.9
400	0.6
500	0.4
1000	0.35
1500	0.17
2000	0.14

Total Irradiance 0.3
Illumination 0.4

Use of the Standards of Total and Spectral Irradiance

These standards require no auxiliary optics. If any are employed, proper correction must be made for their optical characteristics. The lamp is simply placed at a measured distance from the detector or spectrometer slit. If a distance other than 50 centimeters is used, the inverse-square law may be used to calculate the irradiance. (The inverse-square law should not, however, be used for distances shorter than about 35 centimeters.) However, the distance from the front of the base pins to the center of the filament should be taken into consideration.

Values of spectral irradiance for these lamps are tabulated as a function of wavelength in watts per (Square centimeter-nanometer) at a distance of 50 centimeters from center of lamp to receiver. Values of spectral irradiance for wavelength intervals other than one nanometer, say x nanometers, may be found by multiplying the tabulated values by x. Values of spectral irradiance for wavelength not tabulated may be found through interpolation using the adjacent wavelength values.

In measurements wherein two sources (a standard source and a test source) are being compared by the direct substitution method (slit widths kept unchanged, use of the same detector), no knowledge of the spectral transmittance of the spectrometer, nor of the spectral sensitivity of the detector is required. It is necessary, however, to make sure that the entrance slit of the spectrometer is fully and uniformly filled with radiant flux both from the standard and from the test source: and if at any one wavelength the detector response for

the standard is significantly different from that for the test source, the deviation from linearity of response of the detector must be evaluated and taken into account. Furthermore, if the standard and test source differ in geometrical shape, it must be ascertained that the instrument transmittance and detector response are not adversely affected thereby.

Many detectors are highly variable in sensitivity over their surface area and may require diffusion of radiant flux over their surface to insure accurate radiant energy evaluations.

When using the standard to calibrate a spectroradiometer or some other spectrally selective radiometer, care should be taken that the wavelengths are accurately known. This is especially critical in the ultraviolet since the spectral irradiance is decreasing very rapidly with decreasing wavelength. For example, the following table indicates change in the spectral irradiance at various wavelengths for a one nanometer change in wavelength.

Wavelength (nm)	$\Delta E\lambda$ per nm (%)
250	7.5
270	6.0
300	4.0
350	2.5
400	2.0
500	0.88
700	0.25
1000	0.04

The current through the lamp should be increased gradually and great care should be taken that at no time will the current appreciably exceed 8.00 amperes. Stability tests performed on a number of similar lamps indicate that, if handled with care, the calibration should hold to ±1% for a period of 50 hours of use.

These lamps operate at high temperatures such that the quartz envelope is above the flammable point of organic materials. They may thus cause fires, and also the burning of lint, etc. on the envelope,which may result in optical damage to its surface. In no case should the fingers come into contact with the quartz envelope, either hot or cold, as the resulting finger prints will burn into its surface during lamp operation. It should be emphasized that these lamp standards should be handled with the care normally given to other delicate optical components.
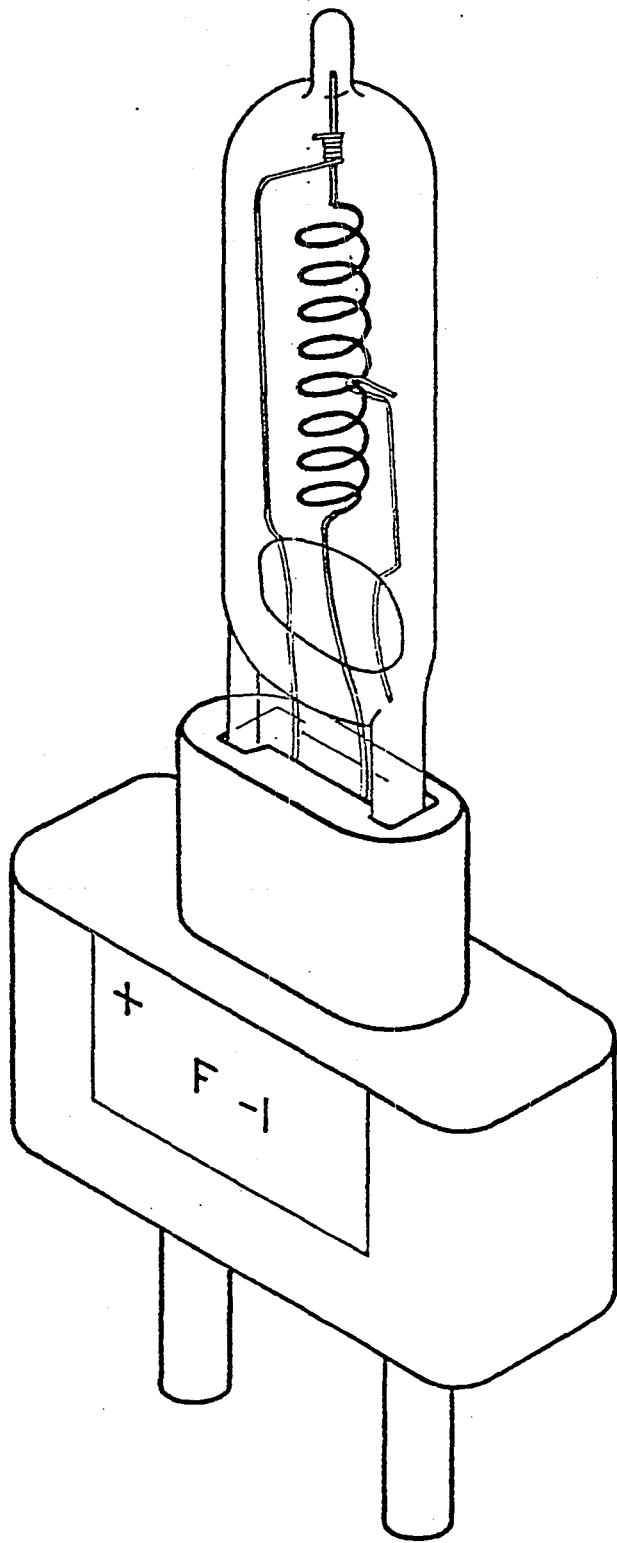
FIGURE 1
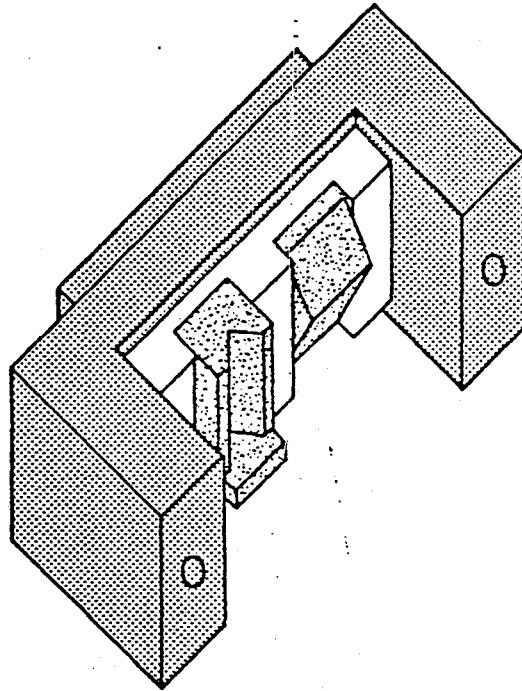
ISOMETRIC VIEW

← TO DETECTOR

(−)

(+)
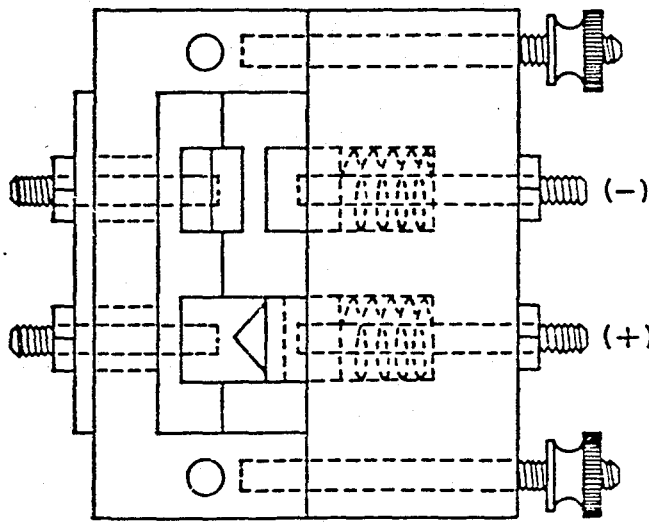
TOP VIEW

KINEMATIC LAMP HOLDER

Figure 2

FRONT VIEW SIDE VIEW

SCRIBED MARK TO LOCATE OPTIC AXIS HEIGHT

FLAT GLASS PLATE FIXED PARALLEL TO PLANE OF TWO RODS

EPOXY ENCAPSULATING COMPOUND

3.750 ± 0.005"

3 5/16"

7/8"

13/16"

0.875" ±0.005

1 7/8"

3/4"
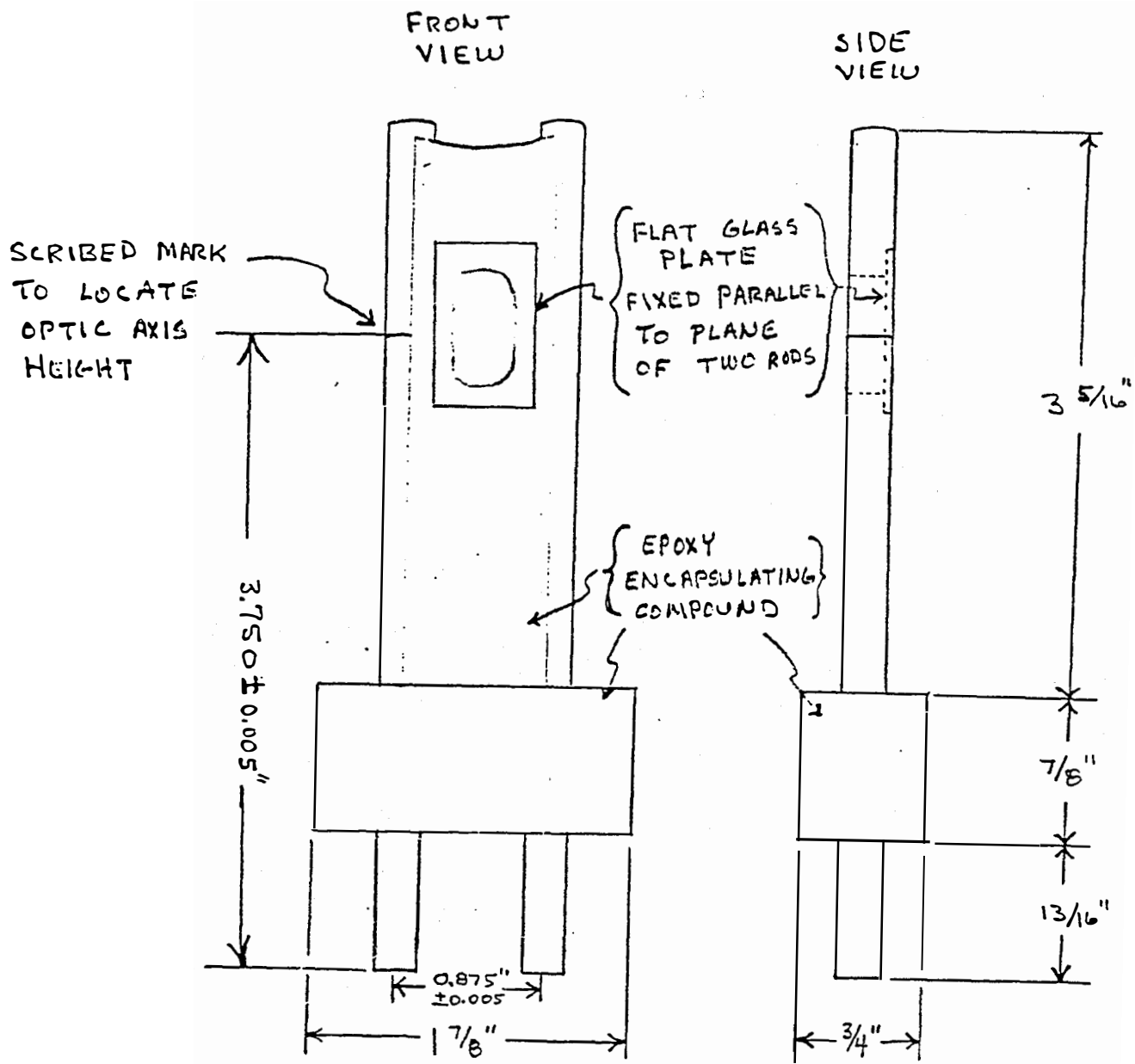
ALIGNMENT JIG
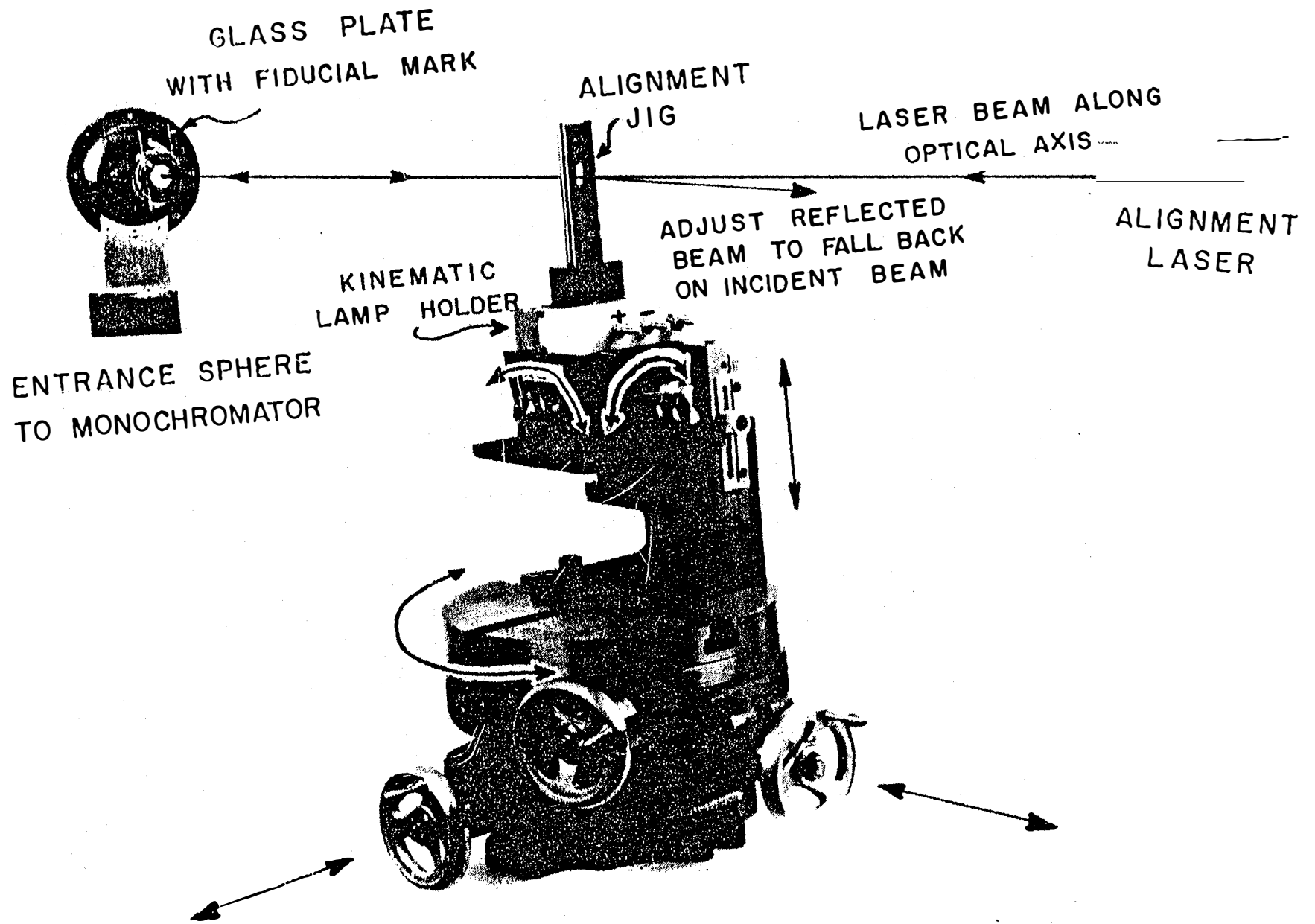
FIGURE 3

FIGURE 4

APPENDIX D
Sample NREL PV Cell Indoor Performance Report

Georgia Inst Tech   Multi-Si

Sample: N6#8

Dec 30, 1995 6:34 PM

ASTM E 892-87 Global

Temperature = 25.0°C

Area = 1.001 cm^2

Irradiance: 1000.0 Wm^{-2}

NREL X-25 IV System
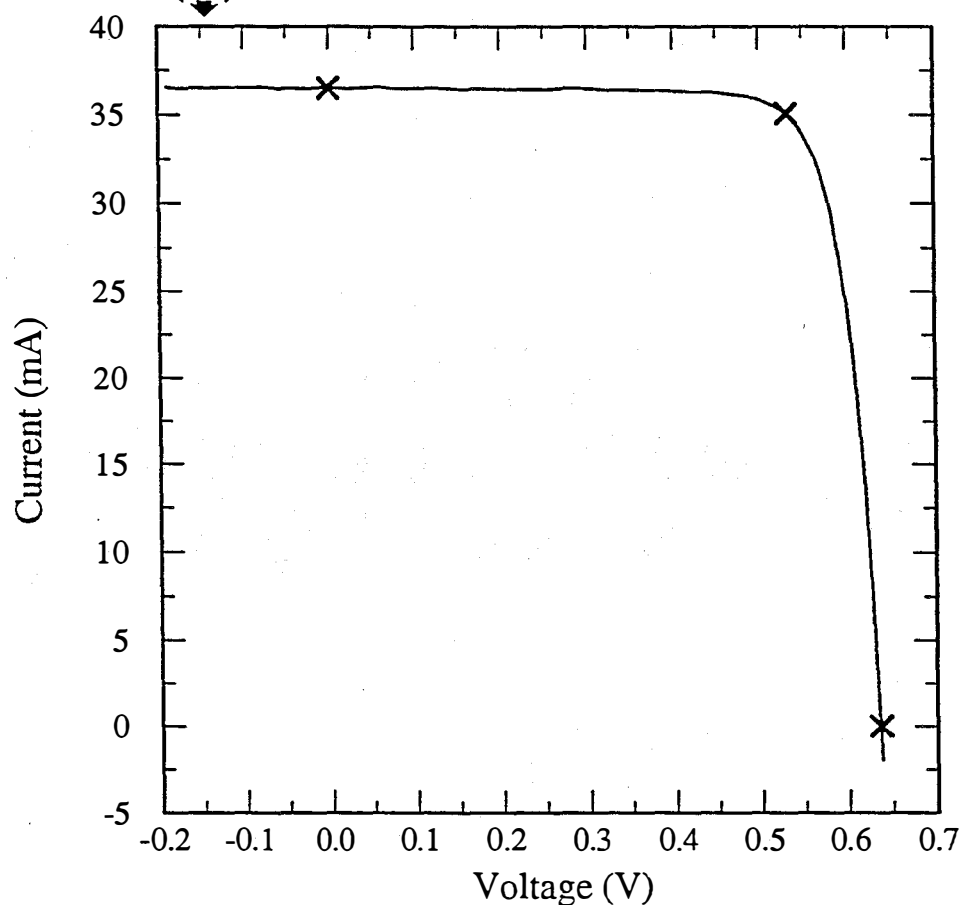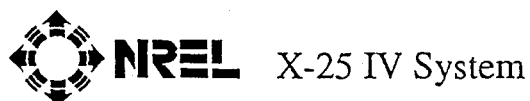
V_{oc} = 0.6360 V

I_{sc} = 36.51 mA

J_{sc} = 36.48 mAcm^{-2}

Fill Factor = 80.36 %

V_{max} = 0.5319 V

I_{max} = 35.08 mA

P_{max} = 18.66 mW

Efficiency = 18.6 %

G.I.T. HEM

APPENDIX E
Manufacturers of Broadband Solar Radiometers

APPENDIX E
Manufacturers of Broadband Solar Radiometers

1.   Ascension Technology, Inc.
P.O. Box 314
Lincoln Center, MA 01773
Telephone (617) 890-8844
Fax (617) 890-2050

2.   Brusag
Chapwiesenstrasse 14
CH-8712 Stafa
Telephone 01-926-74 74
Fax 01-926-73 34

3.   Casella London Limited
Regent House
Britannia Walk
London N1 7ND
Telephone 01-253-8581
Telex 26 16 41

4.   EKO Instruments Trading Co., Ltd.
21-8 Hatagaya 1-chome
Shibuyaku, Tokyo 151
Japan
Telephone 81-3-3469-4511
Fax 81-3-3469-4593
U.S. Distributor:
    SC International, Inc.
    346 W. Pine Valley Dr.
    Phoenix AZ 85023
    Telephone: (602) 993-7877
    Fax (602) 789-6616

5.   The Eppley Laboratory
12 Sheffield Ave
Newport RI 02840
Telephone (401) 847-1020
Fax (401) 847-1031

6.   Kipp & Zonen, Delft B V
P.O. Box 507
2600 AM Delft Holland
Mercuriusweg 1
2624 Delft Holland
Telephone 015-561-000
Fax 015-62-0351
    Division of:
    Enraf Nonoius Co.
    390 Central Ave.
    Bohemia, NY 11716
    Telephone (516) 589-2885
    Fax (516) 589-2068

7.   LI-COR, Inc.
4421 Suprior Street
Lincoln, NE 68504
Telephone (402) 467-3576
Fax (402) 467-2819

8.   Matrix, Inc.
537 S. 31st St.
Mesa, AZ 85204
Telephone (602) 832-1380

9.   Sci-Tec Instruments, USA, Inc.
4240 Bluebonnet Dr.
Stafford, TX 77477
Telephone (713) 240-0404
Fax (713) 240-0428

10.   Solar Light Company
721 Oak Lane
Philadelphia, PA 19126-3342
Telephone (215) 927-4206

11.   Yankee Environemental Systems, Inc.
Montaque Industrial Park
101 Industrial Road
P.O. Box 746
Turners Falls, MA 01376
Telephone (413) 863-0200
Fax (413) 863-0255

APPENDIX F
Sample NREL Broadband Radiometer Calibration Report

NATIONAL RENEWABLE ENERGY LABORATORY

METROLOGY LABORATORY
Management Assessment Office
1617 Cole Boulevard
Golden, Colorado 80401-3393
Building 16, Room 214
Phone: (303) 231-7246

SOLAR RADIOMETER CALIBRATION REPORT

Model #	Serial Number	Samples (N)	Mean CF- uV/W/sqm	Std. Dev uV/W/sqm	CF RANGE % of Mean	Uncertainty % of MEAN
14 PSP	17862F3	271	7.879	0.053	4.5	3.8

Cavity Radiometer   : 68017 WRR (IPC VII) Correction = 0.99977
Diffuse Radiometer : Eppley Laboratory PSP 17802F3 CF = 110.6 W/sqm/mV
Calibration dates : JUN 13 JUN 14 JUN 19 JUN 20 1993
Operators   : J. Treadwell, D. Laudato
Analyzed By   : Chester Wells, Kevin Eldridge

o♭ MEAN CF is for Z = 50 degrees Pyranometers; over ALL Z for Pyrheliometers
o♭ UNCERTAINTY in CF is % of MEAN uncertainty in determination of CF at time
   of calibration.
o♭ All Incidence angles corrected for refraction to APPARENT @ 840 mB, 25 °C.
o♭ Range of Zenith Angles is from 16.1 to 68.4 degrees.

Instruments submitted by: D. Myers

Calibration Event: BORCAL 93-2

Report Date: June 20, 1993

Approved by: _____

NOTICE

NREL SOLAR RADIOMETER CALIBRATION INFORMATION

BORCAL 93-2

INTRODUCTION

The calibration event, designated BORCAL 93-2, was performed by the Metrology Laboratory of the Management Assessment Office (MAO; Branch 3200) at NREL. Data used in the analysis for this report was taken on: June 13, 14, 19, and June 20, 1993.

The solar radiometers listed in Table 1 were simultaneously calibrated outdoors in natural sunlight, at the National Renewable Energy Laboratory's (NREL) Solar Radiation Research Laboratory (SRRL) on South Table Mountain in Golden, Colorado.

All reference times are given in Mountain Standard Time.

RESULTS PRESENTED HERE

The results of the calibration of each instrument are given in Table 1, which includes:

- line number, corresponding to figure number thereafter
- model designation and serial number of the radiometer
- derived calibration factor (CF), in microvolts per watt per square meter (μV/W/m^2)
- standard deviation of the derived mean CF, in μV/W/m^2
- range of values for the CF obtained during the calibration, as a percentage of the derived mean CF.
- uncertainty in CF, as a percentage of the derived mean CF

Figure A is a time-series plot of the three radiation components (direct beam, diffuse, and calculated reference global horizontal irradiance) during the outdoor calibrations.

Figure B is the range of CF values calculated from all the data obtained with zenith angles not greater than 69° during the calibration period, as a percentage of the derived CF. Note that this plot indicates the variability in CF *only during the specific period of calibration.* However, it can alert the user to the probable percentage of random uncertainty appropriate to early-morning and late-afternoon clear-sky data as the result of using the single derived calibration factor.

Figure C is a polar plot of the path of the sun, on the first and last days when calibration data was acquired. The dotted lines at 45° and 55° elevation angles indicate the 55° to 45° zenith (90° - solar elevation angle) and azimuth angle ranges from which data were used to derive the CFs for the pyranometers.

Figure D is a time-series plot of a representative pyranometer case temperature, as sensed by a shaded thermocouple under instrument number 4, of Table 1 during the calibration data

collection. Temperature corrections were not applied to the data acquired from each instrument.

Figures 1 through 42 are calibration factor versus zenith angle plots [1] for each individual instrument. Note that these plots reveal deviations from an ideal angular response for pyranometers (deviations from a true cosine law response, with accompanying azimuthal variations). [1,2,3]

Figures 1-A through 42-A are calibration factor versus true solar time plots [1,4,5] for each individual instrument. Note that these plots reveal any possible asymmetries between the morning and afternoon angular responses for that particular radiometer.

CALIBRATION TECHNIQUE

The calibration technique used (the Component Summation Method) is a modified version of the shading method described in American Society for Testing and Materials (ASTM) Standard E913-82, "Standard Method for Calibration of Reference Pyranometers With Axis Vertical by the Shading Method." [6]

The direct normal irradiance was measured with an absolute cavity radiometer, and the diffuse (sky) irradiance was measured with a pyranometer shaded with a tracking disk. The output voltage of these standards and the radiometers under test were measured at 1-minute intervals throughout each day (weather conditions permitting).

The CF for a pyrheliometer is calculated for each data point by dividing the value of the instrument's output signal by the value of the output signal of the absolute cavity radiometer. The derived CF for pyrheliometers is the mean of the individual CF determinations for all zenith angles.

The CF for a pyranometer is calculated by dividing the value of the instrument's output signal by the computed reference global-horizontal irradiance. The computed reference irradiance is the sum of the diffuse radiation and the vertical component of the direct-beam irradiance. This assumes that the pyranometer does not respond to the horizontal component (i.e., it has a perfect cosine law response). The vertical component of the direct beam is calculated as the product of the measured direct-beam irradiance and the cosine of the zenith angle [1], - corrected for atmospheric refraction effects [7] at the SRRL (based on a mean atmospheric pressure of 840 mBar and an ambient temperature of 25°C).

The derived CF for pyranometers is the mean of the individual CF determinations for zenith angles between 45° and 55°. This effectively normalizes the derived CF for pyranometers to an average response near a 50° zenith angle. Normalization to 50° is done to allow calibration events to be run during a greater part of each year and to compare those results between calibrations. This also permits comparison of these results with calibrations performed at the Solar Radiation Facility at the National Oceanic and Atmospheric Administration (NOAA) in Boulder, Colorado where the CF is the mean from a number of determinations made at 50° zenith angle. CF values determined at different times of the year will be determined over the same zenith angle range, but at different azimuthal positions. Therefore, some variations in CF should still be expected.

2

Only clear-sky data was used to derive the calibration factors. For these calibration purposes, the clear-sky conditions met during BORCAL 93-2 required no obstructions of the direct-beam radiation from the solar disk and a limited diffuse component. The diffuse conditions achieved for this BORCAL event are illustrated in Figure A. Calibration data was collected during 4 days and included both morning and afternoon zenith angle ranges through 45°-55°.

REFERENCE STANDARDS

The direct normal component was measured using a self-calibrating absolute cavity radiometer [8, 9, 10], Technical Measurements Inc., model MK VI, serial number 68017. The diffuse horizontal component was measured by an Eppley PSP pyranometer, serial number 17802F3, mounted under a solar tracking disk [11].

The calibration of the absolute cavity radiometer is traceable to the World Radiometric Reference (WRR) of the World Meteorological Organization (WMO). WRR is maintained by the Physikalisch-Meteorologisches Observatorium Davos (PMOD) in Davos, Switzerland [12]. The accuracy of the cavity radiometer is ± 0.5%. The WRR reduction factor for the NREL reference cavity radiometer was applied to the direct-beam data during data reduction. CF values derived for each instrument will convert its signals to irradiance units with respect to the World Radiometric Reference.

The accuracy of the PSP used to measure the diffuse horizontal component is ± 5%. This inaccuracy contributes to the overall calibration uncertainty by by less than .75%. This is because the diffuse component never exceeds 15% of the global irradiance during the time of calibration.

During each calibration event, one or more radiometers are used as control standards to monitor the calibration process. During this calibration, the control standards were the Eppley PSP, serial number 25825F3, Eppley FPP, serial number 18745 and Eppley NIP, serial number 17836E6. The data from these units is reviewed to monitor the calibration process.

UNCERTAINTY ANALYSIS

NREL staff members evaluated the ASTM E-913 procedure for "typical" pyranometers and pyrheliometers [19] using a standard uncertainty analysis technique [20, 21, 22, 23]. The results indicated that the expected uncertainty in the mean calibration factor of a pyranometer is ±2.8%. Likewise, expected uncertainty in the calibration factor of a "typical" pyrheliometer was ±2.0%.

Another study [18] identified and quantified sources of systematic (bias) and random error contributing to the total uncertainty in the derived CF due to:

- WRR uncertainty
- cavity radiometer uncertainty
- cosine response error
- azimuthal response error
- temperature response error
- spectral response error

- thermal electromotive force errors
- thermal gradient-induced errors
- data acquisition errors
- data reduction (incidence angle computation) errors.

Each instrument is unique, therefore, the uncertainty must be INDIVIDUALLY calculated. This is shown in the zenith angle and solar time plots of CF (Figures 1 through 42 and 1-A through 42-A).

The "CF Range, % of mean" column of Table 1 indicates the percentage errors for the measured irradiance using the derived CF. The error bars in Figure B show the relationship (as a percentage) of the maximum and minimum CF values to the derived CF.

The uncertainty, U_{95}, (as a percentage of CF) in the determination of the derived CF for pyranometers (at the time and under the conditions of this calibration) is

$$U = \sqrt{B^2 + (\frac{CF\ Range}{2})^2}$$

where B is the bias limit, having an estimated value of 3.0% for pyranometers based on recent experience and reference [19].

Similarly, the uncertainty in the determination of the derived CF for pyrheliometers is

$$U = \sqrt{B^2 + (\frac{2\ std.\ Dev}{mean\ CF} \times 100)^2}$$

where B is the bias limit for pyrheliometers having an estimated value of 1.55% [19].

The uncertainty of the CF's for each instrument shown in Table 1 as "Uncertainty % of mean" is uncertainty in the mean CF determined between the 45° to 55° zenith angles. This uncertainty of the CF is only valid at near normal incidence (Z = 45°-50°). The uncertainty that should be applied to data using a single calibration factor for an entire day would be derived from the variability in CF over the day, combined with the uncertainty indicated in Table 1 for that instrument. Individual measurements could reflect uncertainties as great as twice the uncertainty in the derived CF. Integrated data (hourly or daily totals) may have uncertainties approaching the uncertainty in the CF.

ADDITIONAL INFORMATION

NREL's Solar Radiation Research Laboratory is located at 39.74° north latitude, 105.17° west longitude, at elevation of 1828 meters above mean sea level.

The technicians were: James Treadwell and Deborah Laudato.
The analysis was performed by: Kevin Eldridge, Deborah Laudato and Chester Wells.
The data was reviewed by: Chester Wells and Kevin Eldridge.

REFERENCES

[1]   Iqbal, M., An Introduction to Solar Radiation, Academic Press, New York, 1983.

[2]   Coulson, K.L., Solar and Terrestrial Radiation, Methods and Measurements, Academic Press, New York, 1975.

[3]   Anonymous, "Radiation Measurement Instruments," LI-COR, Inc., Box 4425, Lincoln NE, 1986, pp. 20-24.

[4]   Krieth, F., and J. F Kreider, Principles of Solar Engineering, Hemisphere Publishing Corp., McGraw-Hill Book Company, New York, 1978.

[5]   Duffie, J.A., and W.A. Beckman, Solar Energy Thermal Processes, John Wiley & Sons, New York, 1972.

[6]   Anonymous, ASTM Standard E913-82 "Standard Method for Calibration of Reference Pyranometers With Axis Vertical by the Shading Method," American Society of Testing and Materials, Philadelphia, PA, 1982.

[7]   Allen, C.W., Astrophysical Quantities, 3rd Ed., Athlone Press, London, England, 1981.

[8]   Kendall, J.M., Sr., "Primary Absolute Cavity Radiometer," NASA Technical Report 32-1396, Jet Propulsion Laboratory, California Institute of Technology, Pasadena, CA, 1969.

[9]   Kendall, J.M., and C.M. Berdahl, "Two Blackbody Radiometers of High Accuracy," Applied Optics, Vol. 9, 1970, pp. 1082-1091.

[10]   Willson, R.C., "Active Cavity Radiometer Type IV," Applied Optics, Vol. 18, 1979, pp. 179-188.

[11]   Anonymous, "Instructions for the Installation of The Solar Tracking Disk," The Eppley Laboratory, Newport RI, 1978.

[12]   Frohlich, C., "Radiometry at PMOD and the World Radiometric Reference," in Advances in Absolute Radiometry, Proceedings, Atmospheric and Environmental Research, Inc., Cambridge MA, P. Foukal, Ed. June 24-25, 1985.

[13]   Anonymous, "Fourth International Pyrheliometer Comparisons, Third Regional Comparisons (RA VI) 6-24 October 1975," Working Report No. 58, Swiss Meteorological Institute, Zurich, Switzerland, Sept. 1976.

[14]   Anonymous, "Pyrheliometer Comparisons 1980, Results and Symposium", Working Report No. 94, Swiss Meteorological Institute, Zurich, Switzerland, Feb. 1981.

[15]   Anonymous, "Pyrheliometer Comparisons 1985, Results and Symposium," Working Report No. 137, Swiss Meteorological Institute, Zurich, Switzerland, Dec. 1985.

[16]   Anonymous, "International Pyrheliometer Comparisons, IPC VII, 24 September to 12 October 1990: Results and Symposium;" Working Report 162, Swiss Meteorological Institute, Davos and Zurich, Switzerland, March 1991.

[17]   Zerlaut, G., "Solar Radiation Instrumentation," in Solar Resources, R. Hulstrom, Ed. MIT Press, Cambridge, MA, 1989, pp. 242-257.

[18]   Nelson, D., R. Haas, J. Deluisi, and G. Zerlaut, "Results of the NRIP 7 Intercomparison November 18-21, 1985," NOAA Technical Memorandum ERL ARL-161, Air Resources Laboratory, Silver Spring, MD, Nov. 1987.

[19]   Myers, D.R., "Uncertainty Analysis for Thermopile Pyranometer and Pyrheliometer Calibrations Performed by SERI," SERI Technical Report TR-215-3294, Solar Energy Research Institute, Golden CO, Apr. 1988.

[20]   Abernethy, R.B. and Thompson, J.W., Jr. *Handbook, Uncertainty in Gas Turbine Measurements.* AEDC-TR-73-5. Arnold Air Force Station, Tennessee: Arnold Engineering Development Center, February 1973. Available from the National Technical Information Service, Springfield, VA 22161. This was reprinted (but is now out of print) by the Instrument Society of America as: Abernethy, Robert J., "Measurement Uncertainty Handbook, Revised 1980," Instrument Society of America, Research Triangle Park, NC, 1980.

[21]   Anonymous, "Part I - Measurement Uncertainty, ANSI/ASME PTC 19.1-1985," The American Society of Mechanical Engineers, New York, NY, 1985.

[22]   Abernethy, R.B., and B. Ringhiser, "The History and Statistical Development of the New ASME-SAE-AIAA-ISO Measurement Uncertainty Methodology," presented at AIAA/SAE/ASME/ASES Joint Propulsion Conference, July 8-10, 1985.

[23]   Abernethy, R.B., and R.P. Benedict, "Measurement Uncertainty: a Standard Methodology," ISA Transactions, Vol. 24, No. 1, 1985, pp. 74-79.2

Table 1

Summary Statistics for NREL BORCAL93_02

Model #	Serial Number	Samples (N)	Mean CF- uV/W/sqm	Std. Dev uV/W/sqm	CF RANGE % of Mean	Uncertainty % of MEAN
1 NIP	17836E6	1540	8.438	0.020	1.0	1.6
2 PSP	25825F3	287	9.582	0.054	4.2	3.7
3 FPP	18745	213	0.717	0.003	1.6	3.1
4 PSP	21027F3	272	9.405	0.045	2.7	3.3
5 PSP	13365F3	282	7.863	0.045	4.6	3.8
6 PSP	17861F3	280	7.246	0.055	5.6	4.1
7 PSP	17863F3	229	8.063	0.055	3.8	3.5
8 PSP	18039F3	268	7.841	0.042	3.9	3.6
9 PSP	18040F3	287	8.387	0.042	3.5	3.5
10 PSP	20068F3	254	9.793	0.053	2.9	3.3
11 PSP	20079F3	248	9.742	0.046	3.0	3.4
12 PSP	20379F3	265	10.425	0.051	3.4	3.4
13 PSP	20386F3	225	10.361	0.058	2.2	3.2
14 PSP	17862F3	271	7.879	0.053	4.5	3.8
15 PSP	21048F3	267	7.371	0.036	3.1	3.4
16 PSP	23087F3	265	8.347	0.035	2.6	3.3
17 PSP	23620F3	239	8.745	0.041	3.3	3.4
18 PSP	23997F3	235	9.797	0.035	1.7	3.1
19 PSP	28403F3	263	8.671	0.046	2.5	3.3
20 LI-200	PY18104	286	9.454	0.062	6.4	4.4
21 LI-200	PY18105	286	8.426	0.056	7.5	4.8
22 LI-200	PY18106	286	7.930	0.059	7.0	4.6
23 LI-200	PY18107	284	9.094	0.062	6.7	4.5
24 LI-200	PY18108	287	8.477	0.069	6.5	4.4
25 LI-200	PY18109	286	6.962	0.044	5.9	4.2
26 LI-200	PY18110	276	9.460	0.096	6.5	4.4
27 LI-200	PY18111	273	8.285	0.046	5.8	4.2
28 LI-200	PY18112	277	8.057	0.048	6.3	4.4
29 LI-200	PY18113	268	9.210	0.057	4.8	3.9
30 K&ZCM11	850878CM11	253	4.672	0.025	2.0	3.2
31 K&ZCM11	830119CM11	262	5.060	0.019	1.2	3.1
32 K&ZCM11	924319CM11	255	4.764	0.015	1.4	3.1
33 K&ZCM11	924320CM11	242	4.818	0.015	1.6	3.1
34 K&ZCM11	924467CM11	249	4.466	0.011	1.1	3.1
35 K&ZCM21	910002CM21	269	16.813	0.065	2.5	3.2
36 K&ZCM21	920056CM21	252	12.500	0.031	1.7	3.1
37 K&ZCM21	920057CM21	188	14.166	0.032	2.1	3.2
38 K&ZCM21	920058CM21	246	13.696	0.042	2.0	3.2
39 NIP	15239E6	1436	8.380	0.022	1.2	1.6
40 NIP	21620E6	1431	8.721	0.018	1.0	1.6
41 NIP	23385E6	1531	8.554	0.033	1.8	1.7
42 NIP	29001E6	1546	8.418	0.019	1.0	1.6

```
Cavity Radiometer    : 68017 WRR (IPC VII) Correction = 0.99977
Diffuse Radiometer   : Eppley Laboratory PSP 17802F3 CF = 110.6 W/sqm/mV
Calibration dates    :  JUN 13 JUN 14 JUN 19 JUN 20 1993
Operators            : J. Treadwell, D. Laudato
Analyzed By          : C. Wells, K. Eldridge
```

o MEAN CF is for Z = 50 Deg for Pyranometers; over ALL Z for Pyrheliometers
o UNCERTAINTY in CF is % of MEAN uncertainty in determination of CF at time of calibration.
o All Incid. angles corrected for refraction to APPARENT @ 840 mB, 25 C.
o Range of Zenith Angles is from 16.1 to 68.4 Deg.

RADIOMETER CALIBRATION REFERENCE IRRADIANCES
CALIBRATION EVENT: BORCAL93 02

Legend:
+ WRR CAV -68017
+ Dif Irr -17802F3
+ Ref GH -Irr
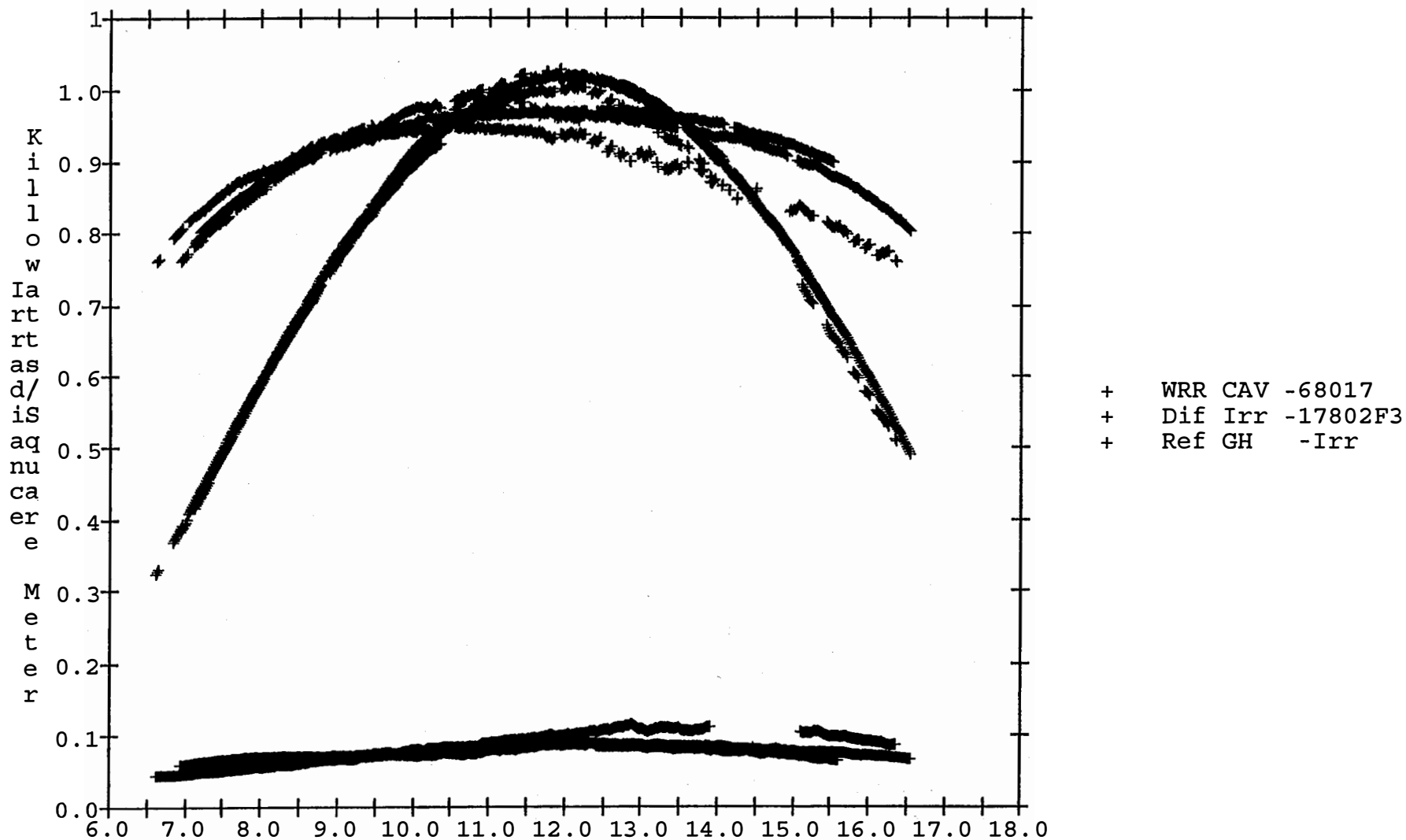
Figure A
Mountain Standard Time

Calibration Dates: JUN 13 JUN 14 JUN 19 JUN 20 1993
Zenith Angle Range: 16.1 to 68.4 Degrees
Reviewed by: Chester Wells and Kevin Eldridge

COMPONENT SUMMATION CALIBRATION UNCERTAINTY
NREL CALIBRATION EVENT: BORCAL93_02

Figure B

Reference Instruments: TMI Cavity serial # 68017, Diffuse-Eppley PSP serial # 17802F3
Calibration Dates: JUN 13 JUN 14 JUN 19 JUN 20 1993
Zenith   Angle Range: 16.1 to 68.4 Degrees
Reviewed by: Chester Wells, and Kevin Eldridge

o Error bars = RANGE of CF Results over period of calibration
o Pyranometer Error Bars about mean of Pyranometer CF @ Z = 50 Deg.
o Pyrheliometer Error Bars about mean of CF for ALL ZENITH Angles

Figure C

Dotted lines bracket calibration zenith angle range, between 45 and 55 Degrees.
Plot is of geometry for period of calibrations.

RADIOMETER CALIBRATION AMBIENT TEMPERATURES
CALIBRATION EVENT:BORCAL93 02
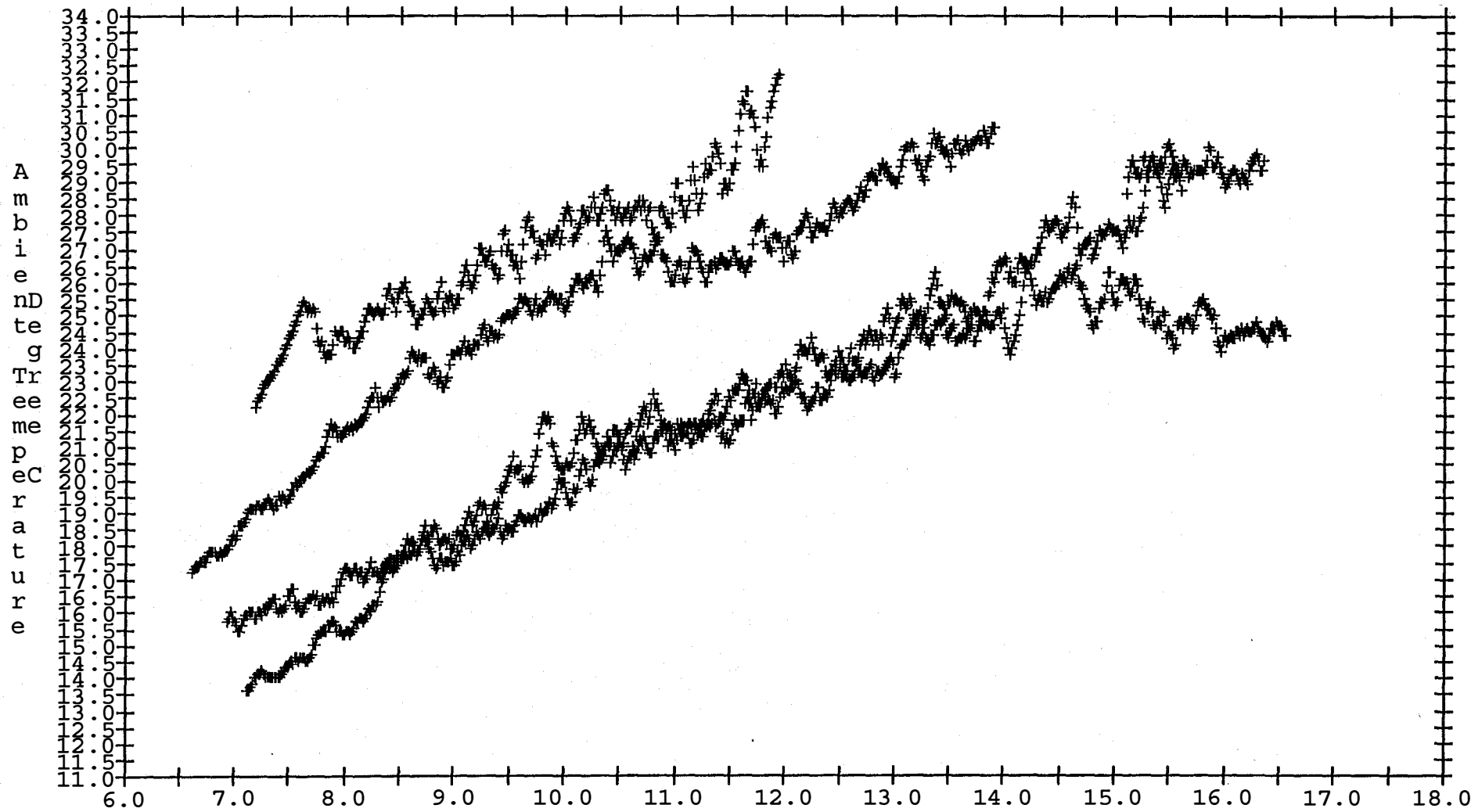
Figure D
Mountain Standard Time

Ref Instruments: TMI Cavity serial # 68017, Diffuse-Eppley PSP serial # 17802F3
Calibration Dates: JUN 13 JUN 14 JUN 19 JUN 20 1993
Temperature Range: 13.7 to   32.3 Degrees C.
Reviewed by: Chester Wells, and Kevin Eldridge

Calibration Factor (Cf) for 17862F3
vs Refraction Corrected ZenithAngle
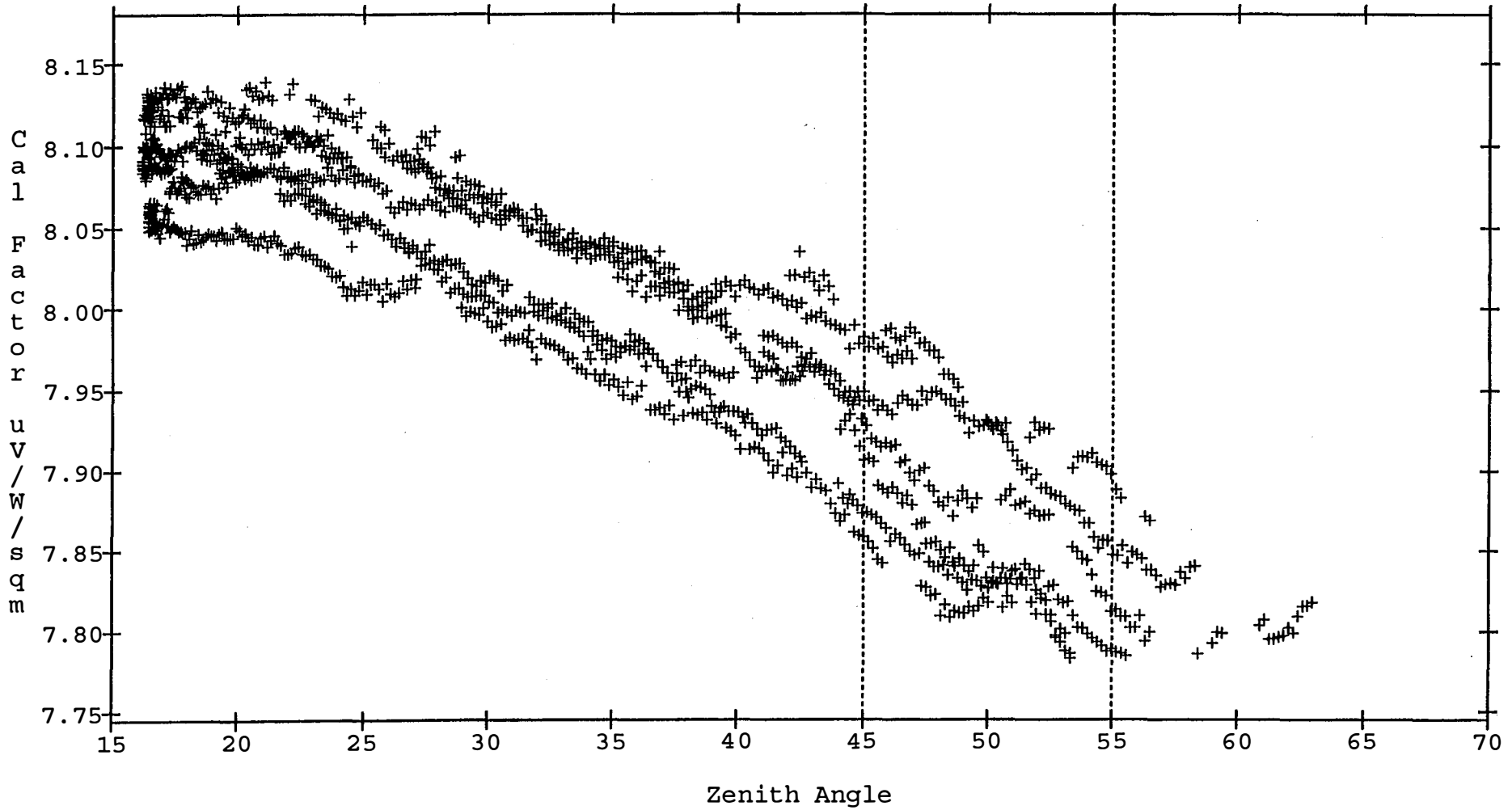
Ref. Radiometer TMI: 68017 (Direct), WRR correction = 0.99977
Diffuse: PSP 17802F3, CF = 110.6 W/sm/mV.
Dates of calibration: JUN 13 JUN 14 JUN 19 JUN 20 1993

NOTE: 16.1 <= Zenith Angle <= 68.4 Corrected for NREL/SRRL site (@ 840 mB and 25 Deg. C)
Dotted lines bracket calibration zenith angle Range

Figure 14

APPENDIX G
Sample NREL PV Module Outdoor (SOMS) Performance Test Report

Requester: Daryl Myers
NREL
Date: September 31, 1996

	Area (cm^2)	Temp. (°C)	V_{oc} (V)	I_{sc} (A)	FF (%)	V_{max} (V)	I_{max} (A)	P_{max} (W)	Aper.η (%)
Arco (mono-crystal Si module)									
XXX									
09/15/95 SPIRE 240A PEAK	1744.3	25	18.01	1.427	74.3	14.61	1.307	19.09	10.95
05/08/96 OUTDOORS SOMS @920 W/m^2	1744.3	28.7	17.17	1.250	70.9	13.61	1.117	15.21	9.47
XXX									
10/19/95 SPIRE 240A PEAK	1744.3	25	17.95	1.431	74.1	14.58	1.303	19.15	11.02
07/08/96 OUTDOORS SOMS @1010 W/m^2	1744.3	24.3	18.05	1.457	71.5	14.32	1.250	17.85	10.01

Sample (#)	Description	Aperture area length (cm)	width (cm)	area (cm^2)	Total area length (cm)	width (cm)	area (cm^2)
ALL	mono-crystal Si module	55.2	31.6	1744.3	56.9	32.5	1849.3

Total area is outside edge of glass to outside edge of glass.
Aperture area was defined as inside edge of frame to inside edge of frame.
Aperture area was used in the efficiency calculation.
Spire 240A measurements were taken with new Peak circuit installed, and running on new NREL software.
Estimated total uncertainty in the NREL Spire measurement efficiency is ±5%.
The SPIRE 240A monitor calibration was set to 128.06 mA using the Si reference cell in a module package sn#150576
    corrected for an estimated 0.97 spectral mismatch error.
Estimated total uncertainty of the NREL Outdoor measurements is ±5%.
Outdoor sample temperature is measured on the back surface and may not represent the actual junction temperature.
The outdoor data was not corrected for the calculated spectral mismatch error (1.00-1.015 range).
NREL Outdoor measurements are not corrected to Standard Reporting Conditions.
The solar spectrum that was taken during the outdoor tests are available.
(Tracking #1230)

Arco   mono-crystal Si

Sample: 536   area used = 1744.3 cm^2

May 8, 1996 9:59 AM MST   920.1 W/m^2 fixed tilt

device temperature = 28.7 °C   Si Ref. cell #294278

NREL   Outdoor I-V
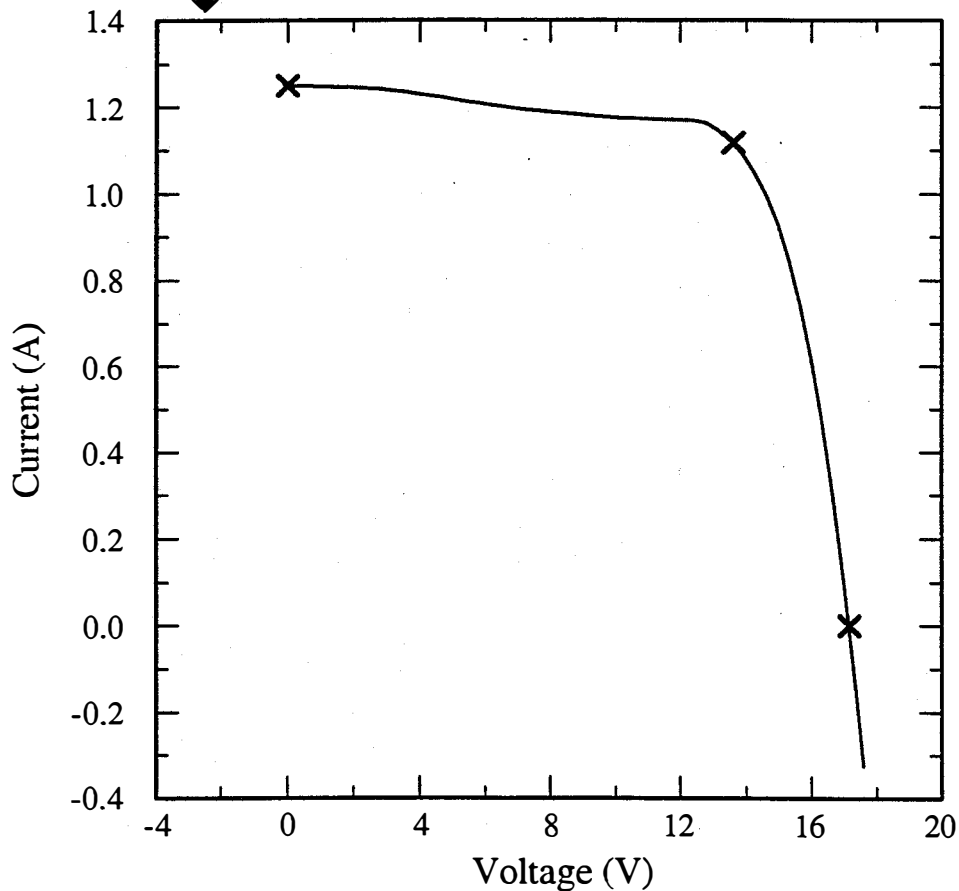
V_{oc} = 17.17 V V_{max} = 13.61 V

I_{sc} = 1.250 A I_{max} = 1.117 A

Fill factor = 70.85 % P_{max} = 15.21 W

Efficiency = 9.47 %

device dimensions = 55.2x31.6

Check out

Air mass = 1.20 , POA sun angle = 28.6°

total irradiance from K&Z CM11 = 918.3 W/m^2

APPENDIX H
Sample NREL PV Module Indoor (Simulator) Performance Test Report

Requester: Daryl Myers
NREL
Date: September 31, 1996

	Area (cm^2)	Temp. (°C)	V$_{oc}$ (V)	I$_{sc}$ (A)	F F (%)	V$_{max}$ (V)	I$_{max}$ (A)	P$_{max}$ (W)	Aper.η (%)
Arco (mono-crystal Si module)									
XXX									
09/15/95 SPIRE 240A PEAK	1744.3	25	18.01	1.427	74.3	14.61	1.307	19.09	10.95
05/08/96 OUTDOORS SOMS @920 W/m^2	1744.3	28.7	17.17	1.250	70.9	13.61	1.117	15.21	9.47
XXX									
10/19/95 SPIRE 240A PEAK	1744.3	25	17.95	1.431	74.1	14.58	1.303	19.15	11.02
07/08/96 OUTDOORS SOMS @1010 W/m^2	1744.3	24.3	18.05	1.457	71.5	14.32	1.250	17.85	10.01

Sample (#)	Description	Aperture area length (cm)	width (cm)	area (cm^2)	Total area length (cm)	width (cm)	area (cm^2)
ALL	mono-crystal Si module	55.2	31.6	1744.3	56.9	32.5	1849.3

Total area is outside edge of glass to outside edge of glass.
Aperture area was defined as inside edge of frame to inside edge of frame.
Aperture area was used in the efficiency calculation.
Spire 240A measurements were taken with new Peak circuit installed, and running on new NREL software.
Estimated total uncertainty in the NREL Spire measurement efficiency is ±5%.
The SPIRE 240A monitor calibration was set to 128.06 mA using the Si reference cell in a module package sn#150576
    corrected for an estimated 0.97 spectral mismatch error.
Estimated total uncertainty of the NREL Outdoor measurements is ±5%.
Outdoor sample temperature is measured on the back surface and may not represent the actual junction temperature.
The outdoor data was not corrected for the calculated spectral mismatch error (1.00-1.015 range).
NREL Outdoor measurements are not corrected to Standard Reporting Conditions.
The solar spectrum that was taken during the outdoor tests are available.
(Tracking #1230)

Manufacturer: ARCO
Sample Type : mono-crystal Si module
Sample #   : S1

Test Date   : September 15, 1995
Test Time   : 9:04 AM
Spectrum   : ASTM E892 Global
File Name   : C:\IV\data\IV7552.xy
NREL Spire 240A solar simulator (peak)
Estimated total uncertainty in efficiency is ± 5 %

Total irradiance = 1000 W/m^2
Temperature   = 24 °C
Aperture Area   = 1744 cm^2

Voc   = 18.01 V
Isc   = 1.427 A
Pmax   = 19.09 W
V at Pmax   = 14.61 V
I at Pmax   = 1.307 A
Fill Factor   = 74.3 %
Efficiency   = 10.95 %

APPENDIX I
Solar Position (SOLPOS) FORTRAN Source Code

APPENDIX I
Solar Position (SOLPOS) FORTRAN Source Code

Subroutine Solpos
(Iyear,Month,Iday,Ihour,Minute,Isecnd,Xlat,Xlon,Tzone,Solzen,Solazm,ETR,ETRN,AMass)

```
*==============================================================*
*
* National Renewable Energy Laboratory
* Technology & Resource Assessment Branch
* 1617 Cole Blvd
* Golden, CO  80401
*
* AUTHOR:
* Martin D. Rymes
* (303) 275-4638
*
* DATE:
* July 23, 1995
*
* DESCRIPTION:
* Computes SOLar POSition factors, given the date, time, and
* location of a site.  The passed parameters are defined below.
* Based on:
*
* Michalsky, Joseph J. (1988).  The Astronomical Almanac's
*   algorithm for approximate solar position (1950-2050).
*   Solar Energy 40 (3); 227-235.
*
* INPUTS:
* --DATE--
* Iyear: Year, e.g., 1990
* Month: Month of year, 1-12, e.g., 4=April
* Iday: Day of month, 1-31
* --TIME--
* Ihour: Hour of day, 0-23
* Minute: Minute of hour, 0-59
* Isecnd: Second of minute, 0-59
*
* Xlat: Latitude in decimal degrees, N +
* Xlon: Longitude in decimal degrees, E +
* Tzone: Time zone number:  Pacific = -8, Mountain = -7,
*      Central = -6, Eastern = -5
*
* OUTPUTS:
* Solzen: Solar zenith angle (angle sun makes with zenith),
*    degrees.
* Solazm: Solar azimuth angle, degrees, 0 = N, 90 = E.
```

```
* ETR: Extraterrestrial global horizontal solar radiation;
*    what Global would read in space.
* ETRN: ETR Normal, what Direct would read in space.
* Amass: Relative optical airmass (the thickness of the
*    atmosphere) normalized to 1 standard atmosphere
*    (sea-level, looking straight up).
*
*=============================================================*
      Integer Month_days(12)

      Data Month_days / 0,31,59,90,120,151,181,212,243,273,304,334 /
      DR = 0.017453292

* Day number (in the year):

      Numday = Iday + Month_days(Month)
      If ( Mod ( Iyear, 4 ) .eq. 0 .and. Month .gt. 2 )
     2   Numday = Numday + 1

* Day angle (Jan 1 = 0 degrees, goes to 360):

      Dangle = 360. * ( Numday - 1 ) / 365.

* Universal (Greenwich) time in hours (1:36 pm = 13.60 hours):

      UTime = Ihour * 3600 + Minute * 60 + Isecnd
      UTime = UTime / 3600.0 - TZone

* Fix for leap year, and adjust for 1949 = day 0:

      If ( Iyear .lt. 100 ) Iyear = 1900 + Iyear
      Delta = Iyear - 1949
      Xleap = Aint ( Delta / 4.0 )

* Our Julian day starts in 1949: ^

      DayJul = 32916.5 + Delta * 365.0 + Xleap +
     2    Numday + UTime / 24.0

      If ( Mod ( Iyear, 100 ) .eq. 0 .and. Mod ( Iyear, 400 ) .ne. 0 )
     2    DayJul = DayJul - 1.0

* GMST is the Greenwich Mean Sidereal Time (in hours):

      EpTime = DayJul - 51545.0

      GMST   = 6.697375 + 0.0657098242 * EpTime + UTime
      GMST = Amod ( GMST, 24.0 )
      If ( GMST .lt. 0.0 ) GMST = GMST + 24.0
```

* XLMST is the Local Mean Sidereal Time:

```
XLMST  = GMST * 15.0 + Xlon
XLMST = Amod ( XLMST, 360.0 )
If ( XLMST .lt. 0.0 ) XLMST = XLMST + 360.0
```

* OBLECL is the Obliquity of the Ecliptic:

```
OblEcl  = 23.439 + 0.0000004 * EpTime
```

* XMANOM is the Mean Anomaly:

```
XmAnom  = 357.528 + 0.9856003 * EpTime
XmAnom  = Amod ( XmAnom, 360.0 )
If ( XmAnom .lt. 0.0 ) XmAnom = XmAnom + 360.0
```

* XMLONG is the Mean Longitude:

```
XmLong  = 280.460 + 0.9856474 * EpTime
XmLong  = Amod ( XmLong, 360.0 )
If ( XmLong .lt. 0.0 ) XmLong = XmLong + 360.0
```

* ECLONG is the Longitude of the Ecliptic:

```
EcLong = XmLong + 1.915 * Sin ( XmAnom * DR ) + 0.020 * Sin (2.0 * XmAnom * DR )
EcLong = Amod ( EcLong, 360.0 )
If ( EcLong .lt. 0.0 ) EcLong = EcLong + 360.0
```

* RASCEN is the Right Ascension (of the sun):

```
Top = Cos ( OblEcl * DR ) * Sin ( EcLong * DR )
Bottom = Cos ( EcLong * DR )
RAscen = Atan2 ( Top, Bottom ) / DR
If ( RAscen .lt. 0.0 ) RAscen = RAscen + 360.0
```

* HANGLE is the Hour Angle (hours):

```
Hangle  = XLMST - RAscen
If ( Hangle .lt. -180.0 ) Hangle = Hangle + 360.0
If ( Hangle .gt.  180.0 ) Hangle = Hangle - 360.0
```

* DECLIN is the declination:

```
Declin = Asin ( Sin ( OblEcl *DR ) * Sin ( EcLong * DR ) ) / DR
```

```
D1 = Dangle
D2 = D1 + D1
S1 = Sin ( D1 * DR )
S2 = Sin ( D2 * DR )
C1 = Cos ( D1 * DR )
```

C2 = Cos (D2 * DR)

* ERV is the Earth-sun Radius Vector (corrects distance from sun):

ERV = 1.000110 + .034221 * C1 + .001280 * S1 + .000719 * C2 + .000077 * S2

Ch = Cos (Hangle * DR)
Cl = Cos (Xlat * DR)
Cd = Cos (Declin * DR)
Sl = Sin (Xlat * DR)
Sd = Sin (Declin * DR)

    Cz = Sd * Sl + Cd * Cl * Ch
If (Abs(Cz) .gt. 1.) Cz = Sign (1., Cz)

* ETRZEN is the solar zenith angle outside the atmosphere:

ETRzen = Acos (Cz) / DR
ETRzen = Amin1 (ETRzen, 99.0)

Ca = Sin (Etrzen * DR)
Sa = Cos (Etrzen * DR)

E = 90. - ETRzen

* Refraction correction:

If (E .gt. 85.) then
  Refcor = 0.
Else
  Te = Tan (E * DR)

  If (E .ge. 5.) then
    Refcor = 58.1 / Te - .07 / Te**3 + .000086 / Te**5
  Else if (E .ge. -0.575) then
    Refcor = 1735. + E * (-518.2 + E * (103.4 + E * (-12.79 + E * .711)))
  Else
    Refcor = -20.774 / Te
  End If
  Refcor = Refcor / 3600.
End If

Solelv = E + Refcor
Solelv = Amax1 (Solelv, -9.0)

Solzen = 90. - Solelv

* SOLAZM is the solar azimuth angle:

```
Solazm = 180.
Al = Ca * Cl
If ( Abs ( Al ) .lt. .001 )  Go to 7000
Caz = ( Sa * Sl - Sd ) / ( Al )
If ( Abs ( Caz ) .gt. 1. ) Caz = Sign ( 1., Caz )
Solazm = 180. - Acos ( Caz ) / DR
If ( Hangle .gt. 0 ) Solazm = 360. - Solazm
```

* Solar constant (W/sq m):

```
7000 Continue
Solcon = 1367.0
```

* ETR is the extra-terrestrial horizontal solar radiation, and
* ETRN is the extra-terrestrial direct normal solar radiation:

```
ETRN = Solcon * ERV
ETR = ETRN * Cos ( Solzen * DR )
If ( ETR .lt. 0. ) then
  ETR = 0.0
  ETRN = 0.0
End If
```

* AMASS is the relative optical airmass (how much air is between us
* and the sun:

```
AMass  = -1.
If ( Etrzen .le. 93. ) then
  Cz = Cos ( Etrzen * DR )
  AMass = 1. / ( Cz + 0.50572 * ( 96.07995 - Etrzen ) ** ( -1.6364 ) )
End If
Return
End
```

APPENDIX J
Spectral Model SPCTRL2 QuickBasic[@] Source Code

APPENDIX J
Spectral Model SPCTRL2 QuickBasic® Source Code

```
' SERI/TR-215-2436 Solar Spectral Model  Oct. 8, 1984
' Developed by Kim Mitchell, ARCO SOLAR
' Slightly modified for Qbasic/QuickBasic environment
' By Daryl R. Myers, NOV 24, 1993 (303)-275-3790
' National Renewable Energy Laboratory
' 1617 Cole Blvd, Golden CO 80401


SCREEN 8
COLOR 14, 1
12 DIM I(123, 8), A$(12), A(12), j(81, 2)
14 DATA 2.305,1.232,3.696,6.577,7.886,8.874,8.209,11.83,11.52,12.46,19.2
15 DATA 30.73,34.42,26.04,30.85,36.24,39.1,40.32,42.48,42.04,43.56,44.25
16 DATA 43.76,46.56,47.55,48.7,48.56,49.03,50.32,48.86,50.39,50.88,51.07
17 DATA 50.82,51.69,50.43,51.24,53.32,52.89,48.15,49.13,50.13,41.47,43.49
18 DATA 49.24,50.93,37.39,46.75,50.98,48.9,47.45,44.4,37.78,40.92,45.49
19 DATA 45.65,45.68,45.22,45.2,42.67,32.44,30.17,31.44,18.25,3.79,12.9
20 DATA 18.39,29.22,33.29,39.97,40.84,41.15,41.94,43.05,43.44,44.14,44.22
21 DATA 43.21,42.37,40.32,34.33
22 FOR x = 1 TO 81
j(x, 1) = .3 + .01 * (x - 1)
READ j(x, 2)
NEXT
25 RPD = .0174533
QX = 4
U = 1
NW = 75
30 XS = 1
YS = 1
XL = 13
YL = 3
x0 = 51 * XS
XEND = 531 * XS
y0 = 20 * YS
yend = 170 * YS
40 DATA I,r,r,a,d,i,a,n,c,e
50 FOR Y = 1 TO 10
READ Y$(Y)
NEXT
70 DATA "Aerosol Optical Depth at 0.5 um, Taus. (0.001-0.6)..........."
71 DATA "Power on Angstrom Turbidity Expression, Alpha(1.14 for Rural)"
72 DATA "Ground Albedo, Rho (0.25 typ)................................."
73 DATA "Ozone Amount, O3(atm cm; 0.01 to 0.3 typ)...................."
80 DATA "Solar Zenith Angle, Z(deg)..................................."
81 DATA "Precipitable Water Vapor, W(cm)..(0.01 to >6.0, typ)........."
82 DATA "Aerosol Assymetry Factor, GG(0.65 used for rural)............"
90 DATA "Angle of Incidence of Direct Beam on Flat Surface, AI(deg)..."
```

91 DATA "Slope or Tilt Angle of Surface, S(deg)........................"
92 DATA "Surface Pressure, SPR(millibars).............................."
100 DATA "Number of Wavelengths for this Run, NW..(max 122)..........."
101 DATA "Julian Day, NDAY......(1-365).............................."
110 FOR x = 1 TO 12
READ A$(x)
NEXT
120 DATA 0.27,1.14,0.2,.34,48,1.42,.65,11,37.5,1013,75,240
130 FOR x = 1 TO 12
READ A(x)
NEXT
140 REM (um) AMO(Wm-2um-1) Awl   Aol   Aul
150 DATA .3,535.9,0,10,0, .305,558.3,0,4.8,0, .31,622,0,2.7,0
160 DATA .315,692.7,0,1.35,0, .32,715.1,0,.8,0, .325,832.9,0,.38,0
170 DATA .33,961.9,0,.16,0, .335,931.9,0,.075,0, .34,900.6,0,.04,0
180 DATA .345,911.3,0,.019,0, .35,975.5,0,.007,0, .36,975.9,0,0,0
190 DATA .37,1119.9,0,0,0, .38,1103.8,0,0,0, .39,1033.8,0,0,0
200 DATA .40,1479.1,0,0,0, .41,1701.3,0,0,0, .42,1740.4,0,0,0
210 DATA .43,1587.2,0,0,0, .44,1837.0,0,0,0, .45,2005.0,0,.003,0
220 DATA .46,2043,0,.006,0, .47,1987,0,.009,0, .48,2027,0,.014,0
230 DATA .49,1896,0,.021,0, .50,1909,0,.03,0, .51,1927,0,.04,0
240 DATA .52,1831,0,.048,0, .53,1891,0,.063,0, .54,1898,0,.075,0
250 DATA .55,1892,0,.085,0, .57,1840,0,.12,0, .593,1768,.075,.119,0
260 DATA .61,1728,0,.12,0, .63,1658,0,.09,0, .656,1524,0,.065,0
270 DATA .6676,1531,0,.051,0,.69,1420,.016,.028,.15, .71,1399,.0125,.018,0
280 DATA .718,1374,1.8,.015,0, .7244,1373,2.5,.012,0, .74,1298,.061,.01,0
290 DATA .7525,1269,.0008,.008,0, .7575,1245,.0001,.007,0
300 DATA .7625,1223,.00001,.006,4, .7675,1205,.00001,.005,.35
310 DATA .78,1183,.0006,0,0, .8,1148,.036,0,0, .816,1091,1.6,0,0
320 DATA .8237,1062,2.5,0,0, .8315,1038,.5,0,0, .84,1022,.155,0,0
330 DATA .86,998.7,.00001,0,0, .88,947.2,.0026,0,0, .905,893.2,7,0,0
340 DATA .915,868.2,5,0,0, .925,829.7,5,0,0, .93,830.3,27,0,0
350 DATA .937,814,55,0,0, .948,786.9,45,0,0, .965,768.3,4,0,0
360 DATA .98,767,1.48,0,0, .9935,757.6,.1,0,0, 1.04,688.1,.00001,0,0
370 DATA 1.07,640.7,.001,0,0, 1.1,606.2,3.2,0,0, 1.12,585.9,115,0,0
380 DATA 1.13,570.2,70,0,0, 1.145,564.1,75,0,0, 1.161,544.2,10,0,0
390 DATA 1.17,533.4,5,0,0, 1.2,501.6,2,0,0, 1.24,477.5,.002,0,.05
400 DATA 1.27,442.7,.002,0,.3, 1.29,440,.1,0,.02, 1.32,416.8,4,0,.0002
401 DATA 1.35,391.4,200,0,.00011,1.395,358.9,1000,0,.00001
402 DATA 1.4425,327.5,185,0,.05,1.4625,317.5,80,0,.011
403 DATA 1.477,307.3,80,0,.005,1.497,300.4,12,0,.0006,1.52,292.8,.16,0,0
404 DATA 1.539,275.5,.002,0,.005,1.558,272.1,.0005,0,.13
405 DATA 1.578,259.3,.0001,0,.04,1.592,246.9,.00001,0,.06
406 DATA 1.61,244,.0001,0,.13,1.63,243.5,.001,0,.001,1.646,234.8,.01,0,.0014
407 DATA 1.678,220.5,.036,0,.0001,1.74,190.8,1.1,0,.00001
408 DATA 1.8,171.1,130,0,.00001,1.86,144.5,1000,0,.0001,1.92,135.7,500,0,.001
409 DATA 1.96,123,100,0,4.3,1.985,123.8,4,0,.2,2.005,113,2.9,0,21
410 DATA 2.035,108.5,1,0,.13,2.065,97.5,.4,0,1,2.1,92.4,.22,0,.08
411 DATA 2.148,82.4,.25,0,.001,2.198,74.6,.33,0,.00038,2.27,68.3,.5,0,.001
412 DATA 2.36,63.8,4,0,.0005,2.45,49.5,80,0,.00015,2.5,48.5,310,0,.00014

```
413 DATA 2.6,38.6,15000,0,.00066,2.7,36.6,22000,0,100,2.8,32,8000,0,150
414 DATA 2.9,28.1,650,0,.13,3,24.8,240,0,.0095,3.1,22.1,230,0,.001
415 DATA 3.2,19.6,100,0,.8,3.3,17.5,120,0,1.9,3.4,15.7,19.5,0,1.3
416 DATA 3.5,14.1,3.6,0,.075,3.6,12.7,3.1,0,.01,3.7,11.5,2.5,0,.00195
417 DATA 3.8,10.4,1.4,0,.004,3.9,9.5,.17,0,.29,4,8.6,.0045,0,.025
428 FOR x = 1 TO 122
FOR Y = 1 TO 5
READ I(x, Y)
NEXT
NEXT
I(0, 1) = .295
I(123, 1) = 4.1
429 GOSUB 550' PRINT HEADER
430 PRINT TAB(15); "SERI/NREL Solar Spectral Model"
PRINT TAB(11); "Developed by R.E. Bird and C.J. Riordan"
PRINT
440 PRINT TAB(20); "1. Input/change Atmospheric Parameters."
450 PRINT TAB(20); "2. Run Calculation."
460 PRINT TAB(20); "3. Plot Data on Screen."
470 PRINT TAB(20); "4. Print Data Table to Screen."
480 PRINT TAB(20); "5. Store/retrieve Data Set to files."
490 PRINT TAB(20); "6. Exit Program."
500 PRINT
PRINT TAB(5); "SELECT CHOICE: 1,2,3....."; 
505 PRINT
PRINT TAB(5); "Tap SPACEBAR after after graphing to return to this MENU."
510 INPUT CX
520 ON CX GOSUB 1000, 570, 1080, 1310, 3000, 540
530 GOTO 429
540  CLS
END
550 SCREEN 8
CLS
PRINT
PRINT TAB(15); "ARCO SOLAR, INC./SERI/NREL ", DATE$
560 PRINT STRING$(80, 42)
PRINT
RETURN
561 SCREEN 8
CLS
PRINT
PRINT TAB(15); "ARCO SOLAR, INC./SERI/NREL", DATE$
562  PRINT STRING$(80, 42)
PRINT
RETURN
563 SCREEN 8
CLS
PRINT
PRINT TAB(15); "ARCO SOLAR, INC./SERI/NREL", DATE$
564    PRINT STRING$(80, 42)
```

```
PRINT
RETURN
565 SCREEN 8
CLS
PRINT
PRINT TAB(15); "ARCO SOLAR, INC./SERI/NREL", DATE$
566    PRINT STRING$(80, 42)
PRINT
RETURN
570 REM Calculate Direct/Diffuse Components of Air Mass
580 GOSUB 561
PRINT
PRINT TAB(15); "Spectral Calculation in Progress...";
590 TAUS = A(1)
ALPHA = A(2)
RHO = A(3)
O3 = A(4)
z = A(5)
W = A(6)
GG = A(7)
AI = A(8)
s = A(9)
SPR = A(10)
NW = A(11)
NDAY = A(12)
DIRT = 0
DIFT = 0
DTOTT = 0
600 OMEG = .945
OMEGP = .095
ALG = LOG(1 - GG)
610 AFS = ALG * (1.459 + ALG * (.1595 + ALG * .4129))
BFS = ALG * (.0783 + ALG * (-.3824 - ALG * .5874))
620 FS = 1 - .5 * EXP((AFS + BFS * COS(RPD * z)) * COS(RPD * z))
630 FSP = 1 - .5 * EXP((AFS + BFS / 1.8) / 1.8)
640 D1 = 6.283185 * (NDAY - 1) / 365
650 d=1.00011+.034221*COS(D1)+.00128*SIN(D1)+.000719*COS(2 * D1)+.000077*SIN(2*D1)
660 AM = 1 / (COS(RPD * z) + .15 * (93.885 - z) ^ (-1.253))
AMP = AM * SPR / 1013
670 FOR x = 1 TO 122
wx = I(x, 1)
H0 = I(x, 2)
IF Q > 15 THEN Q = 1
671 Q = Q + 1
672 PRINT ".";
680 OMEGL = OMEG * EXP(-OMEGP * (LOG(wx / .4)) ^ 2)
690 REM Direct Normal Irradiance
700 TR = EXP(-AMP / (wx ^ 4 * (115.6406 - 1.335 / wx ^ 2)))
710 AMOZ = (1 + 22 / 6370) / (COS(RPD * z) ^ 2 + 2 * 22 / 6370) ^ .5
720 TOZ = EXP(-I(x, 4) * O3 * AMOZ)
```

```
730 TUGA = EXP(-1.41 * I(x, 5) * AMP / (1 + 118.93 * I(x, 5) * AMP) ^ .45)
740 TH20 = EXP(-.2385 * I(x, 3) * W * AMP / (1 + 20.07 * I(x, 3) * W * AMP) ^ .45)
BB = wx / .5
BB = BB ^ (-ALPHA)
750 DELA = TAUS * BB
760 TA = EXP(-DELA * AM)
770 TAA = EXP(-(1 - OMEGL) * DELA * AM)
780 TAS = EXP(-OMEGL * DELA * AM)
790 DIR = H0 * d * TR * TOZ * TUGA * TH20 * TA
800 DIRSUR = DIR * COS(RPD * AI)
810 REM Diffuse Irradiance
820 DRAY = H0 * d * COS(RPD * z) * TOZ * TUGA * TH20 * TAA * (1 - TR ^ .95) * .5
830 DAER=H0*d*COS(RPD * z)* TOZ * TUGA * TH20 * TAA * TR ^ 1.5 * (1 - TAS) * FS
840 TRP = EXP(-1.8 / (wx ^ 4 * (115.6406 - 1.335 / wx ^ 2)))
850 TWP = EXP(-.2385 * I(x, 3) * W * 1.8 / (1 + 20.07 * I(x, 3) * W * 1.8) ^ .45)
860 TUP = EXP(-1.41 * I(x, 5) * 1.8 * (1 + 118.93 * I(x, 5) * 1.8) ^ .45)
870 TASP = EXP(-OMEGL * DELA * 1.8)
880 TAAP = EXP(-(1 - OMEGL) * DELA * 1.8)
890 RHOA = TUP * TWP * TAAP * (.5 * (1 - TRP) + (1 - FSP) * TRP * (1 - TASP))
900 DRGD = (DIR * COS(RPD * z)+(DRAY + DAER)) * RHO * RHOA / (1 - RHO * RHOA)
910 CRC = 1
IF wx < .45 THEN CRC = (wx + .55) ^ 1.8
920 DIF = CRC * (DRAY + DAER + DRGD)
930 DTOT = DIR * COS(RPD * z) + DIF
933 W1 = (I(x + 1, 1) - I(x - 1, 1)) / 2
935 DIRT = DIRT + DIR * W1
DIFT = DIFT + DIF * W1
DTOTT = DTOTT + DTOT * W1
940 REFS = DTOT * RHO * (1 - COS(RPD * s)) / 2
941 A2 = DIR / H0 / d
942 DIFSC = DIF * A2 * COS(RPD * AI) / COS(RPD * z)
943 DIFSI = DIF * (1 - A2) * (1 + COS(RPD * s)) / 2
944 DIFS = DIFSC + DIFSI + REFS
945 DIRS = DIR * COS(RPD * AI)
946 DTOTS = DIRS + DIFS
950 I(x, 6) = DIRS
I(x, 7) = DIFS
I(x, 8) = DTOTS
960 NEXT x
970 GOTO 990
980 CR$ = INKEY$
IF CR$ = "" THEN 980 ELSE 990
990 RETURN
1000 REM Input/change data
1010 GOSUB 563 'PRINT HEADER
1020 PRINT TAB(5); "Enter/change Data Inputs:"
PRINT
1025 PRINT TAB(10); "For Global Normal Spectra: AI=0, S=Z"
PRINT
1030 FOR x = 1 TO 12
```

```
PRINT TAB(5); x; ". "; A$(x); "="; A(x)
NEXT x
PRINT
1040 INPUT "Enter 'Parameter #,New Value' to change, else '0,0': ", z, AZ
1050 IF z = 0 THEN 1070
1060 A(z) = AZ
GOTO 1040
1070 RETURN
1080 REM Plot Data
1090 Q(1) = 2
Q(2) = 6
Q(3) = 7
Q(4) = 8
Q(6) = 8
1100 GOSUB 565
1110 PRINT TAB(20); "Plot Selections:"
PRINT
1120 PRINT TAB(25); "1.  Air Mass Zero Spectrum"
1130 PRINT TAB(25); "2.  Direct Spectrum"
1140 PRINT TAB(25); "3.  Diffuse Spectrum"
1150 PRINT TAB(25); "4.  Total Spectrum"
1155 PRINT TAB(25); "5.  Direct/Diffuse/Total Spectrum"
1160 PRINT
PRINT "Enter/change plot selections:"; QX;
INPUT QX$
1162 IF QX$ = "" THEN 1166
1164 QX = VAL(QX$)
1166 QY = Q(QX)
1172 PRINT
PRINT "SELECT Irradiance Units: 1=W/m2/um, 2=Photons/cm2/sec/um: "; U;
1174 INPUT U$
1176 IF U$ = "" THEN 1180
1178 U = VAL(U$)
1180 SCREEN 8: CLS
1181 PRINT USING "   Air Mass= ##.# Zenith Angle= ### Slope of Surface= ###"; AM; z; s
1182 PRINT TAB(10);"PW (cm)=";W;"Ozone(atm cm)=";O3;"Albedo=";RHO;"Incid.Ang.="; AI
1183 PRINT USING "Irradiance(W/m2):Tot=####.# Dir=####.# Dif=###.#";DTOTT;DIRT; DIFT
1190 FOR Y = 1 TO 10
LOCATE 5 + Y, 1
PRINT Y$(Y)
NEXT Y
1195 IF U = 1 THEN 1200
1197 FOR Y = 0 TO 5
LOCATE (3 + 3.8 * Y), 3
PRINT USING "##"; 10 * (5 - Y)
NEXT
GOTO 1210
1200 FOR Y = 0 TO 5
LOCATE (3 + 3.8 * Y), 3
PRINT USING "####"; 400 * (5 - Y)
```

```
NEXT
1210 SX = 7 * XS
FOR Y = 1 TO 10
SY = Y * (y0 - yend) / 10 + yend
PSET (x0, SY), 3
NEXT
1220 FOR x = 0 TO 10
LOCATE 23, 6 + 5.9 * x
PRINT USING "#.#"; x / 10 + .3
NEXT
1230 LINE (x0, yend)-(XEND, yend)
LINE (x0, y0)-(x0, yend)
1240 SY = 6 * YS
FOR x = 1 TO 10
SX = x * (XEND - x0) / 10 + x0
PSET (SX, yend), 3
NEXT
1250 PRINT TAB(28); "Wavelength (um)";
1260 LOCATE 25, 58
PRINT "KWM   "; DATE$;
1265 IF QX <> 5 THEN 1270
1266 FOR QY = 6 TO 8
1270 PSET (x0, yend), 3
xold = x0
yold = yend
1275 FOR x = 1 TO NW
IF U = 1 THEN UX = .075
1276 IF U = 2 THEN UX = 3 * I(x, 1) * .0503
1280 x1 = x0 + 480 * XS * (I(x, 1) - .3)
y1 = yend - YS * UX * I(x, QY)
LINE (xold, yold)-(x1, y1)
xold = x1
yold = y1
NEXT x
1281 IF QX <> 5 THEN 1283
1282 NEXT QY
1283 IF QX < 6 THEN 1290
1284 PSET (x0, yend), 3
yold = yend
xold = x0
1285 FOR x = 1 TO 81
IF U = 1 THEN UX = .075 / (j(x, 1) * .0503)
1286 IF U = 2 THEN UX = 3
1287 x1 = x0 + 480 * XS * (j(x, 1) - .3)
y1 = yend - YS * UX * j(x, 2)
LINE (xold, yold)-(x1, y1)
xold = x1
yold = y1
NEXT x
1290 CR$ = INKEY$
```

```
IF CR$ = "" THEN 1290 ELSE 1300
1300 RETURN
1310 REM Print Data Table
1320 GOSUB 550
lx = 1
1330 PRINT "uM   "; TAB(10); "AM0"; TAB(20); "Awl"; TAB(30); "Aol"; TAB(40); "Aul"; TAB(50);
"Dir"; TAB(60); "Dif"; TAB(70); "Dtot"
1340 FOR x = 1 TO NW
lx = lx + 1
IF lx > 21 THEN PRINT
IF lx > 21 THEN INPUT "Press Enter to Continue..."; z$
IF lx > 21 THEN lx = 1
IF lx = 1 THEN PRINT "uM   "; TAB(10); "AM0"; TAB(20); "Awl"; TAB(30); "Aol"; TAB(40); "Aul";
TAB(50); "Dir"; TAB(60); "Dif"; TAB(70); "Dtot"
FOR j = 1 TO 8
PRINT TAB(10 * j - 10); I(x, j);
NEXT
NEXT
1350 CR$ = INKEY$
IF CR$ = "" THEN 1350 ELSE 1360
1360 RETURN
3000 REM Store/Retrieve Data Set
3001 GOSUB 550
PRINT
PRINT TAB(5); "Do you want to (1) STORE a data file "
3002 PRINT
PRINT TAB(5); "          (2) RETRIEVE a Data File"
3003 PRINT
PRINT TAB(5); "          (3) RETURN to MAIN MENU"
3004 PRINT
PRINT
INPUT "choose (1) or (2) or (3)..."; SC
3005 IF SC = 1 THEN 3010
3006 IF SC = 2 THEN 3100
3007 IF SC = 3 THEN 429
A:
3010 GOSUB 550
PRINT
PRINT "Save [P]arameters only...or [D]ata and Parameters ?"
PRINT "Note P option allows later recomputation of spectra..."
INPUT "Your Choice [P] or [D] ...."; p$
p$ = UCASE$(p$)
IF p$ <> "P" AND p$ <> "D" THEN GOTO A
PRINT TAB(5); "ENTER FILE NAME for this data set..."
3020 PRINT
PRINT TAB(5); "INCLUDE DRIVE SPECIFICATION !! E.G.; B:fname.ext "; ""
3030 PRINT
INPUT "Your Drive:filename..."; F$
3040 PRINT
PRINT " is " + CHR$(34) + F$ + CHR$(34) + " OK for the file name ? "
```

```basic
3041 INPUT "(Y/N) "; Q$
3050 IF Q$ <> "y" AND Q$ <> "Y" THEN 3010
3060 PRINT
PRINT "SAVING DATA ON FILE "; F$
3061 OPEN F$ FOR OUTPUT AS #1
3064 FOR K = 1 TO 12
WRITE #1, A(K)
NEXT K
PRINT "Parameters saved..."
IF p$ = "P" THEN GOTO B
3065 FOR x = 1 TO 122
FOR j = 1 TO 8
IF j > 1 AND j < 6 THEN GOTO s
PRINT #1, USING "####.#### !"; I(x, j); " ";
PRINT USING "####.#### !"; I(x, j); " ";
s: zz = 0
NEXT
PRINT #1, " "
PRINT " "
NEXT
B: PRINT "Finished saving data..."
3066 PRINT "spectral data saved..."
FOR L = 1 TO 5000
NEXT
3067 CLOSE #1
3070 GOTO 429
3100 GOSUB 563
c: PRINT
PRINT
PRINT TAB(5); "ENTER FILE NAME to RETRIEVE     ..."
PRINT
PRINT "NOTE: Retrieves Parameters only...to recompute spectrum!"
p$ = "P"
3120 PRINT
PRINT TAB(5); "INCLUDE DRIVE SPECIFICATION !! E.G.; B:fname.ext"
3130 PRINT
INPUT "Your Drive:filename..."; F$
3140 PRINT
PRINT " is " + CHR$(34) + F$ + CHR$(34) + " OK for the file name ? "
3141 INPUT "(Y/N) "; Q$
3150 IF Q$ <> "y" AND Q$ <> "Y" THEN 3100
3160 PRINT
PRINT "RETRIEVING    FILE "; F$
3161 OPEN F$ FOR INPUT AS #1
3164 FOR K = 1 TO 12
INPUT #1, A(K)
NEXT K
PRINT "Parameters read...."
3166 PRINT " "
FOR L = 1 TO 5000
```

NEXT
3167 CLOSE #1
3170 GOTO 429

APPENDIX K
Perez Anisotropic Diffuse Irradiance Model
Subroutine QuickBasic© Source Code

APPENDIX K
Perez Anisotropic Diffuse Irradiance Model Subroutine QuickBasic® Source Code

SUB IRRPZ (GH, DN, DF, ZZ, SS, ALB, AINC, DPER)

```
'              Perez Diffuse Radiation Model
'              -----------------------------

' G = GH      = Global Horizontal Irradiance (W/m^2)
' B = DN      = Direct Normal (Beam) Irradiance (W/m^2)
' D = DF      = Diffuse Horizontal Irradiance (W/m^2)
' ZEN = ZZ    = Solar Zenith Angle (Radians), obtained from SOLPOS
' SLOPE = SS  = Surface's Slope (Tilt) (Radians)
' ALBEDO = ALB = Ground Albedo
' AINC        = Solar Incidence Angle on Surface (Radians)

' Routine returns:  DPER = Tilted Diffuse + Reflected Irradiance (W/m^2)
'   (Returns Diffuse on Tilt so compute DN*COS(ZZ) + DPER as Tilted Irradiance
'     i.e., Global POA = DIRECT BEAM + DIFFUSE  in calling program)

' The Tilted Diffuse Irradiance cannot be calculated if G or B is unknown
'   ==> -999 is returned
' If Dew Point Temp. (TD) is unknown, then Precipitable Water (DP) = 2.0 cm
' If Ground Albedo is unknown, then it is assigned the value 0.2


'DEFDBL A-P, R-Z

DIM F11R(8), F12R(8), F13R(8), F21R(8), F22R(8), F23R(8), EPSBINS(8)

F11R(1) = -.0083117#: F11R(2) = .1299457#: F11R(3) = .3296958#
F11R(4) = .5682053#
F11R(5) = .873028#: F11R(6) = 1.1326077#: F11R(7) = 1.0601591#
F11R(8) = .677747#

F12R(1) = .5877285#: F12R(2) = .6825954#: F12R(3) = .4868735#
F12R(4) = .1874525#
F12R(5) = -.3920403#: F12R(6) = -1.2367284#: F12R(7) = -1.5999137#
F12R(8) = -.3272588#

F13R(1) = -.0620636#: F13R(2) = -.1513752#: F13R(3) = -.2210958#
F13R(4) = -.295129#
F13R(5) = -.3616149#: F13R(6) = -.4118494#: F13R(7) = -.3589221#
F13R(8) = -.2504286#

F21R(1) = -.0596012#: F21R(2) = -.0189325#: F21R(3) = .055414#
F21R(4) = .1088631#
F21R(5) = .2255647#: F21R(6) = .2877813#: F21R(7) = .2642124#
F21R(8) = .1561313#
```

```
F22R(1) = .0721249: F22R(2) = .065965#: F22R(3) = -.0639588#
F22R(4) = -.1519229#
F22R(5) = -.4620442#: F22R(6) = -.8230357#: F22R(7) = -1.127234#
F22R(8) = -1.3765031#

F23R(1) = -.0220216#: F23R(2) = -.0288748#: F23R(3) = -.0260542#
F23R(4) = -.0139754#
F23R(5) = .0012448#: F23R(6) = .0558651#: F23R(7) = .1310694#
F23R(8) = .2506212#


EPSBINS(1) = 1.065: EPSBINS(2) = 1.23: EPSBINS(3) = 1.5: EPSBINS(4) = 1.95
EPSBINS(5) = 2.8: EPSBINS(6) = 4.5: EPSBINS(7) = 6.2


B2 = .000005534#
RtoD = 57.29577951308232#:     ' Radians to Degrees
DtoR = .017453292#:          ' Degrees to Radians
ZERO = 0!
CONSTANT = .0871557#:         ' Cosine 85 Deg -- Limit of Model Calculations

G = CDBL(GH):               ' Global Horizontal
B = CDBL(DN):               ' Direct Normal
D = CDBL(DF):               ' Diffuse Horizontal
ZEN = CDBL(ZZ):              ' Solar Zenith Angle (Radians)

ALBEDO = CDBL(ALB):           ' Ground Albedo
INC = CDBL(AINC):            ' Solar Incidence Angle (Radians)
SLOPE = CDBL(SS):            ' Surface Slope (Radians)


IF G = -999 OR B = -999 THEN
  DPER = -999
  GOTO 3000
ELSE
  IF (ZEN < 0) OR (ZEN > 1.5271631#) THEN
    DPER = 0  ^
    GOTO 3000
  ELSE
' For measured data between -10 and 0:
    IF G <= 0 THEN
      DPER = 0  ^
      GOTO 3000
    ELSE
      IF ALBEDO = -999 THEN
        ALBEDO = .2
      ELSE
      END IF

      Cz = COS(ZEN)
      ZENITH = ZZ * RtoD
```

```
    IF Cz >= CONSTANT THEN
      ZH = Cz
    ELSE
      ZH = CONSTANT
    END IF


' The following is used if DIFFUSE is not available:
'  Compute DIFFUSE from available BEAM and GLOBAL

    IF Cz > 0 THEN
      D = G - (B * Cz)
    ELSE
      D = G
    END IF

    D = DF

    IF D = 0 THEN
      DPER = 0   ^
      GOTO 3000
    ELSE
    END IF

    AIRMASS = CDBL(1! / (Cz + (.15 * (93.9 - ZENITH) ^ (-1.253))))
    DELTA = CDBL((D * AIRMASS) / 1367!)
    T = CDBL(ZENITH ^ 3!)
    EPS = CDBL((B + D) / D)
    EPS = CDBL((EPS + (T * B2)) / (1! + (T * B2)))

    FOR I = 1 TO 8
      IF (I = 8) OR (EPS <= EPSBINS(I)) THEN 3100
    NEXT I

3100
    IF ZERO > (F11R(I) + (F12R(I) * DELTA) + (F13R(I) * ZEN)) THEN
      F1 = ZERO
    ELSE
      F1 = CDBL(F11R(I) + (F12R(I) * DELTA) + (F13R(I) * ZEN))
    END IF

    F2 = CDBL(F21R(I) + (F22R(I) * DELTA) + (F23R(I) * ZEN))


    ALBPROD = CDBL(ALBEDO * G)
    COSI = CDBL(COS(INC))

    IF COSI < 0 THEN
      ZC = 0   ^
    ELSE
      ZC = COSI
```

```
        END IF

        A = CDBL(D * (1! + COS(SLOPE)) / 2!)
        BB = CDBL(ZC / (ZH * D) - A)
        c = CDBL(D * SIN(SLOPE))

        DPER = CDBL(A + (F1 * BB) + (F2 * c) + (ALBPROD * (1! - COS(SLOPE))) / 2!)


        GOTO 3000

    END IF
   END IF
END IF

3000

END SUB
```

REPORT DOCUMENTATION PAGE

1. AGENCY USE ONLY (Leave blank)	2. REPORT DATE April 1997	3. REPORT TYPE AND DATES COVERED Technical Report

4. TITLE AND SUBTITLE

Radiometric Instrumentation and Measurements Guide for Photovoltaic Performance Testing

6. AUTHOR(S)

D. Myers

5. FUNDING NUMBERS

C:
TA: PV706401

7. PERFORMING ORGANIZATION NAME(S) AND ADDRESS(ES)

National Renewable Energy Laboratory
1617 Cole Blvd.
Golden, CO 80401-3393

8. PERFORMING ORGANIZATION REPORT NUMBER

9. SPONSORING/MONITORING AGENCY NAME(S) AND ADDRESS(ES)

National Renewable Energy Laboratory
1617 Cole Blvd.
Golden, CO 80401-3393

10. SPONSORING/MONITORING AGENCY REPORT NUMBER

TP-560-21774

DE97000082

11. SUPPLEMENTARY NOTES

12a. DISTRIBUTION/AVAILABILITY STATEMENT

12b. DISTRIBUTION CODE

UC-1250

13. ABSTRACT *(Maximum 200 words)*

The Photovoltaic Module and Systems Performance Engineering Project at the National Renewable Energy Laboratory performs indoor and outdoor standardization, testing, and monitoring of the performance of a wide range of photovoltaic (PV) energy-conversion devices and systems. The PV Radiometric Measurements and Evaluations Team within that project is responsible for measurement and characterization of natural and artificial optical radiation that stimulates the PV effect. The purpose of this document is to address the practical and engineering needs of optical and solar radiometric instrument performance, selection, calibration, installation, and maintenance applicable to indoor and outdoor radiometric measurements for PV calibration, performance, and testing applications. The introduction addresses radiometric concepts and definitions. Next, concepts essential to spectral radiometric measurements are discussed. Broadband radiometric instrumentation and measurement concepts are then discussed. Specific applications and examples of spectroradiometry and broadband radiometry applied to photovoltaic performance evaluation are described. In each case, the need for measurement, calibration and reference standards, and instrument performance and applications (installation, maintenance, and quality assurance) is addressed.

14. SUBJECT TERMS

photovoltaics ; radiometric instruments ; standardization ; testing ; calibrating ; photovoltaic performance testing ; guide

15. NUMBER OF PAGES
151

16. PRICE CODE

17. SECURITY CLASSIFICATION OF REPORT Unclassified	18. SECURITY CLASSIFICATION OF THIS PAGE Unclassified	19. SECURITY CLASSIFICATION OF ABSTRACT Unclassified	20. LIMITATION OF ABSTRACT UL